Universidade de Aveiro Departamento de Química
2018

JOÃO MIGUEL PIMENTA PEREIRA

TETRÓXIDO DE ÓSMIO NUM SISTEMA SUPRAMOLECULAR DINÂMICO

OSMIUM TETROXIDE IN A DYNAMIC SUPRAMOLECULAR SYSTEM

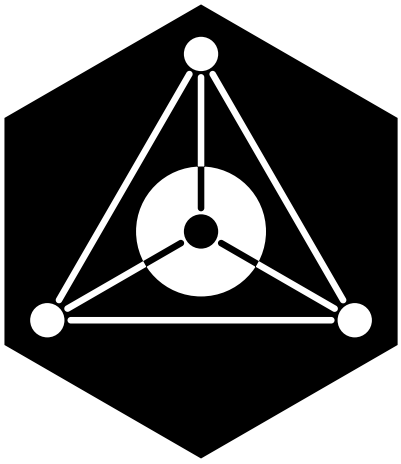

COMPETE
PROGRAMA OPERACIONAL FACTORES DE COMPETITIVIDADE

QUADRO DE REFERÊNCIA ESTRATÉGICO NACIONAL
PORTUGAL 2007.2013

UNIÃO EUROPEIA
Fundo Europeu de Desenvolvimento Regional

FCT
Fundação para a Ciência e a Tecnologia

Universidade de Aveiro Departamento de Química
2018

JOÃO MIGUEL PIMENTA PEREIRA

TETRÓXIDO DE ÓSMIO NUM SISTEMA SUPRAMOLECULAR DINÂMICO

OSMIUM TETROXIDE IN A DYNAMIC SUPRAMOLECULAR SYSTEM

Dissertation submitted to the University of Aveiro to fulfil the requirements for the degree of Master in Chemistry, performed under the scientific supervision of Dr. Artur M. Silva, Full Professor at the University of Aveiro and co-oriented by Dr. Ben S. Pilgrim, Research Fellow at the University of Cambridge.

COMPETE
PROGRAMA OPERACIONAL FACTORES DE COMPETITIVIDADE
QUADRO DE REFERÊNCIA ESTRATÉGICO NACIONAL
PORTUGAL 2007.2013
UNIÃO EUROPEIA
Fundo Europeu de Desenvolvimento Regional
FCT
Fundação para a Ciência e a Tecnologia

SCIENTIA AXIS MUNDI

IGNORANTIA OCCIDIT

o júri

presidente	Professora Doutora Helena Isabel Seguro Nogueira Professora Auxiliar da Universidade de Aveiro
vogal — arguente principal	Doutor Carlos Filipe Reis Alves da Costa Lima Investigador de Pós-Doutoramento na Faculdade de Ciências da Universidade do Porto
vogal — orientador	Professor Doutor Artur Manuel Soares da Silva Vice-Reitor da Universidade de Aveiro

acknowledgements

The path leading me to this stage in my life started with one Teacher in my 7th grade—*Desidério Pires*—to him I owe most of what makes me as a Scientist and Chemist today. Later I came to know three other very influential people in my life: Professors Amparo Faustino, Diana Pinto and Paulo Claro; they were one of the reasons I chose the University of Aveiro as my alma mater. I thank them for all the opportunities they gave me that shaped my course.

The person that had to put up with me for all these last years was Professor Artur Silva. I cannot thank to him enough for his patience and understanding; without his support I would most likely not be handing in any kind of dissertation. I also must thank him for trusting me and let me work autonomously (even though that may not have been the best course of action).

I must give special thanks to Johnathan Nitschke for accepting me as an Erasmus Intern into a leading research group, and to Ben Pilgrim for supervising me. They made me love Supramolecular Chemistry, improved my way of researching, and they put up with my disorganisation. I cannot thank enough for the opportunity to experience and learn from all the talks, all the lectures, all the discussions. I am also grateful to my colleagues in the group, they taught me many lessons and made me grow as a person. Special thanks go to those that made it so that I greatly miss my stay in Cambridge: Ben, Cally, Jack, my mates Jas and Jason, Larissa, the ever-singing Lillian, Marion, Masahiro, Nozomi, and *le* Roy!

Thanks to Florence; for all its little foibles, my work would have not been possible without her dedication in the long nights accompanied by the best of Islay spirits.

To my friends in Portugal, I simply thank the fact that they were there to listen; one can always count on them to jest the depressing moments away.

Finalmente, muito obrigado aos meus pais. De certeza que sem eles não entregaria nenhuma tese. Para além disso, é a eles que tenho que agradecer o meu espírito crítico, curioso e interessado. Agradeço-lhes a compreensão e à minha irmã a motivação para passar esta meta.

Àqueles que não referi: se ajudaram, não precisam de pensar; se precisam de pensar, não ajudaram.

palavras-chave

automontagem de subcomponentes, cinética de associação, complexo hóspede-hospedeiro, di-hidroxilação de alcenos, gaiola de coordenação, ligações dinâmicas covalentes, regulação ortogonal, tetróxido de ósmio

resumo

A Química Supramolecular desempenha um papel importante na obtenção de níveis de complexidade inatingíveis pela Química "clássica", a sua função inclui a criação de redes de sinalização intricadas.

Neste trabalho é feito um relatório da descoberta e caracterização de um complexo supramolecular contendo um catalisador—OsO_4—cuja encapsulação numa gaiola do tipo Fe_4L_6 de ligandos imina permite a regulação da sua catálise de forma não covalente. A surpreendente estabilidade da estrutura supramolecular contendo um oxidante tão poderoso foi estudada e a sua dinâmica caracterizada por RMN. Devido à sensibilidade deste trabalho foram feitas melhorias à síntese do sal de guanidínio da gaiola.

Outros dois complexos hóspede-hospedeiro análogos foram caracterizados contendo 2,5-di-hidrofurano e benzeno como hóspedes. Embora não tenha sido conseguido, isto teve em vista o design de sistemas mais complexos que apresentassem uma variação significativa da cinética de di-hidroxilação normal e demonstrassem regulação ortogonal da catálise.

keywords alkene dihydroxylation, coordination cage, dynamic covalent bonding, host-guest complex, intake kinetics, orthogonal signalling, osmium tetroxide, subcomponent self-assembly

abstract Supramolecular Chemistry plays an important role in attaining levels of complexity in chemical systems that would not be available otherwise, this includes design of complex chemical signalling networks.

Here a report is made on the discovery of a host-guest complex of a catalyst—OsO_4—in an Fe_4L_6 tetrahedral imine coordination cage which enables the regulation of its activity without covalent transformations. The remarkable stability of the assembly hosting this powerful oxidizer is studied as to its stability and dynamics by NMR. Due to the sensitivity of the work, improvements were done on the previously known the synthesis of the guanidinium salt of the cage.

The analogues with 2,5-dihydrofuran and benzene as guests were also characterized. Using these competing guests as signals, the principle of orthogonal regulation of dihydroxylation with OsO_4 was demonstrated. However, no significant deviations from the normal dihydroxylation kinetics were detected in the conditions tested.

Table of Contents

Table of Figures

Table of Tables

Abbreviations and symbols

DHF	2,5-dihydrofuran
DADA	4,4'-diaminobiphenyl-2,2'-disulfonic acid
adj	Adjusted
k	Rate constant
APT	Attached proton test
br	Broad
Bu	Butyl
Bzn	Benzene
δ	Chemical shift
COLSA	Complete Line-shape Analysis
c(X)	Concentration of species X as estimated from solution preparation
CDC	Constitutional dynamic chemistry
CHX	Cyclohexane
y	Degree of association
DF	Degrees of freedom
DMSO	Dimethyl sulfoxide
DA	Donor-acceptor
d	Doublet
DCL	Dynamic covalent linkage
EM	Effective molarity
[G]	Equilibrium concentration of guest
[H]	Equilibrium concentration of host
[HG]	Equilibrium concentration of host-guest complex
eq	Equivalents, molar percentage
EXSY	Exchange spectroscopy
Gdm^+	Guanidinium
HMBC	Heteronuclear Multiple Bond Correlation spectroscopy
HSQC	Heteronuclear Single-Quantum Correlation spectroscopy
HB	Hydrogen bond

K	Equilibrium constant
L	Ligand
LCL	Lower confidence limit
ESI-MS	Electro Spray Ionization Mass Spectrometry
M	Metal
MOF	Metal-organic framework
Me	Methyl
min	Minutes
m	Multiplet
NIOSH	National Institute for Occupational Safety and Health of the United States of America
NMR	Nuclear Magnetic Resonance
NOESY	Nuclear Overhauser Effect Spectroscopy
qu	Quartet
RSS	Residual squared sum
rt	Room temperature
SEXSY	Selective exchange spectroscopy
s	Singlet
Std	Standard
TBA	*Tert*-butanol
$[G]_0$	Initial total concentration of guest
$[H]_0$	Initial total concentration of host
TMA	Trimethylamine
TMAO	Trimethylamine N-oxide
t	Triplet
EXSY	Two-dimensional exchange NMR spectroscopy
UCL	Upper confidence limit
XRD	X-ray diffractometry

Chapter I

Introduction

I.1 Scope of this dissertation

The project leading to this dissertation was brought about by the discovery of a stable host-guest complex with the powerful oxidizer OsO_4 as guest, in the *Nitschke* research group. This discovery is remarkable in and of itself due to the properties of the coordination cage acting as a host. Still, the most important aspect of the observation is that it is about encapsulating a quite reactive dihydroxylation catalyst. This sparked the imagination of chemical systems in solution that, by manipulating the encapsulation of catalyst through other guests, could manipulate the dihydroxylation rate whilst being inert towards every reagent (Figure I.1). One such system, where the guest itself is a substrate for the reaction, would cause the catalysis to be 'turned on' while there is reagent. This kind of system simulates the dynamics and the compartmentalization of active species seen in many self-regulating biological systems. So, all the experiments done were motivated by the wish to build and characterize the dynamics in such a system.

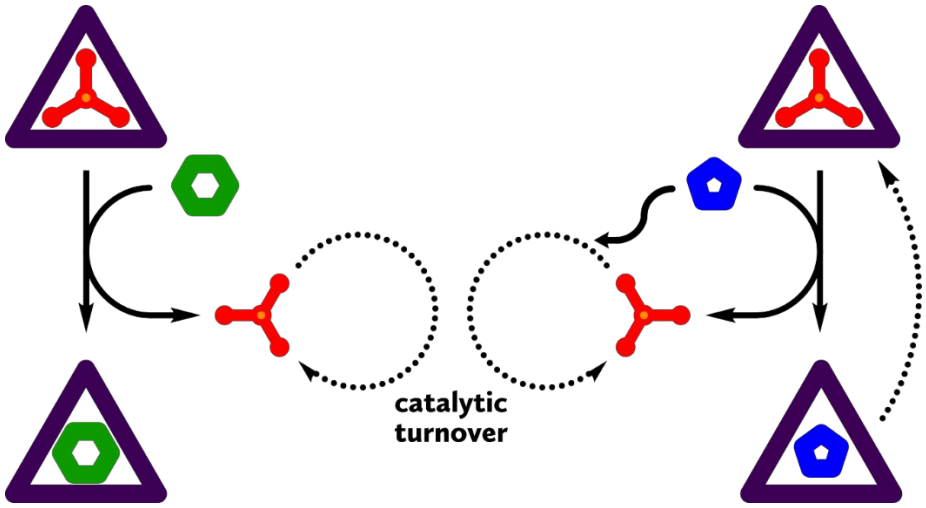

Figure I.1—Cartoon of the idealized reactions that were the final goal of this work. Left: the OsO_4 (red), is simply replaced by another guest enabling catalytic turnover. Right: the displacing guest is itself used in the catalytic turnover with the OsO_4, this returns to the cage after all substrate is spent.

This dissertation starts with an introduction to take the reader trough the same path the author went when entering the field of Supramolecular Chemistry. It goes through the basic concepts needed to understand the motivation behind the experiments. After that, the results of experiments are presented along with brief discussions of results as the subjects are mostly independent and a general discussion is thus avoided.

I.2 Beyond the molecule, before the systems

It can be said that the first scientist to focus their research effort on molecular interactions was *Johannes Diderik van der Waals*. He revolutionized the approach to the thermodynamic properties of fluids not only with the assumption that molecules exist, but that they feel a mutual attraction force, stating that "gaseous and ordinary liquid states are (...) forms of the same condition of matter"—not a universal belief at the time.

Intermolecular forces had been referred before as the cause for unexpected behaviour of gases, but the concept of particles interacting with each other still met some opposition until the beginning of the 20th century. In the late 19th century, *van der Waals* publishes his work "On the continuity of the gaseous and liquid state".[1]

Although understanding intermolecular forces is fundamental to the field of Supramolecular Chemistry, the concepts introduced by *van der Waals* cannot define the field as we know it today. For many years, the effects of these interactions were studied on the bulk of a material (particularly liquids and gasses) or on their general effects on a reaction. However, to do Supramolecular Chemistry is to manipulate and take advantage of intermolecular interactions at the single molecule level and its neighbouring environment; to do Supramolecular Chemistry is to think of all non-covalent interactions in the vicinity as relevant (solvent included); the "mechanical configuration" of a molecule is as important as its electronic configuration.

Emil Fischer was the first to capture this kind of mindset when studying enzymes and their specificity. Although incomplete, his model for the mechanism of enzyme catalysis—the "lock and key principle"—captured the idea of molecular recognition; that the conformation and configuration of a molecule well beyond the reactive group mattered.[2] This was the first hint at chemistry beyond the molecule.

I.3 Beyond Der Waals

After *Van der Waals* laid the ground work for the study of molecular interactions, many researchers sought after the causes of the attractive force he postulated. The work that followed in the subject of non-covalent interactions is summarized in this section as a review of the fundamentals. Other driving forces relevant to the Supramolecular field are also discussed.

I.3.1 Electrostatic interactions

Almost all intermolecular interactions are, in one way or another, electric in nature. Figure I.2 shows examples of these interactions with observed examples.

Interactions depending on permanent electric charges are the strongest; though sometimes included under the umbrella term Van der Waals Forces, they are not part of this group *sensu stricto*. Nonetheless, the ionic interactions are essential to the conformational stability of some proteins (e.g. carboxylate-ammonium salt bridges) and to the activity of some prosthetic groups (e.g. polarization of diatomic oxygen before binding to the iron in the haem group). On the other hand, electrostatic repulsion can also be a barrier for the assembly of certain highly charged supramolecular architectures.

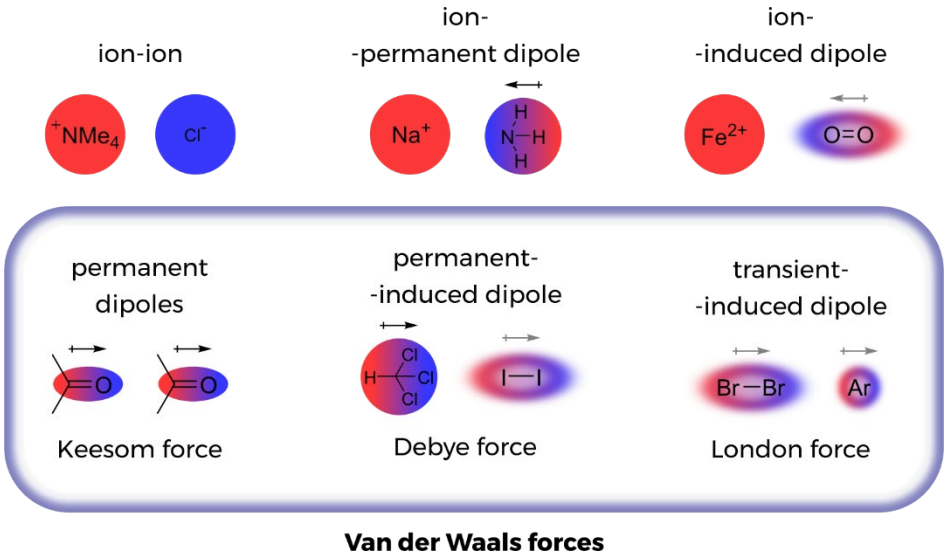

Figure I.2—Illustration of the simplest intermolecular electrostatic interactions in real cases. Note that, strictly speaking, the Van de Waals forces involve only uncharged particles.[3]

There are three kinds of *Van der Waals* interactions, all illustrated in Figure I.2. The interaction through London forces is the only one through which all molecules interact since all particles are polarizable to some extent. Therefore, though theoretically the weakest, these interactions are not to be ignored in supramolecular systems. London forces dominate whenever the molecule is not small enough for its polar momentum to be a major force over its whole volume.

I.3.2 Stacking π

There is a "family" of interactions often called **π-interactions** that deserve a bit of attention of their own due to the chemical moieties involved. It is in fact argued that the species involved are the only thing uniting these under an umbrella term; the interactions can have contributions from very different physical properties of the molecule.[4] Here, I present just a few examples—illustrated in Figure I.3—representative of the possible interactions.

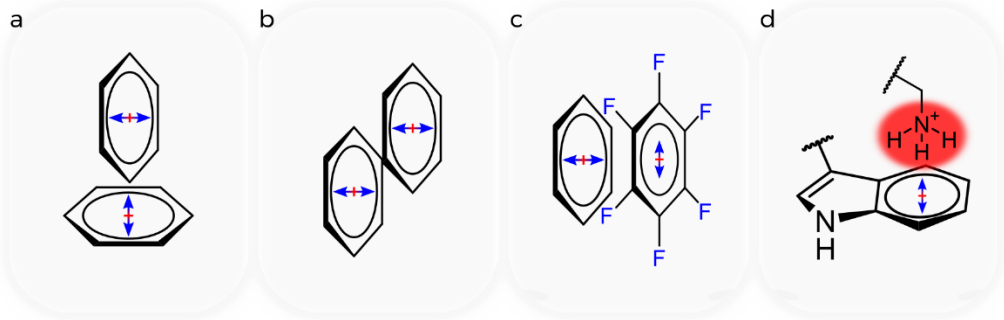

Figure I.3—Several possible π-interactions showing the relevant quadrupoles. a) Perpendicular stacking of benzene molecules. b) Parallel offset stacking of benzene molecules. c) Parallel face-centred stacking of two aromatic systems with opposite quadrupoles. d) π-cation interaction in between the ammonium ion in acetylcholine and a tryptophan residue, observed in the nAChR.

Quadrupolar moment interactions are the basis for the electrostatic interpretation of the simplest interactions involving π- systems such as the one in benzene. The interaction of two benzene molecules is most favourable in two configurations: perpendicular (Figure I.3a) or parallel offset (Figure I.3b). The latter is most often referred to as **π-stacking**. This phenomenon, when cooperative, can severely influence the macroscopic physical properties of a supramolecular assembly such as a gel or polymer[5–7] and affect the behaviour of sensors[8,9].

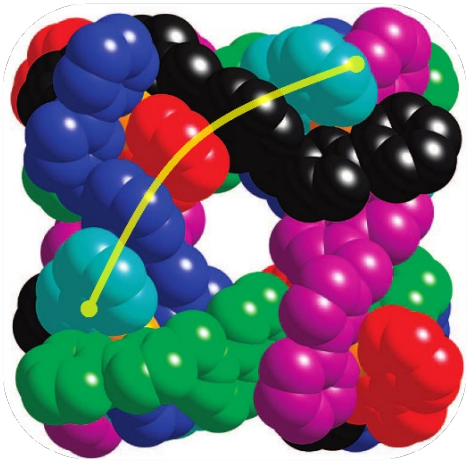

Figure I.4—An octanuclear cobalt coordination cage with charge 16^+. The yellow line is highlighting one of the stacks of "alternating aromatic of naphthyl/pyridyl-pyrazole units". [16] The cage has six of these stacks driving its assembly and conveying interesting luminescence properties. Adapted with permission from *Tidmarsh et al.*[10]. Copyright 2008 American Chemical Society.

Parallel face-centred stacking can be favourable, for example, in between benzene and hexafluorobenzene in which the quadrupolar moment in a π-system is reversed (Figure I.3.c).[11,12]

While the electrostatic quadrupole model works qualitatively to explain most of the phenomena mentioned, it soon fails in predicting interactions between large π-systems such as expanded porphyrins, nanotubes or nanobelts where a great dispersive component might be present. In these systems, the whole potential surface and polarizability must be considered, not simply reduced to a point charge with a quadrupolar electric moment. It also does not explain well substituent effects which can interact directly through space (and not through the aromatic system) with adjacent π-electron clouds.[4,13]

I.3.3 Ion-π

Ion-π interactions are easy to understand from the electrostatic point of view presented earlier. **Cation-π** interactions can easily be seen in water where, due to lack of solvation of the aromatic system, the energy of the interaction can more than double that of salt bridges. These interactions are biologically relevant for ion channels and receptors such as the nicotinic acetylcholine receptor (nAChR) in which acetylcholine interacts with a tryptophan residue.[14] **Anion-π interactions** also exist when the electron density is reversed and sometimes have analytical and biomedical applications since many enzyme cofactors and substrates are anionic.[11,15,16]

I.3.4 Donating and accepting pies

Another type of interaction between π-systems that is also not explained from a simple electrostatic model are **donor-acceptor** (**DA**) **interactions**. These happen between electron rich and electron poor aromatic systems acting as donor and acceptor respectively. This interaction results from a partial charge transfer from donor's HOMO to the acceptor LUMO. To minimize its energy, a DA complex maximizes the overlap between orbitals unlike simple approximation of zone of opposite polarity.

DA interactions can be quite strong where there is a significant contribution from charge transfer. By alternating electron-rich and electron-poor rings (hetero-stacking), strongly bound stacks can self-assemble. Typical binding Gibbs free energies in D-A-D stacked pairs are in the order of 10 $kJmol^{-1}$. The structure in Figure I.4 has 24 of those stacks cooperating which, overall, constitute a great driving force for its assembly (which is needed to overcome the high charge concentration).[10,17]

I.3.5 Bonds, H–bonds

Water is composed of atoms with hard electron clouds: hydrogen has the smallest possible electron cloud of any element and oxygen is too electronegative to enable extensive polarization. Having this in mind, water should be a poorer solvent than many organic ones. Even worse when comparing to a chlorinated solvent with its soft polarizable electron cloud around the chlorine atoms. The reason water can be such a great solvent is due to its ability to be both a good donor and acceptor of hydrogen bonds (**HB**).

Hydrogen bonds are quite varied in nature to the point of causing controversy.[18] It was initially thought to be a purely electrostatic interaction between a hydrogen bonded covalently to an electronegative atom (electron deficient region, **X**) and another atom with lone pairs (electron rich region, **Y**)—**X-H···Y**. The archetypal example being that of water (X=Y= O) with $-\Delta H$ on the order of 10 $kJmol^{-1}$ in liquid.[19] **Ionic hydrogen bonds** are present, for example, in salt bridges.[20] Not long after the concept was born, less conventional HB with a more dispersive character were being observed even involving π-electrons—e.g. **X-H···π** and **M-H···N**.[21] Observations proved that these bonds had at least some covalent character, show directionality and even charge and polarization transfer.[21]

Figure I.5 illustrates with approximate geometry a bit of the diversity of structures involving HB; knowledge of their geometry enables the engineering of supramolecular assemblies and crystals.

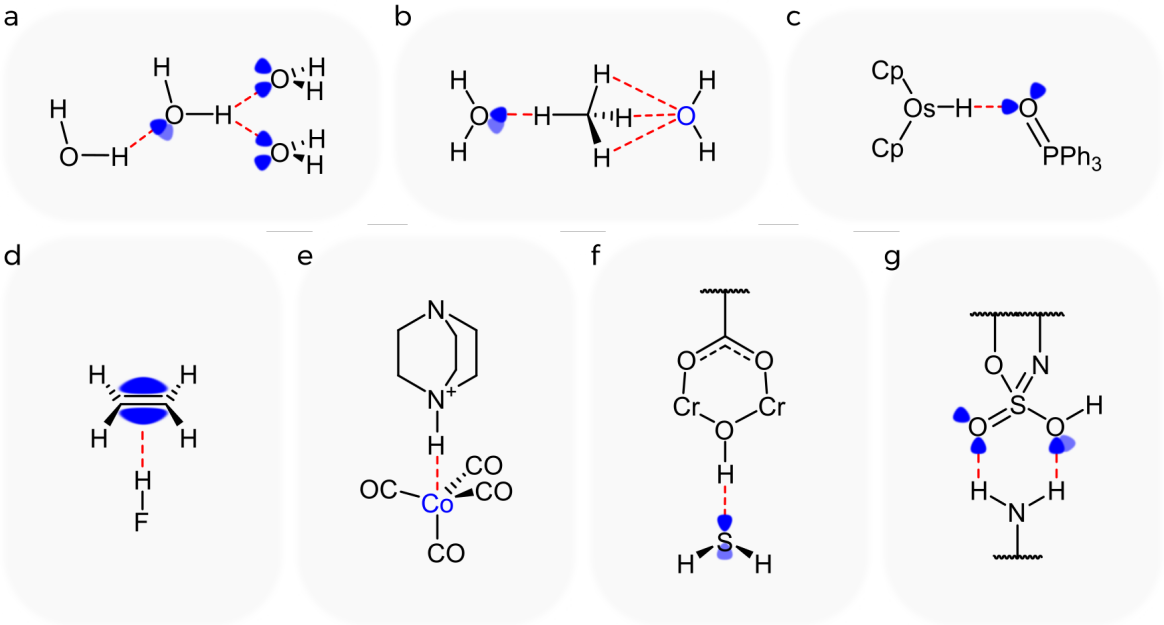

Figure I.5—Several examples of HB structures. a) Two possible HB in H_2O, linear conformation is preferred but bifurcated HB are possible.[19] b) Possible weak HB of H_2O and methane ($\Delta H \approx -2$ kJmol^{-1} and -0.3 kJmol^{-1} respectively).[22] c) HB bond in an osmium organometallic complex.[23] d) Strong HB between HF and ethylene, perpendicular to the π-bond nodal plane.[24] e) HB of X-H···M type in an fluxional organometallic compound.[23] f) Part of a MOF structure capable of adsorbing H_2S with a weak HB to a sulphur atom.[25] g) Part of a cyclamate-urea adsorbate showing HB cooperativity.[26]

Nowadays, it is recognized that H-bonds arise from varying contributions, often difficult to discern and characterize: polarization, dispersion, electrostatic, multipolar interactions etc.[27] Reflecting the hazy nature of H-bonds and accentuating the requisite for evidence, the latest **IUPAC** recommendation states the following:

> "The hydrogen bond is an attractive interaction between a hydrogen atom from a molecule or a molecular fragment X–H in which X is more electronegative than H, and an atom or a group of atoms in the same or a different molecule, in which there is evidence of bond formation."[28]

I.3.6 The force of entropy

In the supramolecular field and whenever dealing with many particle systems, entropy is a key factor in the planning of their dynamics. In elementary synthetic or analytical chemistry, there is not a habit of considering entropic effects as a determining factor to enable/inhibit the desired result. In this section, I briefly discuss some entropic effects to be taken into account when planning/observing supramolecular systems.

I.3.6.a Hydrophobic effects

The adage '*similia similibus solvuntur*' comes from the empirical observation that polar and non-polar substances are only soluble between themselves. However, in section I.3.1, we see that water can interact with non-polar molecules mainly through dispersive interactions. Their interaction is thermodynamically favourable, so why does it appear that those substances actively repel? This emergent behaviour is often called hydrophobic 'force' or hydrophobic 'interaction'. Even though it might be convenient to refer to hydrophobic effects in those terms when talking about the bulk effect, it perpetuates the misconception about their origin.

A factor contributing to the hydrophobic 'interaction' is simply the greater polarizability of hydrocarbon moieties versus that of water. This makes the enthalpic balance of *Van der Waals* interactions favour interactions between hydrocarbons themselves more than between hydrocarbons and water. But one has to have in mind that the interactions in between water molecules are not much stronger, with all of these being on the order of 10 kJ/mol.[29] Hence, solvation can be enthalpically favoured. So, if most hydrophobic molecules do not have water 'phobia', why is there a 'hydrophobic force'?

The **classical hydrophobic effect** case is that of a convex molecule that interacts poorly with water, surrounded by H_2O molecules (Figure I.6), causing a disruption in the network of H-bonds. This discontinuity serves, effectively as a boundary layer not too dissimilar from that at the surface of water in a glass. The anisotropy of forces acting on the molecules restricts their movement; Locally, it forces the solvent into a state with less degrees of freedom. Therefore, aggregation of hydrophobic species is **entropy driven** since ordered water is "released" into the bulk.[30–33] Beware that, although this behaviour

might be clathrate-like, no rigid cage forms, there is evidence that the key factor in entropy reduction is the reduction in mobility, H-bond over-coordination and defects.[34,35]

On the other hand, when the hydrophobic surface is highly concave or fully encapsulates water molecules, there is a **non-classical hydrophobic effect**. Water molecules, whilst in the cavity, have great freedom of rotation and dangling H-bonds. When association of a hydrophobic moiety to the cavity occurs, the displaced water molecules meet with the bulk water and can bond to other ones. Therefore, in this case, the change in free energy upon aggregation is **enthalpy driven** due to the new H-bonds.[36]

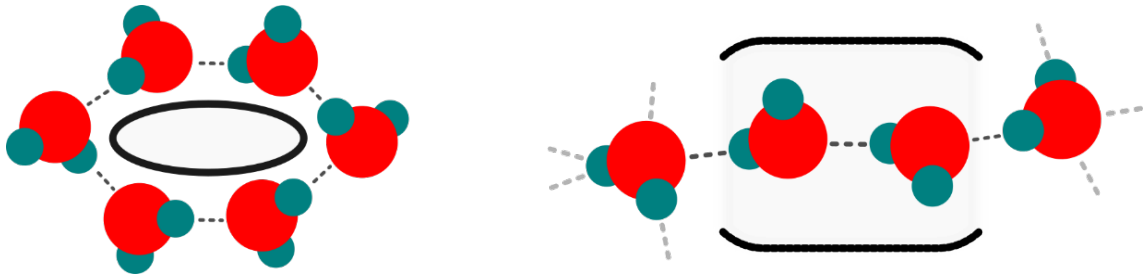

Figure I.6—Left: an illustration of the classical hydrophobic solvation; a convex surface is surrounded by water molecules reducing their mobility. Right: an illustration of a non-classical case of hydrophobic solvation; surrounding water molecules, a concave surface increases their mobility but prevents them forming as many HB as they would in the bulk.

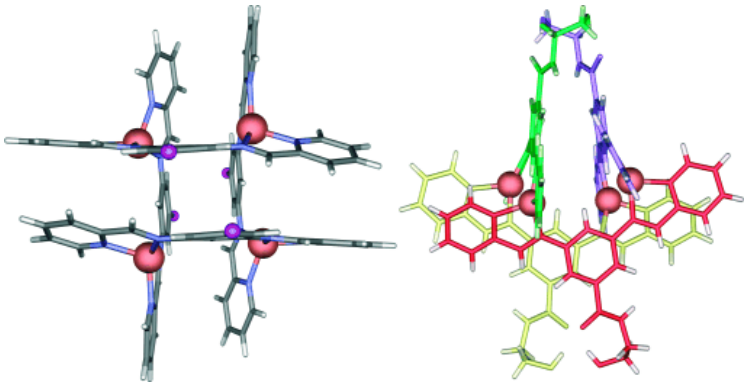

Figure I.7—X-ray crystal structure of a Cu(I) grid whose self-assembly is drive by hydrophobic effects. In all solvents tried, this structure is not obtained except in water. Adapted from 37—Copyright © 2004 WILEY-VCH Verlag GmbH & Co. KGaA, Weinheim.

The phenomena of **hydrophobic solvation** or any **solvophobic effects** remind us of one concept particularly relevant in supramolecular chemistry: the structure of the solvent. Harnessing the power of solvophobic effects allows the assembly of unexpected architectures such as the one in Figure I.7, designing better reaction conditions,[38] and is essential to the stability of macromolecules such as proteins.[39]

I.4 Molecular organization

Control of the relative position of molecules is key throughout Chemistry. Still, in Synthesis, one does not worry much about that in an equilibrium state. Most reactions are controlled kinetically, and it is the transient orientation of molecules at their encounter that matters. Controlling and understanding the entropy changes upon binding of molecules in receptors allows for more intelligent non-covalent (supramolecular) and even covalent synthesis.

Whenever a chemical reaction or a binding event depends on multiple components floating around in the reaction medium, an encounter in the proper fashion to react is always left to chance; the more components needed, the less likely their encounter. From a macroscopic point of view, there must be an ordering of the reagents to increase the efficacy of the encounter: there is a reduced in the number of favourable microstates.

Pre-organization of reagents is a strategy that orders the reactant moieties in space to make their reaction more likely. At a molecular level, pre-organization is done by restricting mobility in some way to reduce the number of possible microstates prior to reaction. This effectively makes the entropic balance of a multicomponent reaction less negative. Decreasing solvation of reagents is also a key factor.[40]

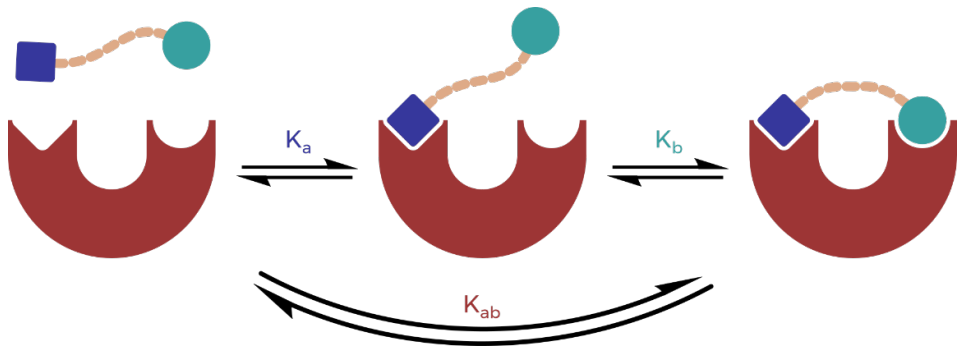

Figure I.8—Illustration of a two-site receptor sequentially binding a bivalent ligand with a flexible bridge.

To better understand the effect that preorganization has in multicomponent events, more specifically host-guest chemistry, the simplest system one can interpret is that illustrated in Figure I.8: a rigid receptor with two binding sites binding a ligand with two complimentary guest moieties linked by a flexible bridge.

With this picture in mind, it easy to see that a first binding event 'pre-organizes' the unbound ligation site lowering the entropic cost of the second binding event. It is as if the ligand had a higher effective concentration. Considering each binding event separately (**a** and **b**) we can think of two independent equilibrium constants, $K_{a'}$ and $K_{b'}$, with a global association constant K_{ab}. The **effective molarity** (***EM***) is a factor serving as some measure of the **binding cooperativity** as is defined in equation I.1.

$$K_{ab} = \boldsymbol{EM} \times K_{a'} \times K_{b'} \quad \textbf{(I.1)}$$

EM can also be defined in kinetic terms as the ratio between intramolecular and intermolecular reaction constants. It is also evident that (having the ideal geometry) the more rigid the bridge, the more the second ligation site is forced into the binding site even if there is not a strong affinity—the entropic penalty is very low. Consequently, the second event is promoted to a higher degree—it is said that the complex **self-assembles**.[41] In this case, there's very little of any intermediate with only one site bound. As a result, these systems show a sigmoidal binding curve (fully bound complex *vs* ligand concentration) upon titration, going from mostly totally unbound to fully bound faster than a non-cooperative system.[42]

The specific case presented in Figure I.8 is an example of **intramolecular cooperativity**, also called **chelate effect (**more often in metal complexes**)** or **configurational cooperativity**. It is the type of cooperativity that drives folding of proteins into complex 3D structures.[43,44]

Other effects are also variations on the theme of pre-organization and mobility restriction, namely the **macrocyclic effect** and the **cryptate*** **effect**. These effects produce a higher stabilization of a complex with a macrocycle as a ligand, when compared to that of noncyclic (open) analogues (Figure I.9).[45,46] Yet, stabilization effects can be difficult to quantify as a good standard is difficult to find; observations might be overwhelmed by other effects (e.g. different bulkiness, solvation, polarity) which are difficult to account for.[47–49]

* Cryptands are polydentate polycyclic ligands that coordinate a multitude of cations and surround them inhibiting their unbinding, in some cases, mechanically.

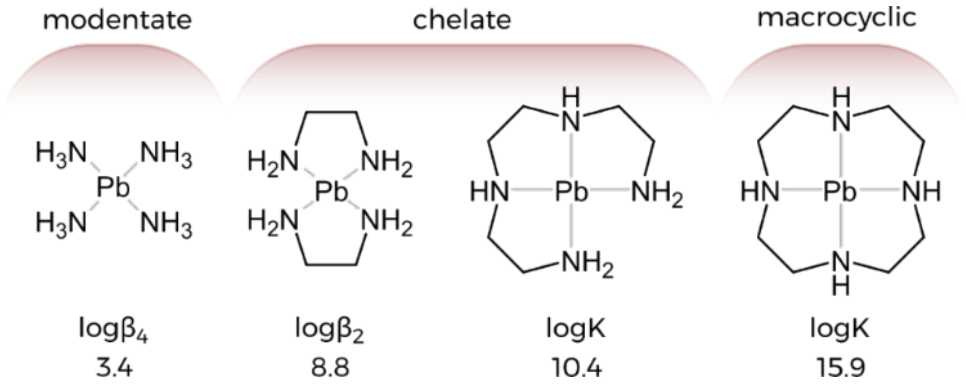

Figure I.9—Series of different amine Pb(II) complexes and their estimated formation constants showing their increasing stability as intramolecular cooperativity increases.[46] It is not possible to compare this sequence with a bicyclic cryptand complex since the structures differ too much.[50]

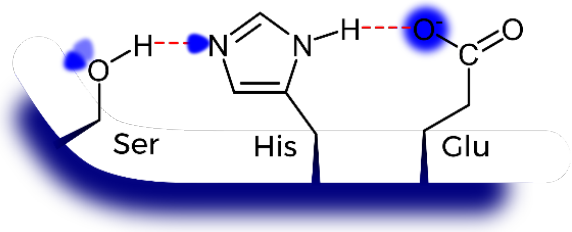

Figure I.10—Scheme of the catalytic triad in the active site of acetylcholine esterase. The Ser residue acts as nucleophile, His residue as a base, and a Glu residue as acid. HB aid in proton transfer which eases the nucleophilic attack of Ser.[51]

Supramolecular catalysis uses pre-organization to drive reactions faster or increase selectivity. Enzymes are a blatant example of supramolecular catalysts; one ubiquitous motif in hydrolases is illustrated in Figure I.10.[52]

Template directed synthesis can be regarded as a special use of pre-organization in supramolecular synthesis (Figure I.11 shows two examples). If the reactions conditions allow **annealing***, a **thermodynamic template** can help achieve synthesis species otherwise unstable.[37] **Kinetic templates**, on the other hand, act by stabilizing intermediate species in a reaction. [53]

There are also examples of "**negative templating**", which inhibit the formation of a specific product. The effect is usually attained through the stabilization of an inactive species or one that leads do different products.[54]

* Annealing is the setup of a systems conditions so that a globally minimum energy state is reached; much like the slow cooling of glass upon solidifying to even out any mechanical strain.

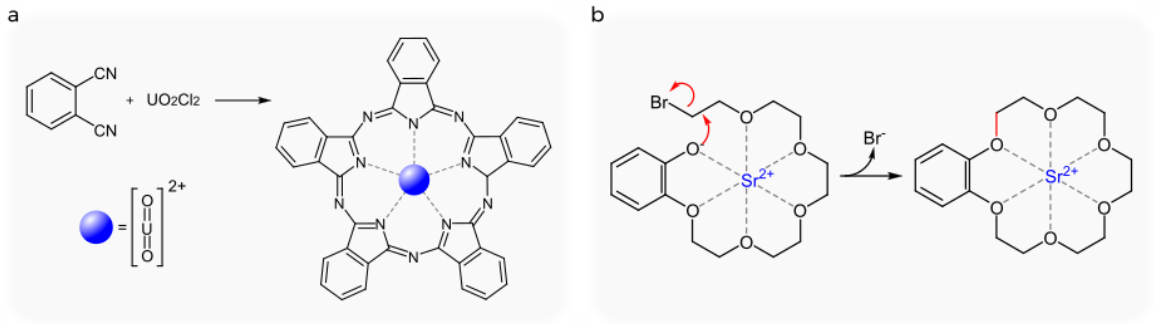

Figure I.11—Reactions with template examples. a) Synthesis of a superphthalocyanin with uranyl ion as thermodynamic template.[55] b) Formation of 18-crown-6 with strontium ion as kinetic template.[56]

I.5 Promiscuous bonds

The concepts introduced in previous sections focus mainly in fleeting non-covalent interactions. These provide supramolecular assemblies with **physical dynamics**. But, there is interest in making rigid enduring molecular subcomponents *in situ*. However, supramolecular chemistry demands versatility in bond formation. So, to not perturb the rest of the structure and enable thermodynamic control, *in situ* assemblies need mild enough conditions for bond formation and reversibility, providing **chemical dynamics**. Because of this, coordination to metals and **dynamic covalent bonds** are a very important tool in supramolecular architectures to build dynamic blocks for supramolecular assemblies. Together, chemical and physical dynamics provide a molecule with **constitutional dynamics** and allow a system to anneal.[57]

I.5.1 Metal centres

The defined coordination geometry, dynamicity and simple fabrication of metal centres make them valuable for **Constitutional Dynamic Chemistry** (**CDC**). Metal centres have two convenient properties: they present a large range both in terms of lability and of local symmetries.

Any polytope is totally defined by the number of vertices and their connection geometry and by the number of edges and their lengths. In chemical structures these are translated into parameters such as: **coordination numbers**, **coordination vectors and planes**, **vertex distance**, **twist angles**, and **approach angles** (see Figure I.12). Through these, directed

changes can be done to metal-organic networks, but control is limited; dynamic systems can become very complex with different networks forming in the same conditions as ligand's conformational space comes into play.

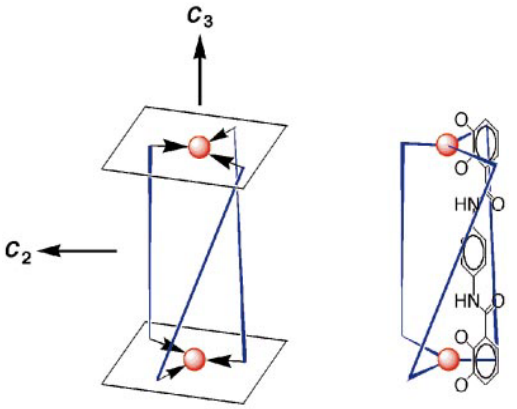

Figure I.12—On the left: the arrows show the coordination vectors inside the coordination planes and the axes of symmetry on an M_2L_3 complex. On the right: example of such a structure—three catecholate ditopic ligands coordinated to two Fe(II) metal centres. Reproduced from 58 with permission of The Royal Society of Chemistry.

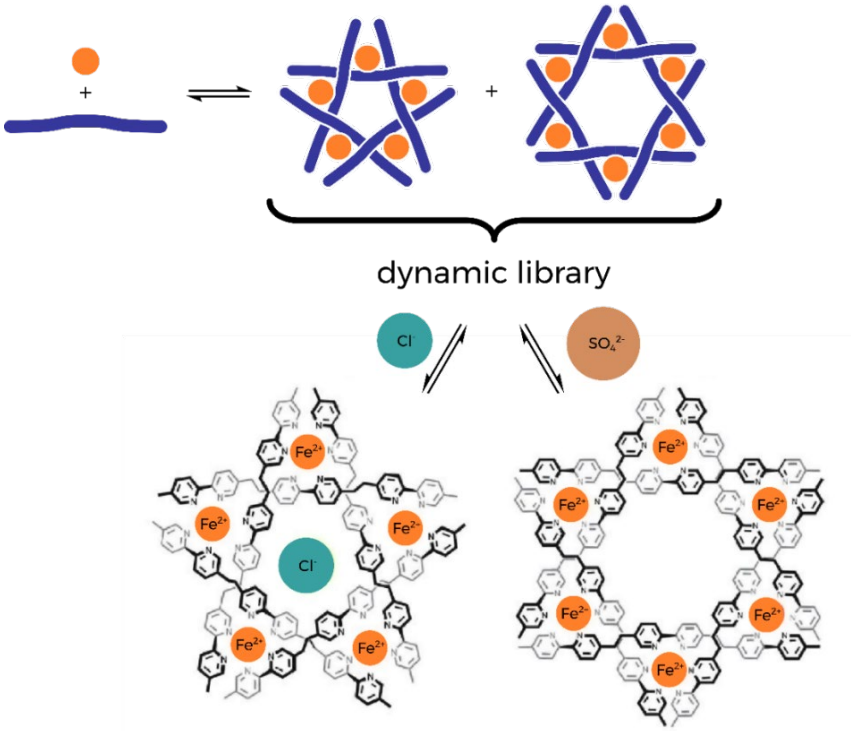

Figure I.13—Scheme of the self-assembly of circular helicates. The pentanuclear helicate forms if Cl^- is present, otherwise the hexanuclear helicate forms. The Cl^- ion templates its formation. Bigger ions (such as sulfate) will not select this—they will not fit inside the cavity and not stabilize the pentanuclear complex. In the presence of bromide (intermediate radius) both species are observed. In part from reference 59 with permission of The Royal Society of Chemistry.

Figure I.13 illustrates an example of the added complexity brought about by the use of coordination centres in assemblies from the work of *Hasenknopf* et al.[59] The ligand is hexadentate, but tritopic, with the coordination vectors preferring an approximate anti-parallel position between them. Due to the lability of the coordination and the slight

flexibility of the ligand, a **virtual combinatorial library** of the different possible oligomers is obtained. It is 'virtual' since only some of the constituents are expressed depending on conditions—a **selection** is said to occur upon self-assembly.

Changing the metal ion can effectively change the **vertex distance** of an assembly. This has an impact in pore and cavity sizes, affecting host guest chemistry and stability. *Nitschke* and co-workers compared the host-guest chemistry of an $[M_4L_6]^{4-}$ tetrahedral cage with different metals: Fe(II), Ni(II) and Co(II).[60] The cages had significantly different host guest chemistry. For example, the Fe(II) based cage could not encapsulate cycloheptane contrary to both the Co(II) and Ni(II).

Lability is another controllable parameter relevant mainly to the kinetics of an assembly's reactions. The more labile a complex is, the faster ligand exchange will be. Aqua metal complexes from different elements shows water exchange rate constants spanning 20 orders of magnitude. On this matter, some trends are worth pointing out: higher charges, smaller ionic radii and greater ionic bond character (generally higher in the periodic table) contribute to more labile complexes. Even so, one should be wary of exceptions, of which as *Jahn-Teller* complexes[61] (more labile than expected) are just one example.

These lability trends have consequences in the use of different metals in complexes and it is easiest to see them in biologic systems: alkali metals and calcium are so labile they're used mostly for recognition/signalling; less labile, magnesium has some structural and fast catalytic function; metals with moderate lability and with capacity for electron transfer (e.g. Fe, Co, Ni) are useful for catalytic purposes (redox mainly); metals such as Pd, Rh and Pt, in addition to their scarce bioavailability are too inert to find catalytic use under biocompatible conditions.[61] Nonetheless, platinum group metals are very useful in forming stable assemblies where kinetic inertness is an advantage.

Due to the diverse coordination geometry, metal centres impart rich stereochemistry to assemblies. Even considering only facial isomers there is already the possibility of two stereoisomers: Δ and Λ. Figure I.14 illustrates how a simple M_4L_6 system with only two types of subcomponents can generate a dynamic combinatorial library.

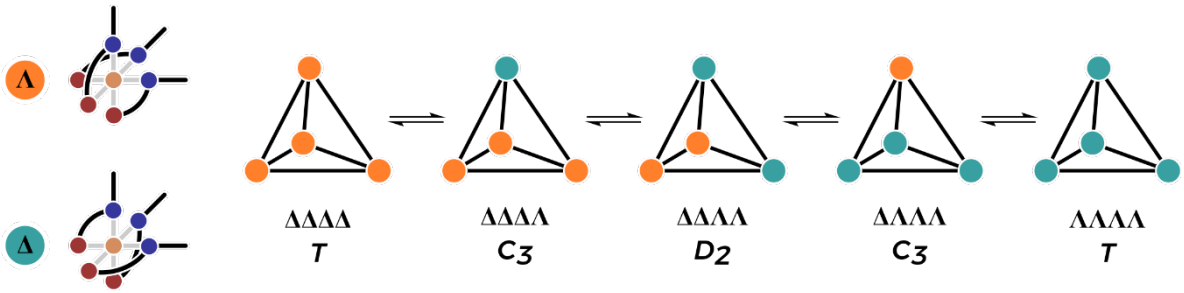

Figure I.14—*Fac* ML_3 complexes and their Δ and Λ isomers. The five possible isomers of tetrahedral cages with *fac* corners (and their overall symmetry point groups). Note that the first and last, as the second and fourth form enantiomeric pairs.

Metal centres, due to their rich electrochemistry, can also contribute to interesting electronic properties of coordination networks (e.g. guest dependent redox activity and magnetism).[62]

I.5.2 Dynamic covalent linkages

Throughout supramolecular developments we see the importance of bond reversibility. What if one wants to covalently link various subcomponents *in situ* without resorting to metal centres? What if one wants to be able to activate the bonds reversibility at will? **Dynamic covalent linkages** (**DCL**) help solve these issues.

There are several reactions that form covalent bonds and are reversible in the right conditions. Figure I.15 shows some examples of reactions forming DCLs. Note that, where exchange reactions are shown, the respective synthesis reactions are just as useful. Exchange reactions just add to the complexity of system where exchange can occur with already assembled entities. The most useful reactions are asymmetrical, that is: the moieties from which the linkage originate are not the same. Asymmetrical reactions originate less complex product libraries since exchange can only occur in one way. Because of that, symmetrical reactions like disulphide exchange demand a bit more control to be useful (e.g. use of symmetrical reagents.)

The relatively mild conditions for most DCLs allow for control of the kinetic activity of the products. Without destroying the system, the reaction can be regulated by a signal which generates a response, thus being useful for chemical transduction. Vesicles responsive to pH are an example[63]. Dynamic covalent reactions can also be orthogonal (i.e. chemically independent), enabling them to be used simultaneously in the same system.

For example, **boronate ester exchange** can happen in the same conditions as **disulphide exchange** allowing quite complex libraries to be built with multifunctional subcomponents.[64]

A remarkable example of orthogonality of DCLs is that reported by *Bonifazi et al* that makes use of disulphide, boronate, and acyl hydrazone formation to link dyes onto a peptide scaffold with programmable spatial positioning.[65]

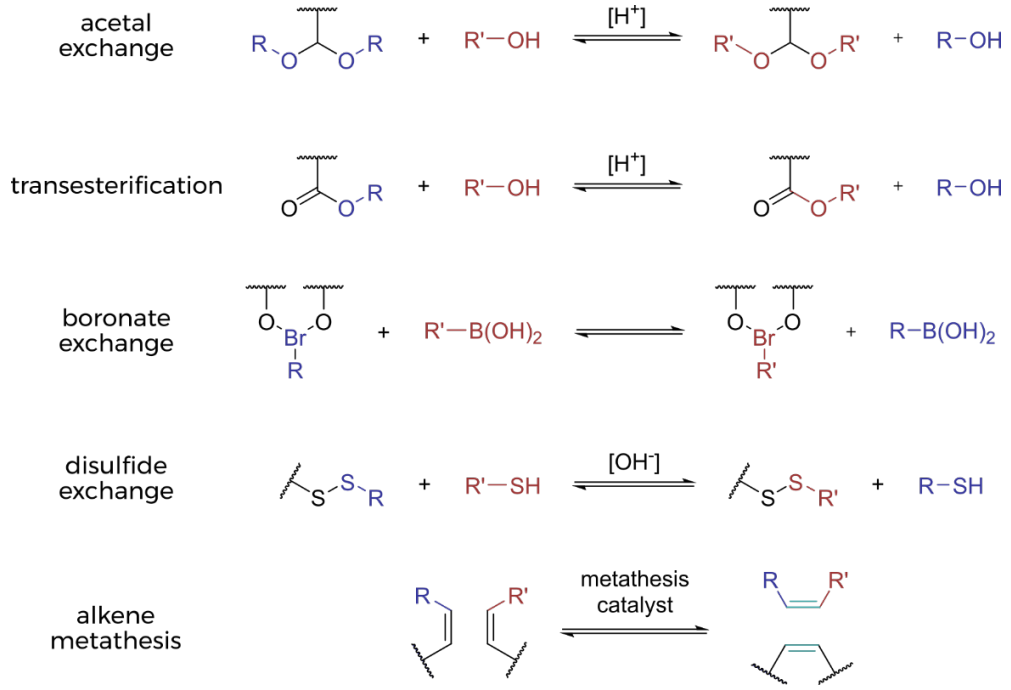

Figure I.15—Some examples of reactions useful in dynamic covalent chemistry.

Olefin metathesis is a quite outstanding case of formation of a DCL. The C-C bonds involved are among the least sensitive is this family of reactions, making the reactants kinetically inert in the absence of a metathesis catalyst such as *Grubbs catalyst*. This results in very stable assemblies (e.g. polymers) once the catalyst is inactivated. Alkyne metathesis is a similar reaction providing more rigid bonds.[66]

One of the most used reactions for the formation of DCLs is **imine synthesis**. Its use is particularly prominent when dealing with metal-organic assemblies as the imine moiety coordinates easily to most metal centres—bringing together dative and covalent dynamics.[67] Figure I.16 shows the mechanism of imine synthesis from condensation of an aldehyde and an amine. Note that the reaction can be catalysed by acids including metals that coordinate to the aldehyde.

Imine exchange (transimination) and **imine metathesis** are also used. All these reactions are reversible; some kind of driving force is needed to shift the equilibrium (e.g. dative bond formation, different amine acidity, cooperativity). This is especially relevant in aqueous solution where, given a 1:1 mixture of aldehyde and amine, imines are often the minor species.[68,69] Yet, stable imine-based architectures can form in water (see example in section I.7.1).

Another noteworthy characteristic of imine based dynamic assemblies is that they can be turned kinetically inert or "fixed" by reduction to amines. Due to change in bonding nature, the scaffold turns more flexible and can be more soluble.[70] Similarly to imines, hydrazones and oxymes also find their role as DCL and tend to be more stable due to increased conjugation.[66,71,72]

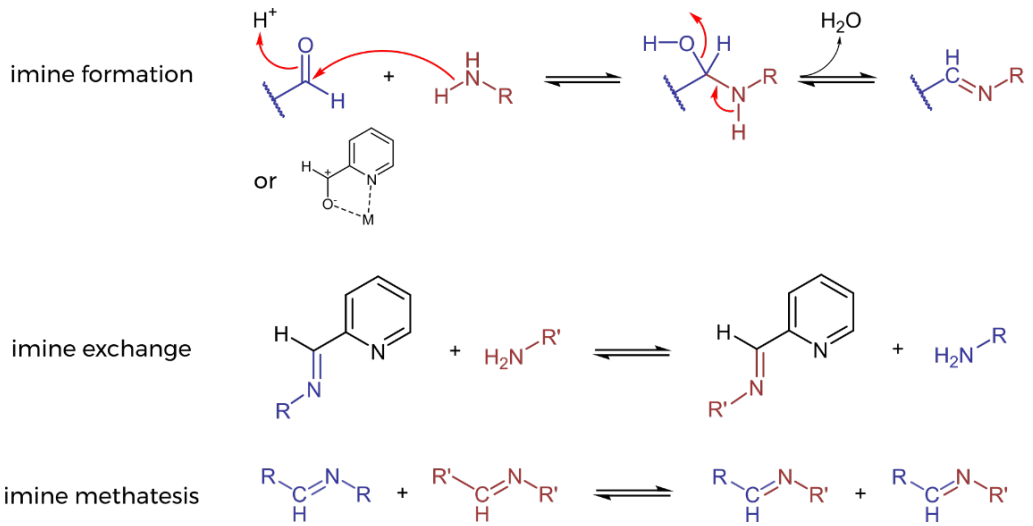

Figure I.16—Simplified mechanism of imine formation in water from an aldehyde and amine, reaction schemes of an imine exchange and metathesis.

I.6 Bonds, mechanical bonds

Chemists always ambitioned for more complex molecules both geometrically and topologically. Mechanically interlocked molecules were especially interesting due to the purely physical nature of their interaction. Nevertheless, the **mechanical bond** was the latest major "type of bond" to become a tool in chemist's toolbox. The difficult in synthesis of architectures with complex topology is due to the required restriction of movement. It was not until specific strategies were developed to overcome this entropic barrier that research in molecular topology became common.

In the 1960s, *Frisch* and *Wasserman* performed synthesis of interlocked molecules, but the reactions were statistical and the yields very low.[73] Breakthroughs in the field were made by *Jean-Pierre Sauvage* and *Fraser Stoddart*. *Sauvage* used metal ions as templates to make catenane (a method illustrated in Figure I.17).[74] In 1995 the same research group reported the synthesis of a [2]rotaxane using the same core complex.[75]

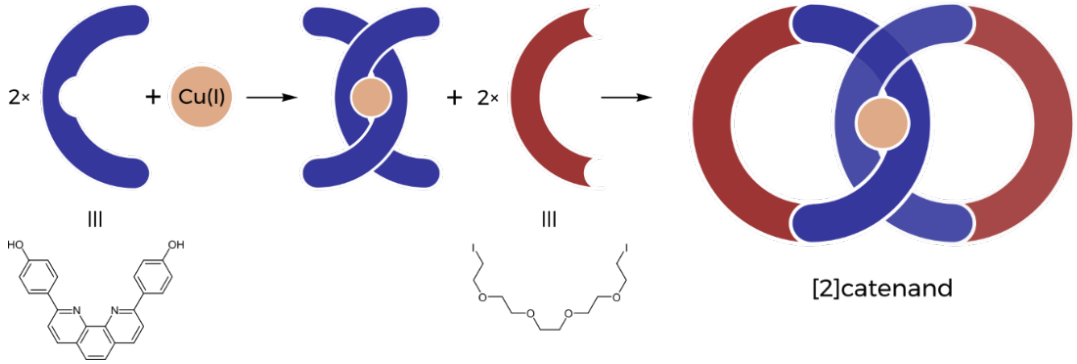

Figure I.17—Illustration of the cuprocatenand synthesis developed by *Sauvage*'s group in 1984. A complex of a phenanthroline Cu(I) complex that is then closed by Williamson ether synthesis. After demetallation a [2]catenane is produced.[74]

In using metal ions as templates (see example in Figure I.17), *Sauvage* observed that the dissociation of the complexes was much slower in the catenanes that in open analogues. This **catenand effect** is attributed to the lower conformational space of the molecule when mechanically restrained.[74,76] This relates to the concept of **confinement** in supramolecular chemistry (see section I.7 for examples of its application).

Stoddart and co-workers designed several syntheses of rotaxanes* using non-covalent templates. With careful engineering of interactions between axle and rings, they achieved good yields often with simple and mild conditions.[77]

During the 1980s and 1990s, the two scientists mentioned previously developed techniques to improve yields and get new mechanically functional architectures. This development was rewarded, in 2016, with the attribution of the Nobel Chemistry Prize to *Sauvage*, *Stoddart* and *Bernard Feringa* 'for the design and synthesis of molecular machines'.[78–80]

* Rotaxanes are equivalent in confinement to catenanes in that they both consist of a molecule threaded through another molecule's cavity. The difference being that the threaded part in rotaxanes in open and stoppered to prevent unthreading.

The stabilizing effect of confinement in rotaxanes lead to their use in protecting unstable chemical moieties without having to alter their chemical constitution. One remarkable example is the stabilization of the highly sensitive squaraine dyes (in the axle) when surrounded by the rotaxane ring. This allows their use for cell imaging.[81,82]

The template approach to mechanical links is very powerful, having already permitted the synthesis of quite convoluted molecular linkages and knots; **Borromean rings, trefoil knots** and **suitanes** are some examples.[83]

I.7 Thinking inside the box

In this section I will present various reported host-guest systems that present interesting behaviour that would not be expected in more conventional 'molecular chemistry'. Often, the unexpected strange properties of these host-guest systems are related to the concepts of confinement and compartmentalization.

Confinement effects are observable whenever limitation of space around a molecule causes a change in behaviour from what would happen in a free environment. A simple effect that results from it is the non-classical hydrophobic effect discussed before (section I.3.6.a). The increased stability of the squaraine dyes in rotaxane is also a confinement effect; the tight space around the squaraine moiety protects it from nucleophilic attack, prevents dissociation (reducing photobleaching), increases rigidity and reduces quenching by water, improving quantum yields. Enzyme catalysis also uses confinement to preorder the substrates and drive reactions.

Compartmentalization is the most natural strategy to make incompatible systems work together. Essentially, a Chemist does this every time they do a multi-pot reaction. It is often simpler to separate incompatible reaction steps than adapt the reagents to make them compatible (and this is not always possible).

In nature, compartments separate every system that operates in different conditions; compartment walls maintain the necessary gradients. Indeed, compartmentalization is necessary for the very definition of a living being's body.

It was only recently that Chemists started to harness the power of compartmentalization. Early uses of this strategy were based on organic/aqueous systems and were very passive like micro-emulsions for polymerization.[84] With the progress of supramolecular synthesis, structures that allowed compartmentalization at a molecular level started to be developed: partially or fully enclosed capsules, dynamic capsules, programmable openings.[85] This control over separation of chemicals *in situ* permits orthogonality between reactions as well as signalling and regulation.

I.7.1 Boxing rings

In 2008, *Mal et al* reported the synthesis of the salt of a tetrahedral cage "by aqueous subcomponent self-assembly" with the motif M_4L_6;[86] Figure I.18 shows a scheme of it.

Observe that a base (tetramethylammonium hydroxide) is needed to deprotonate the ammonium termini. Only then can the free amino groups react with the 2-pyridinecarboxaldehyde templated by the Fe^{2+} ions. Cage **1** forms with a 4^- charge due to the sulfonate substituents in the ligand's bridge, this allows it to be soluble in water. The authors managed to obtain single crystals of the structure by precipitating the compound from an aqueous solution through acetone vapour diffusion. The XRD characterization of the structure revealed the Me_4N^+ acting as counterion to the cage and one acetone molecule inside the cage's void (with partial occupancy).

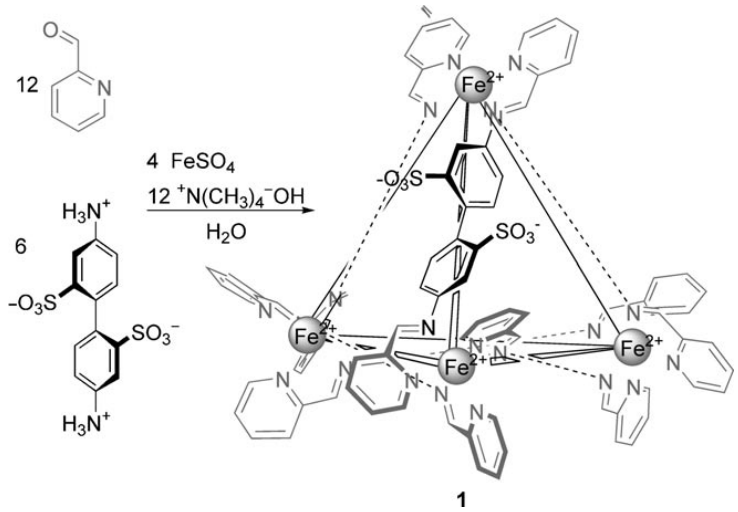

Figure I.18—Scheme of the synthesis reported by *Mal et al* with the structure of the final tetrahedral structure **1** (only one ligand is explicitly shown for clarity). Reproduced from reference 86—Copyright © 2008 WILEY-VCH Verlag GmbH & Co. KGaA, Weinheim.

Since no chiral information is communicated to the system, the cages form a racemate with all the metal centres in either Δ or Λ configuration. Owing to the tetrahedral symmetry of cage **1**, the NMR spectra are very simple, with only one set of signals. This makes NMR very easy to interpret and ideal to study inclusion of compounds inside the cage.

The relative rigidity and bulkiness of the ligands prevents the sulfonate groups from turning into the cage's cavity. Hence, the cavity is mainly hydrophobic without much flexibility to adapt to guest molecules. This is proposed to be the cause as to why only neutral, relatively hydrophobic molecules were found to form host-guest complexes with the cage; Even though the cage is polyanionic, no cations were ever found to bind in the cavity. Indeed, the rigidity of the pores is such that kinetic discrimination between cyclopentane and cyclohexane (**CHX**) was demonstrated in solution. In the solid state cyclopentane did not remain inside the cage, contrary to CHX.[87]

DCL are what brings together the subcomponents of **1**. The dynamic character of the structure means that the equilibrium of the system is affected by manipulating the stability of the subcomponents. In the work of *Mal et al*, the controlled release of a CHX was demonstrated with both reverse and irreversible signals (see Figure I.19).

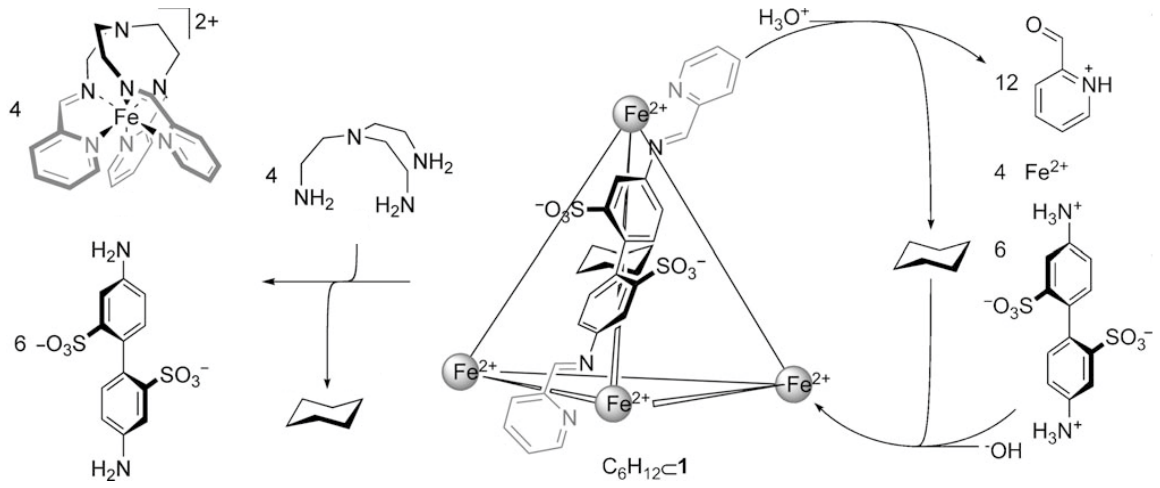

Figure I.19—Scheme showing two kinds of signal used to induce guest release. To the left: addition of a chelating amine irreversibly substitutes the linking bridge forming smaller 'corner' complexes. To the right: addition of acid reversibly inhibits imine formation by protonation of the amine. Adapted from reference 86—Copyright © 2008 WILEY-VCH Verlag GmbH & Co. KGaA, Weinheim.

I.7.2 White phosphorus in a violet cage

Later work, by *Smulders et al*[87], focused on an extensive study of host-guest thermodynamics of $(Me_4N)_4$**1** (by ^1H NMR). This analysed correlation of guest properties with their binding strength; found a negative correlation with dipole moment and a positive correlation with logP, the size of a molecule (below a maximum) didn't seem to govern binding strength. They also found a great influence of molecular shape in intake kinetics, with rigid and flat molecules being the quickest to enter the cavity (e.g. acetone is faster than chloroform although it binds weaklier).

In 2009, *Mal et al* reported the notable discover that **1** binds one molecule of P_4 (white phosphorous) in its cavity.[88] Various aspects to this report are noteworthy: the stability of a highly reactive reducing P_4 molecule inside the cage (even in contact with oxygen), the discovery of a way to solubilize P_4 in water and of releasing it from the cage in a controlled fashion.

The stability of P_4 inside **1** arises through confinement and not compartmentalization since oxygen can pass through the cage's pores. The stabilization is said to be **constrictive**, that is: reaction of the guest would involve bigger intermediates that would force deformation of the cage. Hence, kinetic inhibition is the cause for the great stability (over 4 months) of the $P_4\subset$**1** complex against oxidation. The dynamics of the cage, once again, proves valuable: the P_4 molecule can be displaced by competitive binding with benzene without destroying any part of the system.

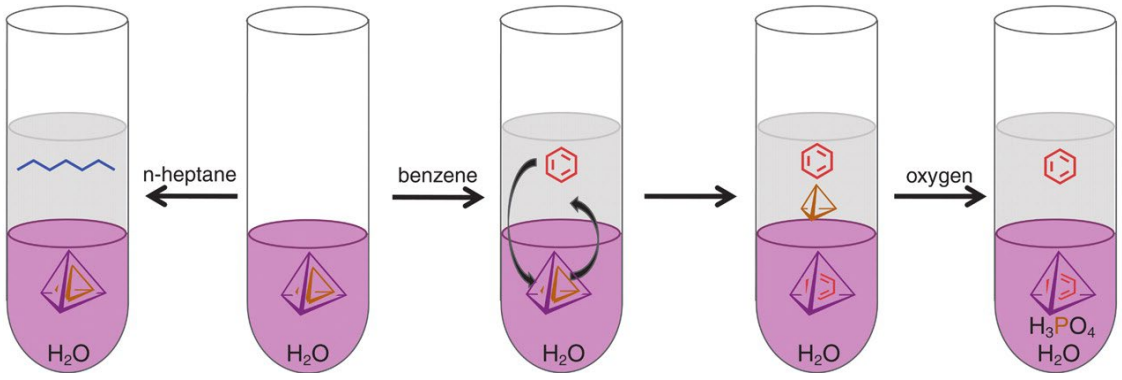

Figure I.20—Experiment reported by *Mal et al* showing that simple extraction of P_4 is not sufficient to remove it from inside the cage; A displacing/competitive guest (such as benzene) is needed. From 87—Reprinted with permission from AAAS.

I.7.3 Closing doors

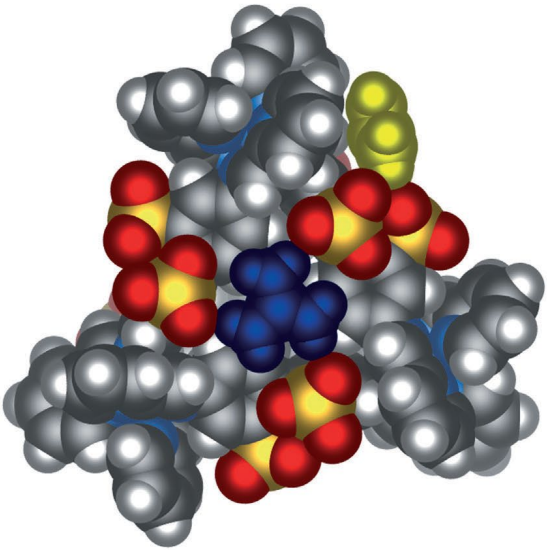

Figure I.21—XRD structure of Gdm$_4$**1** viewed along one of the pseudo C_3 axes of symmetry. In blue and yellow are two Gdm$^+$ ions. Adapted from 88—Copyright © 2012 WILEY-VCH Verlag GmbH & Co. KGaA, Weinheim.

In 2012 the structure of cage **1** was the subject of a report by *Zarra et al* stating the preparation of a guanidinium (**Gdm**$^+$) salt of **1**. Its synthesis is attained, very simply, by the replacement of the base used previously with guanidinium carbonate.[89]

The single crystal XRD structure of Gdm$_4$**1** revealed that the Gdm$^+$ ions could bind to the faces of the capsule through HB to the sulfonate groups. Although, in the solid state, the cations were not observed to cap all the faces, the dynamics of the structure in solution allows for this to happen very fast. This was observed by the fast exchange of signals on the NMR timescale maintaining the number of individual signals. The binding constant was measured at (263 $\pm$ 63) M^{-1} by titration (assuming no cooperativity between binding events on each face, which was proven reasonable).

The binding of the Gdm$^+$ ions to the faces was observed to affect guest intake kinetics. This is expected as the bound ions cover the pores on the faces of the cage; thermodynamic analysis of host-guest intake showed the most likely intake mechanism to be 'through pore'. Therefore, Gdm$^+$ ions can act as a 'labile gate' for guest exchange. Additionally, Gdm$^+$ seems to improve the stability of the cage against oxidation in air when heated.

I.8 Complex kinetics

In this section, the discussion will focus on reports of host-guest systems that exhibit complex behaviour over time while interacting with kinetically controlled 'classic' reactions.

The behaviour of such systems is summarized by the notion of **self-organization**. These systems are, fundamentally, a closer imitation of the kinetic complexity and interconnectivity in biological systems. This is also because of their **dissipative nature**: the behaviour only emerges as long as energy is dissipated. Any non-equilibrium phenomena (e.g. auto-catalysis, oscillating reactions, weather patterns) are dissipative systems said to exhibit dynamic self-organization.[41]

What makes biological systems stand out in from other dissipative systems is their exceptionally complex signalling networks, namely their high dimensionality; the same component can perform a variety of functions while maintaining some independence with other components. Using the terms of a pioneer in networked systems, *Jean-Marie Lehn*: simulating this complex **adaptive chemistry**, is the foundation for programmable, functional, **Informed Matter**.[90] The latter concept he coined to refer to molecular systems that do more than just statistically bump into each other and can perform functions with their emergent behaviour.

I.8.1 Ford's molecular dream

More than a century after Henry Ford's plan for an assembly line,[91] *Salles et al* published a report of a "chemical assembly line" represented schematically in Figure I.22.[92] The reported 'assembly line' consists of three 'stations' (catalytic cycles) transforming reagents and producing compounds to be used in the next cycle. The overall reaction uses furan to produce 5-hydroxy-3-(nitromethyl)dihydrofuran-2(3H)-one.

Firstly, methylene blue is activated by UV light, produces singlet oxygen and oxidizes furan resulting in an endoperoxide. The second catalytic cycle is composed of $(Me_4N)_4$**1** which seems to accelerate the decomposition of the endoperoxide to produce fumaraldehydic acid. The cage also increases the selectivity towards this product as the endoperoxide is unstable and is readily hydrolysed and oxidized to other side products. Finally, the fumaraldehydic acid is alkylated in a third organocatalytic cycle. In this cycle, proline catalyses the addition of nitromethane and the resulting compound cyclizes giving the final product.

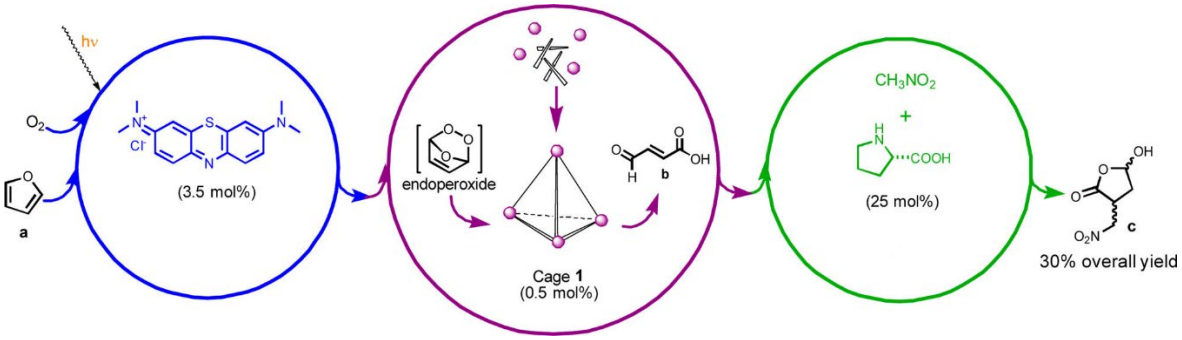

Figure I.22—Scheme of the system reported by *Salles et al*. Showing the three catalytic cycles involved. Adapted with permission from 92—Copyright 2013 American Chemical Society.

The authors tested the reaction in various conditions, selectively removing necessary subcomponents. The mechanism is still very unclear, but none of the subcomponents catalysed the endoperoxide decomposition as effectively as cage **1** itself.

In brief, a system was designed in which different catalytic cycles coexisted in solution with one of those being a dynamic supramolecular assembly whose persistence was essential to the process.

I.8.2 Delayed guest

Smulders and Nitschke, in 2012, published a paper about the use of a host-guest system to regulate a reaction's kinetics.[97] Their system used cage **1** as a 'whole molecule protecting group', with furan binding in its cavity ($K = (8.3\pm0.7) \times 10^3\ M^{-1}$).

Furan reacts with maleimide through a Diels-Alder reaction but only if it is in solution. The cavity of **1** is too small for the reaction to take place inside. The reactants are compartmentalized: separated (to some degree) until a perturbation is introduced. The authors used this property as a means to regulate the reaction kinetics by regulating the binding of furan. Benzene can outcompete furan for binding in **1** ($K = 3.0\pm0.6\times10^3\ M^{-1}$) if a great excess is added. So, this was a possible signal to accelerate the reaction easily identifiable by ^{1}H NMR.

According to the report, with the addition of benzene, the reaction rate could be accelerated by as much as 25 times. The authors did the experiment at 5°C to maximize the effect by slowing the spontaneous release of furan.

The reaction could also be "signalled" to accelerate at a later point in time with the rate improving by the same factor. In this system, 87% of the furan was bound, in a system where this can be improved to close to 100%, the signal (competing guest) would, effectively, be an on-off switch for the reaction.

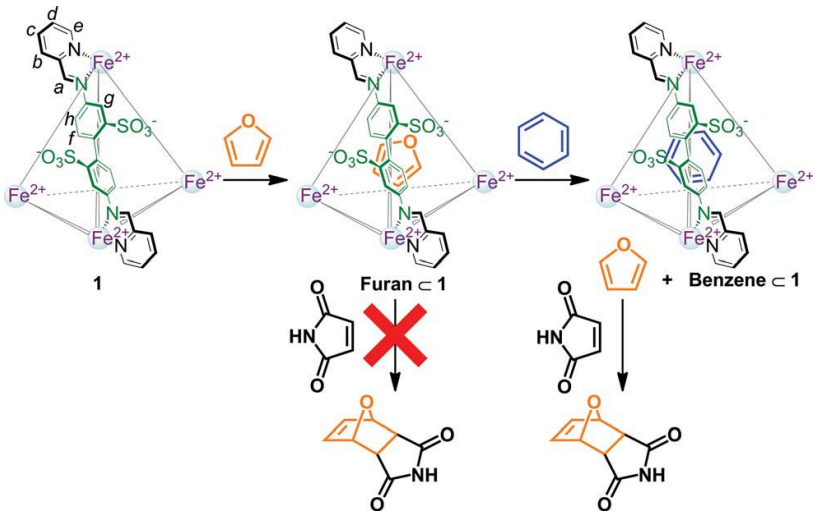

Figure I.23—Scheme of the system demonstrated by *Smulders and Nitschke*. Reproduced from reference 93 with permission of The Royal Society of Chemistry.

I.9 The wonderful oxide of Os

Osmium tetroxide (OsO_4) is a clear, crystalline, volatile solid slightly soluble in water and highly soluble in non-polar solvents. The molecule is tetrahedral with the central Os atom in the form of Os(VIII). The bonding nature is largely covalent and intermolecular interactions are relatively weak in the solid.[94] It is used regularly in the staining of biological samples for microscopy.[95,96]

Osmium has interesting speciation equilibria in aqueous solution. Both VI and VIII oxidation states form various hydroxoosmates; formally salts of osmic acids. However, the composition of these solutions has not been comprehensively studied outside strongly alkaline conditions. Although some species of OsO_4 can be studied directly by UV-Vis spectrophotometry and NMR (only with organic ligands) they have been mostly observed indirectly through partition, reactivity studies or by using chromogenic reagents.[97–102]

In Organic Chemistry, OsO_4 is mainly used as an oxidising agent. Due to its cost, this is often in catalytic amounts with a terminal oxidizer to close the catalytic cycle. The typical

reaction for which this is done is the dihydroxylation of alkenes. The most used terminal oxidizers are H_2O_2 and amine oxides (when the reactants are sensitive to the former).[103,104] Alkaline conditions are known accelerate the reactions due to the formation of the more reactive $[OsO_4(OH)_2]^{2-}$, this is only a major species in strongly alkaline solutions.[97]

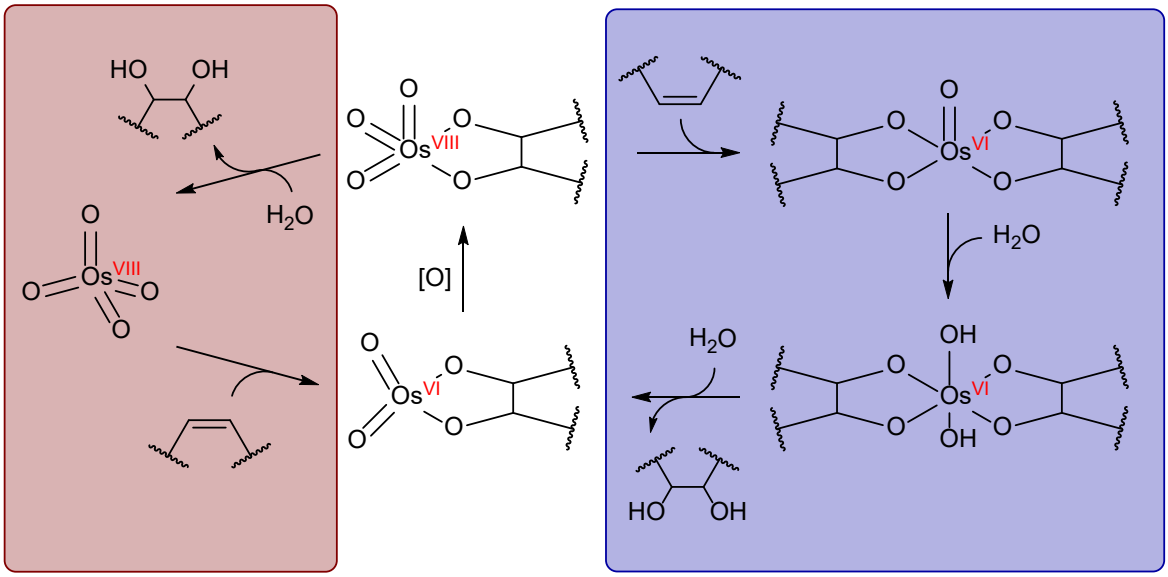

Figure I.24—General scheme of the first (red) and second (blue) catalytic cycles of OsO_4 in the dihydroxylation of alkenes without additional ligands present. Adapted from 105—Copyright © 2002 WILEY-VCH Verlag GmbH & Co. KGaA, Weinheim.

Although there is still some debate as to the precise mechanism of the OsO_4 cycloaddition the overall catalytic cycle is well established.[103,106] As can be seen from Figure I.24, there are two possible catalytic cycles performed by OsO_4 in the simplest conditions: neutral aqueous solution without additional promoters. In the first and shortest cycle there is a simple alternation between cycloaddition of alkene and elimination of glycol. In the first cycle, further hydration and deprotonation of OsO_4 may happen but to a small extent. In the second cycle the active catalyst is the osmium glycolate. This second cycle is responsible for lower enantiomeric selectivity in asymmetric dihydroxylation. During this second cycle, speciation of Os is also more complex. One must be aware that, in alkaline conditions, any of the H_2O molecules involved may be replaced by a OH^- to form the corresponding osmate oxoanions. Moreover, the progress through the second cycle might be halted by 'locking' the Os in the bisglycolate form. This happens in strongly alkaline solutions (pH>12) where the diglycol adduct can deprotonate forming a dianion inert towards hydroxylation.[105,107]

In previous works, it has been observed that the turnover-limiting step tends to be the either the monoglycolate (or bisglycolate) hydrolysis or the reoxidation step. Notwithstanding, in some conditions, specially without a great reoxidant excess, the reoxidation of Os(VI) can be the rate-limiting step or even the cycloaddition step. Furthermore, since the first cycle has a much slower turnover than the second, an auto-acceleration effect can be expected in the right conditions (as glycolate would promote the second cycle).[106,108]

Finally, an additional barrier for the efficient turnover of OsO_4 is the disproportionation of Os(VI) species which is prevented when in anionic form (possibly due to repulsion).[109]

I.10 NMR and Supramolecular systems

Even though MS and microscopy techniques are improving and becoming more powerful, NMR is still the most versatile technique. It is often the easiest to use also; NMR spectra are easy to interpret, and the signals do not need intricate calibration techniques to be made meaningful.[110]

NMR is quite powerful to study dynamics but is limited by the timescale of the experiments and relaxation/exchange dynamics. Although, in some specific cases this aspect might give additional sensitivity. The advantage of NMR in field of Supramolecular Dynamics is the rainbow of possible techniques that most of the time allows one to find tailored experiments for the systems under study.

I.10.1 NMR and Chemical Exchange

Chemical exchange is any process by which a moiety switches between more than one chemical environment changing its properties under observation. From the perspective of an NMR technique, the entity being observed is a particular nuclide (or set of nuclides) that can exchange between different sites where it will be under different magnetic fields. The technique may or may not be sensitive to this as the timescale of interaction varies; Figure I.25 shows the average lifetimes of states during certain molecular events. Note that chemical exchange can happen at any of the NMR experiment timescales, so experiment selection must be done carefully.

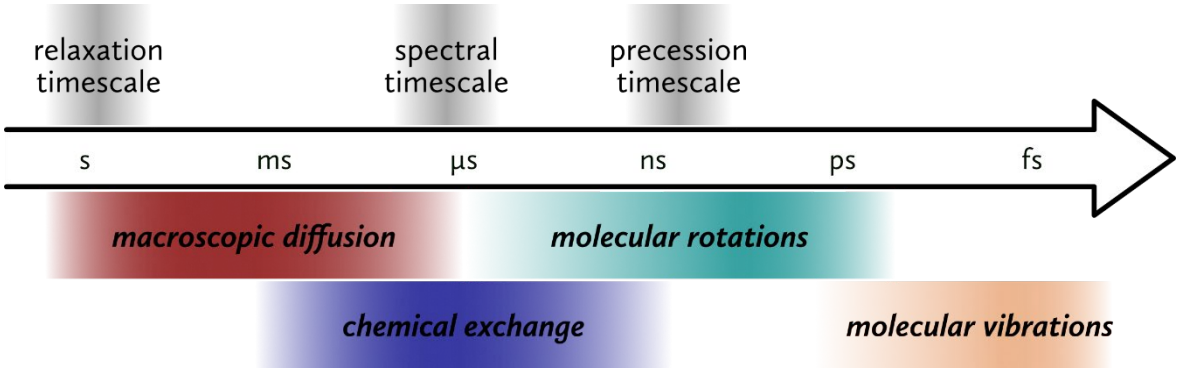

Figure I.25—Typical timescales of NMR experiments along with a rough notion of the average timescales of molecular events. The arrow indicates increasing order of magnitude in time. Adapted from [111]—Copyright © 2013 Woodhead Publishing Limited.

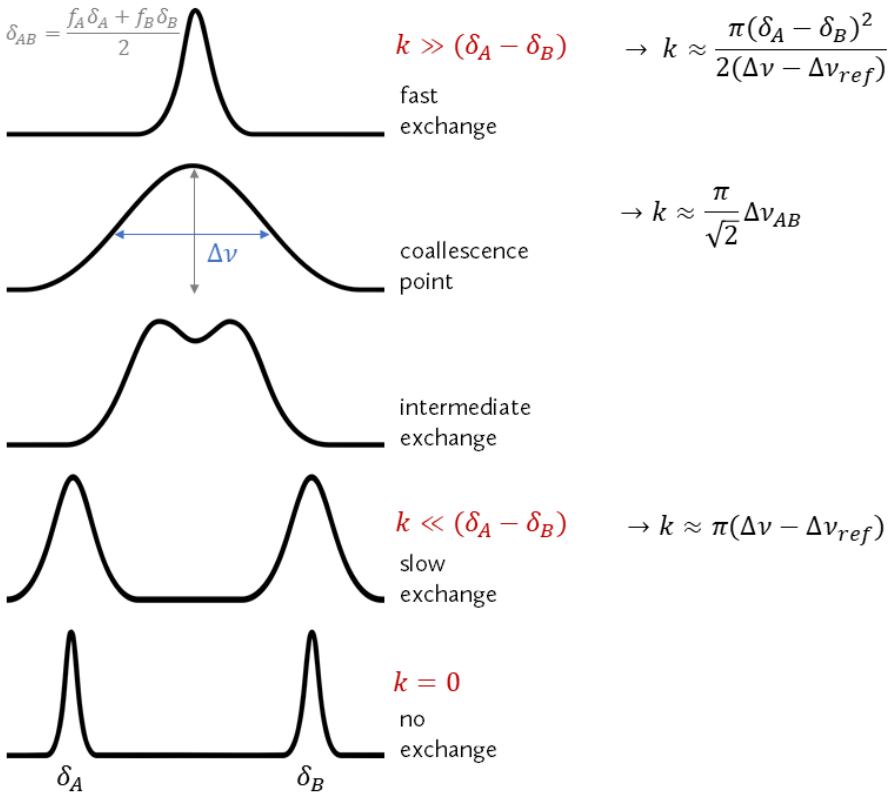

Figure I.26—Illustrative examples of NMR signal line-shapes for an uncoupled two-site system at various exchange regimes. Approximate equations estimate the exchange rate constant (k) are show along with application conditions for each case.[112] *f*: molar fraction. *ref*: reference peak without exchange

The relation of a state's average lifetime to the measurement time has substantial effects on the features of the NMR spectrum. Figure I.26 illustrates these changes. If the site exchange rate is significantly lower than the frequency difference between signals of each

site, the spectrum will show to non-overlapping signals and the system is in a slow exchange regime; each signal will be broadened in frequency in approximately direct proportion to the exchange rate. If the site exchange rate is much faster than the frequency difference between signals of each site, then the spectrum will show just one peak and the system is in fast exchange; In this limit, the signal broadening will be inversely proportional to the exchange rate. The chemical shift of this signal is the average of chemical shifts of the originating signals (without exchange) weighed by the molar fraction of the components.

In between these regimes there is that of intermediate exchange and, most importantly, the coalescence point: the rate at which the two signals coalesce into one.[110,112,113] Beware the conditions shown here for the evaluation of the exchange regimes are simplified. Non-Lorentzian line-shapes may be present and compromise quantification.[114]

Analysis of signal broadening can give some estimate of exchange rates. These estimations are, nonetheless, prone to positive bias and are very sensitive to out of ideal conditions (e.g. asymmetric populations and signal distortion). The most reliable way of quickly estimating the exchange rate from a 1D NMR spectrum is at the coalescence point. Variable temperature NMR may help attain this.

For a more precise and accurate estimation of rate constants from signal line-shapes, Complete Line-shape Analysis (**COLSA**) is the best tool. The fundamental improvement in COLSA is the lack of assumptions as to the state of a system. This makes the technique quite powerful and versatile. COLSA involves modelling the signals' line-shape using the Modified Bloch Equations. These expand the model of spin relaxation in a magnetic field to include chemical exchange. Fitting of the models to the obtained line-shapes is quite straightforward with today's computing power and user-friendly software, making this a fast way to obtain very good estimates of exchange rates. Nevertheless, COLSA demands high quality data with very good reference points which might be hard to obtain in noisy supramolecular systems.

Since simple 1D NMR experiments can only detect the exchange effects on the line-shape, advanced dynamic NMR techniques must sometimes be used even if often being

more time consuming. The key aspect those is the use of polarization transfer to measure rate of exchange of nuclides between sites.

The most relevant 2D NMR experiment to measure chemical exchange is Exchange Spectroscopy (**EXSY**). EXSY is essentially a special purpose NOESY experiment with a variable mixing time to allow for cross-polarization to evolve. The exchange rate constant is estimated from the volume of cross-peaks against that of the diagonal peaks thus accounting for relaxation. For all its versatility, EXSY as some limitations as to its sensitivity; the mixing time must be chosen well, too high and relaxation prevents observations of any signal, to low and not enough exchange is observed. In general, EXSY (as other polarization exchange experiments) work in the gap between relaxation and spectral timescales but can have difficulties in the higher end of the range. Ideally, the exchange rate is similar to or greater than the spin-lattice relaxation time but lower than the nuclide frequency difference between sites.[115]

Selective EXSY (SEXSY) can also be used in conjunction with COLSA. 1D SEXSY essentially selects for a given exchange rate measuring de amount of polarization transfer at a given rate. The implementation of SEXSY-COLSA is more complicated with more parameters in the pulse train to optimise and thorough analysis, but can give very accurate measurements of several binding thermodynamic parameters simultaneously.[116]

I.11 Titrations and binding

The most straightforward way to determine binding constants in solution is by titration. With the titration data, the most accurate way to determine the binding constant is to perform a regression to fit a titration isotherm model to the data points. This has the great advantage of automatically estimating the errors in the results. With the computing power available to most scientists nowadays, linearized models are to be avoided as this distorts the data. The best route is using non-linear regressions for fitting.

The best isotherm model to be used depends on the available data and assumptions that can be made on the system. For this, it helps to gather the maximum amount of information about the system prior to titration.[117]

In a one ligand one site binding system, the host (H) to guest (G) reaction stoichiometry is 1:1. Thus their mass balances can be written as shown in the equations **I.1** and **I.2** , the binding constant (*K*) as in **I.3** and occupied host molar fraction (or host's degree of association) as in **I.4**.

$$[H]_0 = [H] + [HG] \qquad \textbf{(I.1)} \qquad [G]_0 = [G] + [HG] \qquad \textbf{(I.2)}$$

$$K = \frac{[HG]}{[H][G]} \qquad \textbf{(I.3)} \qquad y_{HG} = \frac{[HG]}{[H]_0} \qquad \textbf{(I.4)}$$

From **I.3** and **I.4** a general binding isotherm can be expressed through a hyperbolic curve as follows.

$$y_{HG} = \frac{K[G]}{1 + [G]} \leftrightarrow \frac{[HG]}{[H]_0} = \frac{K[G]}{1 + [G]} \qquad \textbf{(I.5)}$$

The use of **1.5** as a model has a big caveat: it needs the equilibrium guest concentration to be known. This is often not possible and so a more specific binding isotherm model must be devised. This is done using the mass balances **I.1** and **I.2** to substitute [G] and [H] as independent variables in **I.5** so that in the end the model depends only on total concentrations (easier to measure) and [HG]. The substitution results in the quadratic equation **1.6** which possesses only one meaningful root which rearranged results in the model expressed in **1.7**.

$$[HG]^2 - [HG]\left([H]_0 + [G]_0 + \frac{1}{K}\right) - [H]_0[G]_0 = 0 \qquad \textbf{(I.6)}$$

$$[HG] = \frac{1}{2}\left([H]_0 + [G]_0 + \frac{1}{K}\right) - \sqrt{\left([H]_0 + [G]_0 + \frac{1}{K}\right)^2 - 4[H]_0[G]_0} \qquad \textbf{(I.7)}$$

Equation **1.7** can be divided by $[H]_0$ to result produce a model with y_{HG} as dependent variable; this is often easier to measure and interpret and makes isotherms comparable across different systems.

Chapter II

Materials & Methods

II.1 NMR Instrumentation and Methods

NMR spectra were obtained using the following instruments: 400 MMHz Avance III HD Smart Probe (for routine ^{1}H NMR); DCH 500 MMHz dual cryoprobe (for high-resolution ^{1}H and ^{13}C NMR). Tuning and matching of NMR probes was done automatically as well as 90° pulse calibration (for ^{1}H experiments). All spectra were acquired at 298.2 K.

Samples used D_2O as solvent with tert-butanol as internal standard; all spectra were referenced to its signals: ^{1}H NMR δ reference at 1.24 ppm and ^{13}C NMR δ reference at 70.36 ppm.

In all equilibrium titration experiments using OsO_4, J. Young NMR tubes were used for safety reasons; enabling a good seal against leakage of OsO_4. In kinetics experiments, due to the necessity of quick addition of reagents to the tube and auto-sampler use, regular 5 mm tubes were used capped with rubber septa (tightly wrapped in parafilm).

Whenever there was demand for quantitative results in integral analysis, T_1 (longitudinal) relaxation times were estimated. For this an inversion-recovery experiment was performed using the Bruker pulse program *t1ir1d*.

All spectra were processed using Topspin or Mestrenova software. All spectra are presented with their baseline corrected automatically (by a polynomial function). 1D spectra were automatically phase corrected; 2D spectra were manually phase corrected.

NMR signal multiplicity is reported using the following abbreviations: **s**, singlet; **d**, doublet; **t**, triplet; **qu**, quartet; **m**, multiplet; **br**, broad.

II.2 Materials and equipment

II.2.1 Cleaning of glassware

Good cleanliness of all reaction containers proved to be important to guarantee quality results. Care was taken to clean the glassware in a reliable manner. Any organic or inorganic oxidizable residue in the tubes affects results by accelerating degradation of the OsO_4. Any ions contaminating the host-guest system and its counterions can interfere.

Keeping the inside of the NMR tubes as clean and hydrophilic as possible also helps with smooth insertion and agitation of aqueous solution.

For cleaning, firstly, the glassware was immersed in freshly prepared *aqua regia* for at least 30 min followed by a thorough wash with deionised water. Secondly, a wash with methanol. Finally, the glassware was dried in an oven (if not volumetric) and cooled under as stream of N_2.

Materials containing metal were cleaned with a thorough wash with deionized water and then methanol.

Micro-syringes and plungers that met solutions containing OsO_4 were first washed with acetone to carry all residue more easily and only then washed with water, methanol and finally painstakingly dried with a flow of N_2.*

II.2.2 Degassing of solvents

Whenever a degassed solvent or solution was needed, the freeze-pump-thaw method was used. With this method, evaporation and change of composition is kept to a minimum. To begin with, the solvent is placed in a sealed container connected to a Schlenk line which is flushed with N_2. Then, using a liquid N_2 bath, the liquid is frozen. After that the container is evacuated through the Schlenk line and left under vacuum for 5 min. Finally, the flask is resealed, and the liquid thawed. This freeze-pump-thaw cycle was carried out four times for each liquid to be degassed.

II.2.3 Reagents

4,4'-Diaminobiphenyl-2,2'-disulfonic acid (DADA) was acquired from Alfa Aesar (with a maximum water content of 30%); elemental analysis measurements were consistent with a 15.8% water content. Some unknown impurities in this reagent were found to persist in some cage samples, observable at 1.91 ppm and 8.46 ppm in some ^{1}H NMR spectra.

* Do not play down the importance of cleaning and drying the syringes thoroughly, else you will be presented with black syringes from the osmium residue in the frosted bore. If this happens, a quick wash with dilute nitric acid is recommended, followed by the normal waste disposal and cleaning procedure.

All other solvents and reagents were used as supplied.

Deuterated water with *tert*-butanol internal standard was prepared in batches of 100 mL; the TBA was weighed in a sealed, tared vial, on an analytical balance and then quantitatively transferred to a 100.0 ml volumetric flask then filled with D_2O.

II.3 Handling of OsO_4

Osmium tetroxide is a powerful oxidizer and quite reactive towards unsaturated organic matter with its hydrophobicity helping permeate lipid membranes. These properties make it quite useful for fixing biological samples and as microscopy stain.[96,118] But it is those very qualities, in conjunction with its physical properties—with a vapour pressure higher than that of mercury[94,119]—that make it quite a hazardous material to work with.

According to NIOSH, OsO_4 has a Time Weighted Average Recommended Exposure Limit of 0.002 mg/m^3 (as Os).[120] For comparison, the most dangerous form of mercury—alkyl mercury—has that same limit set at 0.01 mg/m^3 (as Hg).[121]

Several precautions were put in place with the risks of OsO_4 handling in mind. For storage of the solid OsO_4, two screw-cap vials were used, one inside the other, both capped, and sealed with paraffin film. These were put inside a lidded metal canister visibly labelled.

As for disposal of any liquid waste containing osmium, solutions were treated with an excess of $Na_2S_2O_3$ before disposal into the appropriate waste container. Regarding solid waste, every piece of material was washed with a saturated solution of $Na_2S_2O_3$ before disposal. The same was done before washing any experiment paraphernalia that came into contact with OsO_4 (except for microsyringes).

Chapter III

Be my guest

III.1 Improving the synthesis of Gdm_4**1**

The synthesis of Gdm_4**1** reported by Zarra et al[89] calls for the use of Schlenk apparatus making the synthesis a bit cumbersome. In addition, the use of acetone in the work up of the reaction is also undesirable; it remains inside **1** in the solid-state interfering with further host-guest studies.

Meanwhile, it was found that cage **1** possesses a remarkable stability against oxidation in the presence of Gdm^+. With care taken, the synthesis can be performed in air without much loss of yield. Attention has to be paid so that all of the ligand's subcomponents are dissolved and available to react as soon as the Fe(II) salt is added. The purple colour typical of Fe(II) complexes in a hexa-imine coordination environment instantly appears as the salt dissolves. Heating should begin only after homogenization to enable the annealing of the system while preventing oxidation of the Fe(II) by O_2.

The issue about the presence of acetone was dealt with by decreasing the amount of water used in the reaction and simplifying the workup. With less water, the cooling of the reaction mixture to room temperature proved enough to precipitate most of the Gdm_4**1**. Then, filtration and drying can be used to isolate the solid product without any interfering guests.

Notwithstanding the remarkable stability of Gdm_4**1** even in the presence of strong oxidants such as OsO_4, some of the latter seemed to decompose when mixed in a solution of cage (see section III.2.3). Adding to this, the observation of a brown solid (probably mixed iron oxides) retained upon filtration of solutions of Gdm_4**1**, lead to the conclusion that some purification could be needed.

By deviations from the ideal stoichiometry there is the possibility of organic impurities. Minor contamination, from the DADA stock, was observed by NMR. (see II.2.3) However, tests seemed to show this to be relatively inert towards OsO_4 and that decomposition still occurred.

It was also hypothesized that decomposition of OsO_4 could be caused by inorganic impurities (invisible in the NMR), namely excess Fe(II), which can also arise from stoichiometric imbalances. The reduction of OsO_4 by Fe(II) is irreversible even in the presence of an oxidizer (such as TMAO) due to precipitation of mixed oxides.

To try and eliminate these impurities, successful recrystallization of Gdm_4**1** in water was achieved (by dissolution in a minimum of hot water and slow cooldown). Despite the elimination of most organic impurities, there was still decomposition: detected by the formation of a small amount of brown/grey precipitate in a NMR tube with Gdm_4**1** and OsO_4 in D_2O (observed in initial binding titration attempts)

It has been shown that hexa-aqua metal complexes can act as counterions, aiding in the production of good quality crystals for XRD. More specifically, **1** can be crystallized as $[Fe(H_2O)_6]_2$**1** when excess Fe(II) present.[60] Figure III.1 shows the crystal structure of this compound. The report noted that the quality of such crystals was superior to those of $(NMe_4)_4$**1**. Considering this, a hypothesis was postulated: the recrystallization could be making matters worse by increasing the deficiency of the solid in Gdm^+ cation and increasing the amount of excess Fe(II).

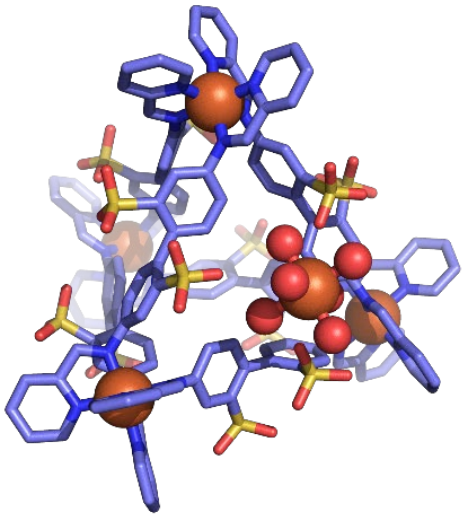

Figure III.1—Structure of **1** and a $[Fe(H_2O)_6]^{2+}$ counterion (spheres) as they stand in a crystal of $[Fe(H_2O)_6]_2$**1**—CCDC 903563. Hydrogen atoms in the cation are disordered. Hydrogens and solvent omitted for clarity.

Having this in mind, an improved procedure was designed that proved efficient in consistently producing Gdm_4**1** pure enough for experiments to be done without unmanageable amounts of decomposition in the observed timescale. The new procedure uses an excess of Gdm_2CO_3 (2 eq. per **1**). The excess is added in a second batch to prevent premature precipitation (before annealing) and occlusion of impurities. The yields also improve due to this excess and the smaller amount of water.

III.1.1 Procedure for synthesis of $Gdm_4$1

Figure III.2 illustrates the following process. 4,4'-Diaminobiphenyl-2,2'-disulfonic acid (510 mg, 1.04 mmol) and guanidinium carbonate (184 mg, 1.01 mmol), were dissolved in water (20 mL) in a 50 mL round bottom flask containing a magnetic follower. 2-formylpyridine (200 µL, 2.08 mmol) was added and the solution stirred for 5 min at room temperature. Iron(II) sulphate heptahydrate (200 mg, 0.712 mmol) was added, the round bottom flask sealed with a rubber septum and the mixture heated 50 C for 1 h. Then, another portion of guanidinium carbonate (65.0 mg, 0.357 mmol) was added, the flask resealed, and the reaction was stirred at 50°C for 24 h.

After this period, the mixture was slowly cooled to room temperature over the course of 2 h under slow stirring. The dark purple slurry was filtered through a sintered glass funnel (1 cm diameter). 10 mL of an aqueous solution of Gdm_2CO_3 (0.1 gmL^{-1}) were then used, in two portions, to wash the flask and the solid in the filter and finally with the 5 mL of water. This was dried under a flow of nitrogen for an hour. The resulting wet powder was transferred to a tared vial and dried overnight in a desiccator, under vacuum, over P_2O_5. This produced a dark purple powder of Gdm_4**1** (521 mg, 0.145 mmol, 82%).

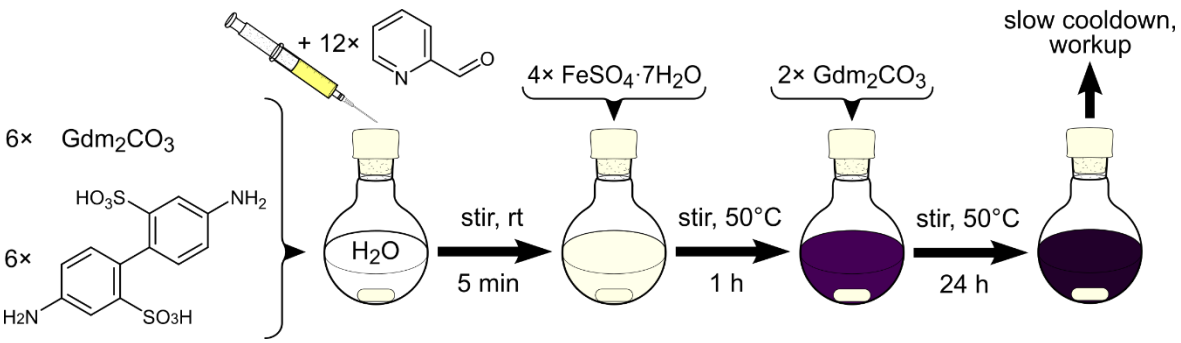

Figure III.2—Illustration of the improved procedure for the synthesis of Gdm_4**1**.

III.1.1.a Further considerations

As has been demonstrated in a previous report,[89] the synthesis of Gdm_4**1** can be driven towards a quantitative yield by adding a great excess of GdmCl. In this work, a choice was made not to use GdmCl nor a great excess of Gdm_2CO_3. While, a large excess of Gdm_2CO_3 would have had the same effect, it could have the undesired effect of causing the precipitation of iron carbonates and hydroxides. On the other hand, the use of the GdmCl would add yet another anion to the system, possibly interfering with the solid's composition and with subsequent experiments.

The precipitation of Gdm_4**1** using an excess of a Gdm^+ salt, as stated in the report mentioned above, can be used to purify old batches or contaminated batches. This would start by dissolving the solid in a minimum of water and adding the Gdm^+ salt until Gdm_4**1** precipitates out.

For experiments where the presence of chlorides is not an issue, the use of GdmCl to induce precipitation of Gdm_4**1** or solid washing is preferable. This is because any impurities that may form salts are likely to be more soluble with chloride as counterion.

Degasification of the water did not seem to affect yields or product quality. Nevertheless, for work especially sensitive to the presence of Fe(III) it is a step that might help in avoiding contamination without much effort.

III.1.2 $Gdm_4$1 NMR characterization

The NMR data is consistent with previous reports.[89] Figure III.3 shows the ^1H NMR spectrum of $Gdm_4$1 in D_2O, with the peaks labelled with their source nuclides. Note that, no major impurities are observable in the aromatic region, meaning that no significant free ligand or its subcomponents are present.

Due to the large cooperativity between binding events at the corners, the only possibility for free subcomponents to be observed is to have a stoichiometric unbalance

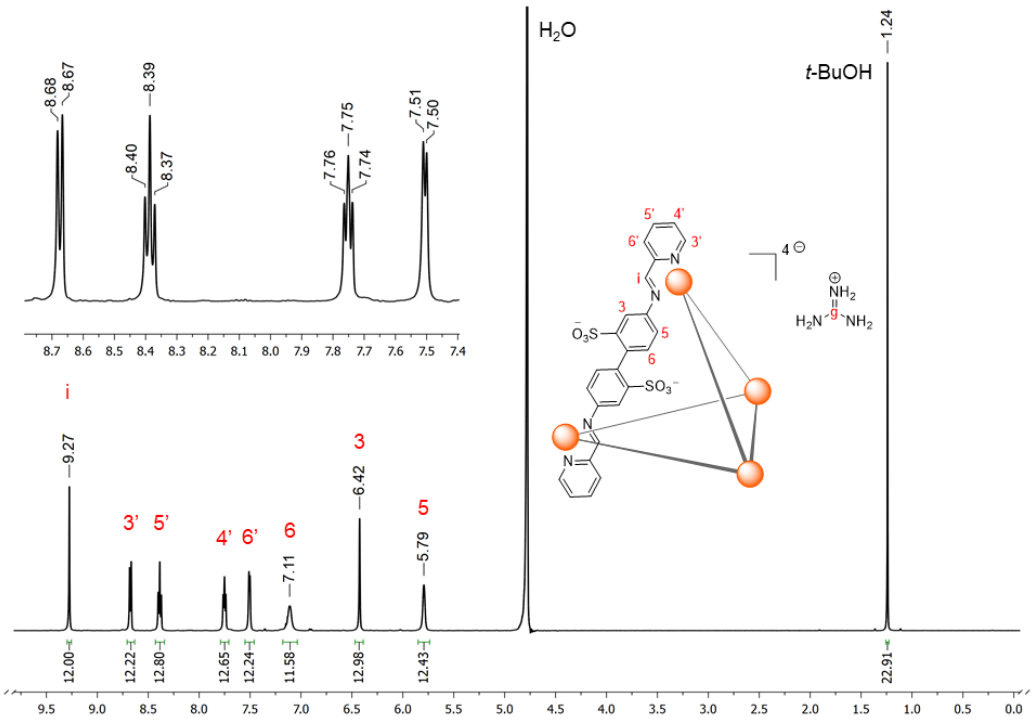

Figure III.3—^{1}H NMR spectrum of Gdm$_4$1 2.42 mM (500 MMHz spectrometer) with labelled peaks and their relative integration.

Table III.1 shows the ^{1}H NMR data extracted from the previous spectrum respectively, with peaks assigned to their source nuclides. The imine signal is the one with highest frequency. It appears as a narrow singlet quite isolated from the others at 9.27 ppm. This makes the imine signal the ideal one to track for host-guest studies. Overlap is also the least likely to occur for the imine signal as it is the most sensitive to guest presence. This is probably due to variation of Fe-N distance, and consequent variation of the imine bond polarization, as the cage is deformed by the guest.

Table III.1—^{1}H NMR signals of Gdm$_4$1 with the assigned source nuclide, their number, chemical shift, multiplicity and observed coupling constants.

^{1}H nuclide	N° nuclides	δ / ppm	Multiplicity	*J* / MHz
i	12	9.27	s	—
3'	12	8.67	d	7.8
4'	12	8.39	t	7.8
5'	12	7.75	m	13 (range)
6'	12	7.51	d	5.3
6	12	7.11	s (br)	—
3	12	6.42	s	—
5	12	5.79	s (br)	—

Table III.2—^{13}C NMR signals of Gdm$_4$**1** (in D_2O, 126 MHz spectrometer).

^{13}C nuclide	δ / ppm
i	176.9
1'	158.7
g	158.6
6'	156.6
4	150.8
2	143.6
4'	140.5
1	136.7
6, 3'	132.6
5'	130.5
5	122.3
6	121.6

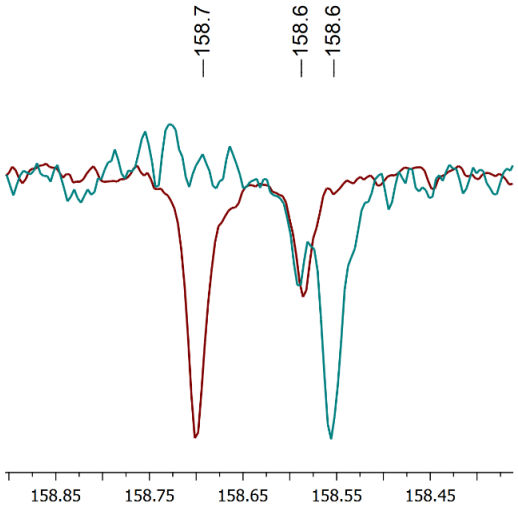

Figure III.4—Overlay of a portion of the ^{13}C NMR spectra of Gdm$_4$**1** (red) and OsO_4⊂ Gdm$_4$**1** (blue); the signals of **C1'** and **Cg** are visible.

It is interesting to note that ^{1}H signals from H5 and H6 are broadened singlets whereas one should observe splitting due to homonuclear *J*-coupling. This signal broadening can be attributed to fast chemical environment variation upon rotation around the C1-C1 bond. This rotation is not totally free, however, as it is hindered by the sulfonate groups and bound guanidinium ions. Most notably, in all observed host-guest complexes of **1**, these signals are narrow and split into the expected doublets due to hindrance of this rotation by the guest.[87]

Unequivocal assignment of the ^{13}C NMR peaks of **1** was a little harder due to some overlapping and similar coupling patterns (as observed in the HSQC and HMBC—see spectra in Figure A.5 and Figure A.6). Namely, the C atoms with no attached protons in the ligand's rings. Table III.2 shows the observed ^{13}C NMR chemical shifts identified with the help of the couplings shown in Figure III.5.

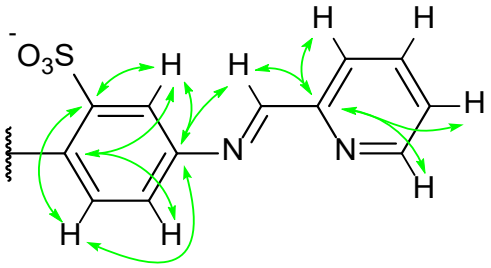

Figure III.5—Diagram showing the most relevant heteronuclear couplings in resolving the NRM peak assignment.

Even though admittedly superfluous, an attempt was made to distinguish the NMR signals of **C1'** and **Cg**. This was possible since these were not overlapping in the spectrum, unlike the case of the C6 and C3' signals. Comparing the spectra of empty **1** and $OsO_4 \subset$**1**, as shown in Figure III.4, one detects that the signal at 158.6 ppm varies just slightly. Given that the chemical environment of the carbon atom in Gdm^+ should be the least affected by the presence of a guest inside **1**, it can be said with some confidence that the signal at 158.6 ppm is that of **Cg**.

III.2 The cage and the beast

The $OsO_4 \subset Gdm_4$**1** complex was the most studied of all the presented in this work purely due to the novelty of having highly oxidative incompatible guest in a oxidizable dynamic system. The potential use as a OsO_4 storage medium and as an analytical device also called for a good characterization.

III.2.1 Subcomponent (in)stability—*As weak as they are divided*

After the discovery of the compatibility of Gdm_4**1** and OsO_4, perhaps the most remarkable aspect is the fact that the subcomponents of **1** are all incompatible with the latter. Notwithstanding, the cage's assembly is dynamic. The relative stability of the systems seems to stem from the assembly itself: the cooperation of metal coordination centres and imine formation seems to obstruct the availability of susceptible moieties to meet effectively and react with OsO_4.

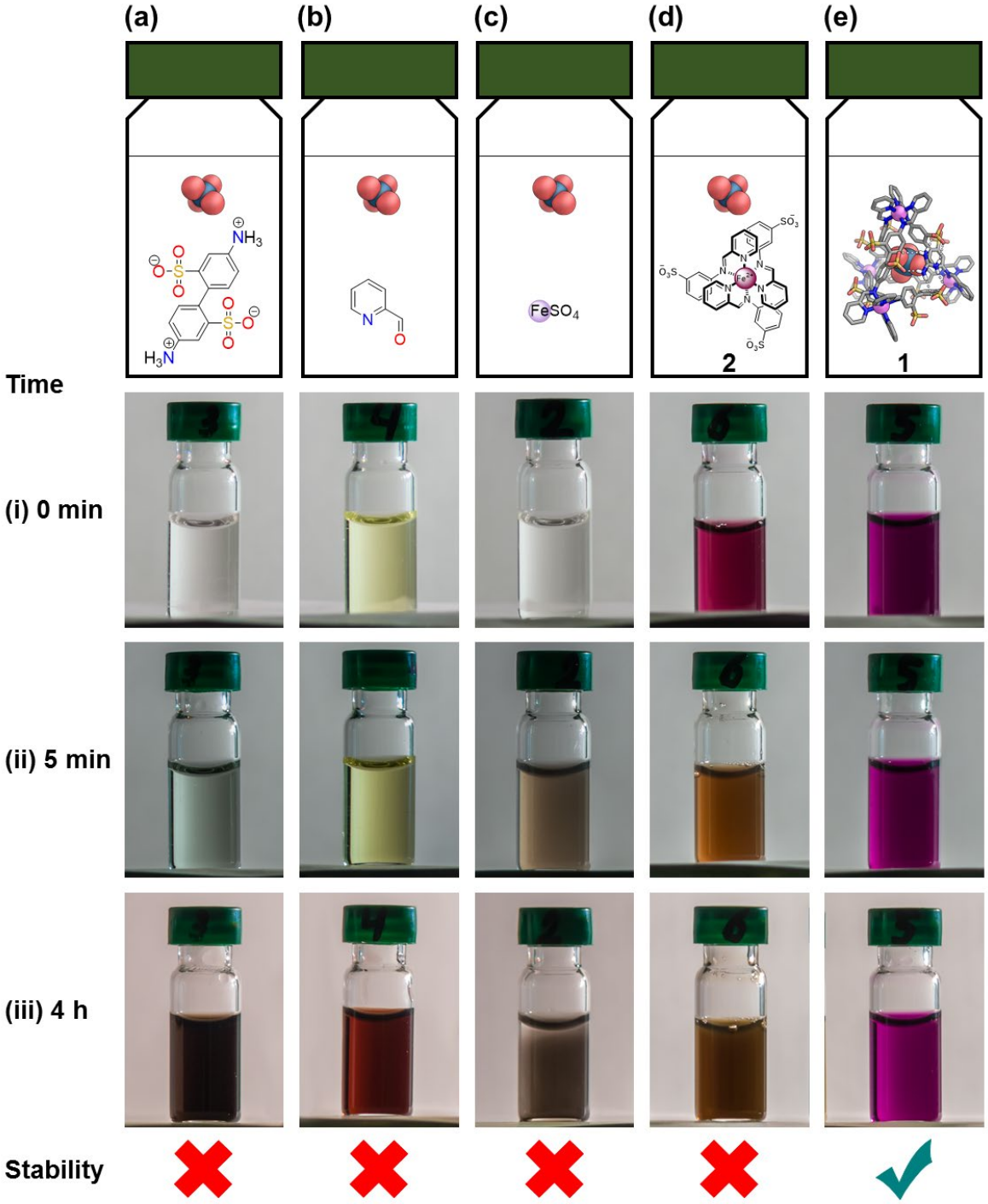

Figure III.6—Qualitative assessment of the stability of the subcomponents of **1** in the presence of OsO_4. Note that the solution changes colour or turns cloudy in all cases except when all subcomponents are present in the form of $Gdm_4\mathbf{1}$.

Figure III.6 shows photographs of an experiment assessing the stability of the subcomponents of **1**. Vial ***a*** contained 3.4 mg (10 mmol) of dissulfonic acid with 1.7 mg (20 mmol) of $NaHCO_3$ to solubilize the former. Vial ***b*** contained 1.2 µL (12 mmol) of pyridine carboxaldehyde. Vi al ***c*** contained 1.4 mg (5 mmol) of $FeSO_4 \cdot 7H_2O$. Vial ***d*** contained 7.1 mg (10 mmol) of **2**. Vial ***e*** contained 1.8 mg (0.1 mmol) of Gdm_4**1**. All the vials also contained 1.0 mL of water. After dissolution of all reagents the vials were capped. 100 µL of OsO_4 solution were added through the septum to each vial.

It is observed that both the $FeSO_4$ and mononuclear complex **2** react very quickly (vials ***c*** and ***d***). Changes in the solution are observable a mere couple of seconds after addition of OsO_4; a visible precipitate forms within 5 min.

However, changes in the vials containing the DADA and the carboxaldehyde (vials ***a*** and ***b***), are slower; visible degradation appears gradually about 1 h after addition of OsO_4. The DADA quickly forms a pale blue solution and produces a dark precipitate about 4 h after. The pyridine carboxaldehyde quickly forms an orange solution darkening to brown in the following 4 h.

Finally, the appearance of the vial containing **1** (vial ***e***) remains unaltered even after a day, showing the remarkable stability of the assembly compared to its components. The stability was further confirmed by observing no changes to the ^{1}H NMR spectrum of $OsO_4 \subset Gdm_4$**1**.

A note on the complex **2**: it serves to emulate the corners of the cage, without the cooperativity of the rest of the assembly. The isolated corner is much more labile and sensitive to O_2. The batch used had been synthesised sometime before. Before using it, the compound was recrystalized from degassed methanol by precipitating with degassed acetone. The synthesis has been reported before by *Salles et al*[92] and the ^{1}H NMR spectrum of the solid obtained was consistent with the previous results.

III.2.2 $OsO_4 \subset Gdm_4 1$ NMR characterization

The binding of OsO_4 observed by ^1H NMR with the appearance of another set of peaks, as the spectrum in Figure III.7 shows. This indicates a binding interaction in a slow exchange regime at the NMR timescale. Because the number of signals is the same, it is reasonable to assume that the complex preserves an overall tetrahedral symmetry upon binding.

As expected, the coupling patterns increase in complexity. The rotational and vibrational freedom of the cage decreases as its void is occupied by the guest; additional couplings become observable, bond angles are altered and so do coupling constants.

The volume of the cavity of **1** is 141 $Å^3$ (estimated from the crystal structure by probe scanning)[86] and the average molecular volume of OsO_4 is 81.7 $Å^3$ (estimated from the crystal structure parameters)[95]. Therefore, OsO_4 fills roughly 58% of the cavity's volume once inside **1**. This is well within the ideal (55 $\pm$ 9) % shown by Mecozzi and Rebek[122] for a good host-guest interaction within a cavity. Hence, as expected: the OsO_4 does not seem to force much distortion to the cage since the imine signal shift is only of 0.10 ppm (see Table III.3); the distortion seems to be mostly accommodated by bond angle variation throughout the rather flexible ligand.

Table III.3 and Table III.4 show the ^1H and ^{13}C NMR data extracted from spectra presented in Appendix Section A.2. Automatic deconvolution was performed to enable calculation of real coupling constants for the signals with significant peak distortion (due to small coupling and great peak width), namely H-3 and H-5. In the (apparent) triplet signals, deconvolution was attempted to extract the true coupling constants. However, the values were meaningless since the signals are distorted beyond true triplets and too wide and overlapping to be deconvoluted with confidence. In these cases, the constants reported are only apparent.

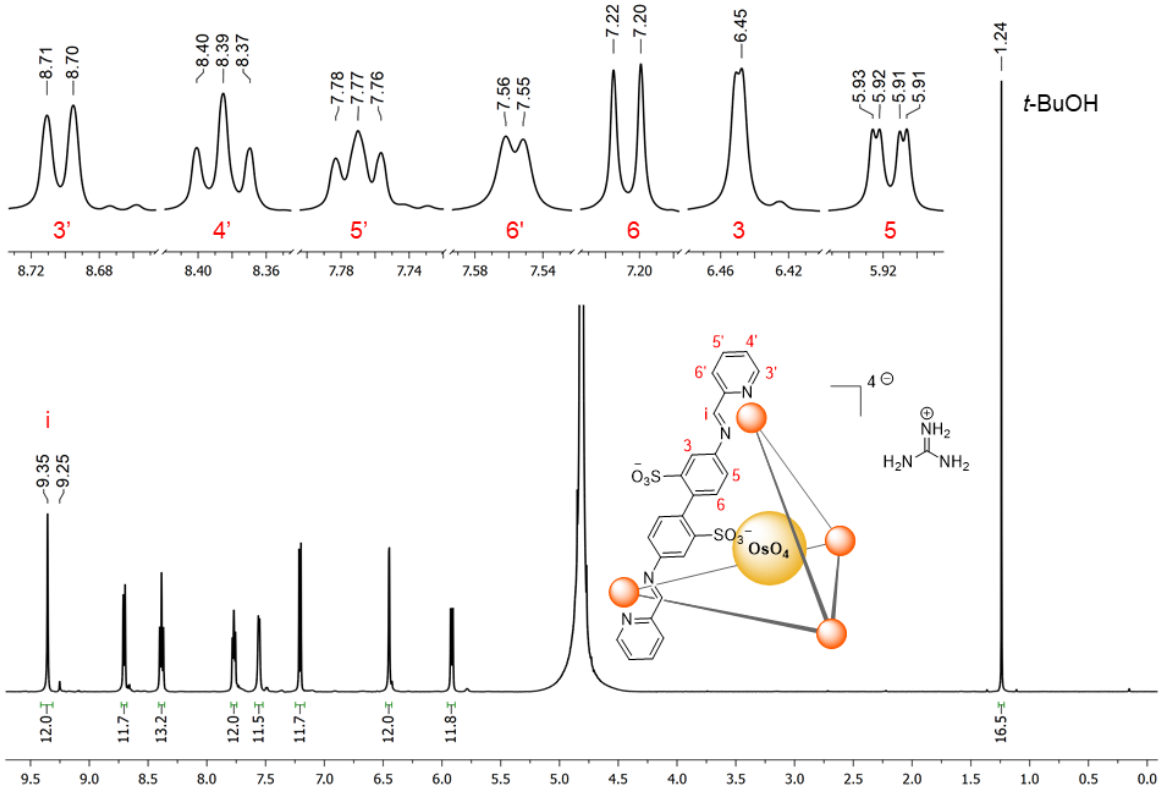

Figure III.7—^{1}H NMR spectra of OsO_4⊂Gdm$_4$1 with 1.48 mM of total host and 8.6 mM of total guest (500 MHz spectrometer).

Table III.3—^{1}H NMR signals of OsO_4⊂Gdm$_4$1. [a] From deconvolution.

^{1}H nuclide	N° nuclides	δ / ppm	Multiplicity	*J* / MHz	Δδ / ppm
3	12	6.45	d	2.3[a]	0.03
5	12	5.92	dd	8.0; 2.3[a]	0.13
6	12	7.21	d	8	0.10
3'	12	8.7	d	7.8	0.03
4'	12	8.39	t	7.8	0.00
5'	12	7.75	t	6.7	0.00
6'	12	7.56	d	5.1	0.05
i	12	9.35	s	—	0.08

Table III.4—^{13}C NMR signals of OsO_4⊂$Gdm_4$1.

^{13}C nuclide	δ/ ppm	$\Delta\delta$/ ppm
1	136.7	0
2	143.3	-0.3
3	121.6	0
4	151.2	0.4
5	122.5	0.2
6	133	0.4
1'	158.6	-0.1
3'	132.8	0.2
4'	140.5	0
5'	130.8	0.3
6'	156.6	0
g	158.6	0
i	176.7	-0.2

III.2.3 OsO_4⊂$Gdm_4$1 binding titration

Due to the slow exchange rate of the host-guest complex, binding of OsO_4 is easy to follow by ^{1}H NMR during a titration to determine the binding equilibrium constant. Intuition might lead one to use as much of the cage's signal as possible. However, some preliminary studies revealed that the quality of data is best using only the H-i signal data. It was found that integration of all the signals, even if not overlapping, resulted in too much noise in the processed data. The width of the ^{1}H peaks (other than H-i) demands that integration regions must be large to be accurate or risk biases in the data because not all of the signal is integrated. All the quantitative NMR studies presented use only the H-i peak integration as signal for the concentration of **1**; simplifying the steps of signal processing.

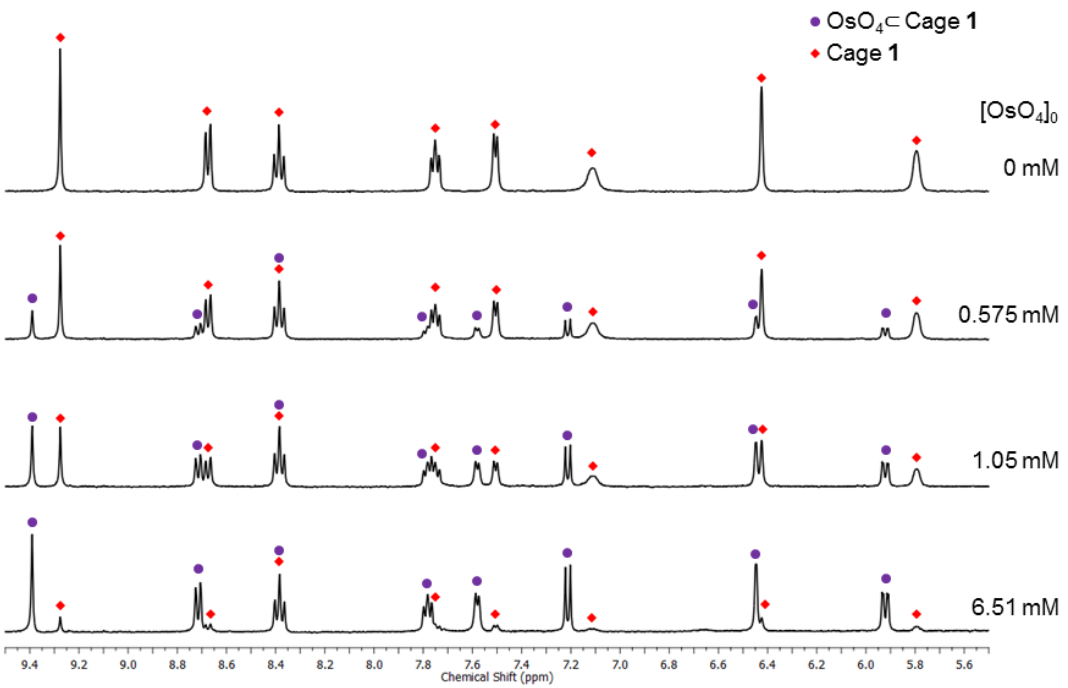

Figure III.8—Representative ^{1}H NMR spectra of the progress of a titration of Gdm$_4$1 with OsO_4.

As shown in Section III.2.1, even though the cage **1** is stable in a solution containing excess OsO_4, the subcomponents of **1** are not. Even if samples appeared clean by ^{1}H NMR analysis, the total absence of free diamine and aldehyde components cannot be guaranteed. The same can be said about NMR silent species such as Fe^{2+}. Due to these impurities, the procedure previously presented by *Hristova* et al.[123] was adapted to enable greater precision, accuracy and throughput.

Following that procedure, a solution of guest—OsO_4—was titrated into a solution of host **1**. The titrant did not contain host and so was made as concentrated as practical (but always well below saturation—0.2 M)[124]. This kept the host concentration from varying too much although the aliquots of titrant must be kept at a minimal volume to be measured accurately.

After some initial titration trials, widely varying values for the binding constant were being obtained with fitted isotherm curves presenting unacceptable residual biases. This was in spite of a constant effort to improve the purity of the cage's samples and the cleanliness of the glassware. A slight trend in the results was noticed: the binding curve

seemed to flatten the longer the time taken until the end of the procedure; another approach was then needed. Since most of the decomposition of OsO_4 seemed to happen during an initial period, a long "equilibration" period was introduced as a way of increasing accuracy. With the titration proceeding in parallel using various NMR tubes, the procedure is also sped up.

With this, one can assume that the decomposition of OsO_4 during the titration is negligible. The regression model, however must be adapted to account for the initial decomposition. While this could be estimated from titration point where the degree of association starts to increase, a high resolution in the concentration domain would be needed to properly assess it.

The quantity of added OsO_4 must be estimated from the solution preparation data as the OsO_4 is not easily observable in Os. The approach chosen for this titration, was that of letting an unknown parameter ($\boldsymbol{x_0}$) be subtracted to the added guest concentration ($\boldsymbol{c(OsO_4)}$) to estimate the effective total guest concentration. This can be interpreted as said initial decomposition. NMR. Furthermore, unlike previous work, given that the variation in total host concentration cannot be ignored ($\boldsymbol{[H]_0}$), it is considered an independent variable (estimated via the *t*-BuOH standard). Also, using the host's degree of complexation ($\boldsymbol{y}$) as the dependent variable revealed to be more precise than using the concentrations of its species directly. On that account, deduced from equations **I.5** and **I.7** the mathematical model used expressed in equation **III.1**.

$$y = \frac{1}{2[H]_0}\left([H]_0 + [G]_0 - x_0 + \frac{1}{K}\right) - \sqrt{[1 + K([H]_0 + [G]_0 - x_0)]^2 - 4K^2[H]_0([G]_0 - x_0)} \quad \textbf{(III.1)}$$

The model and the data points (shown in Figure III.9) were then imported into the *Origin* software. The first 6 data points (blanks and equilibration) were masked to be excluded from the calculations, leaving 27 points. Using the *Non-Linear Curve Fit function*, the model's parameters were restricted to positive values and initialized at the arbitrary value of 1. The model then converged resulting in the parameters as shown in Table III.5.

For the complete *Origin* non-linear regression output, including regression statistics and residual plots, see Appendix Section Chapter VIIB.1.1.

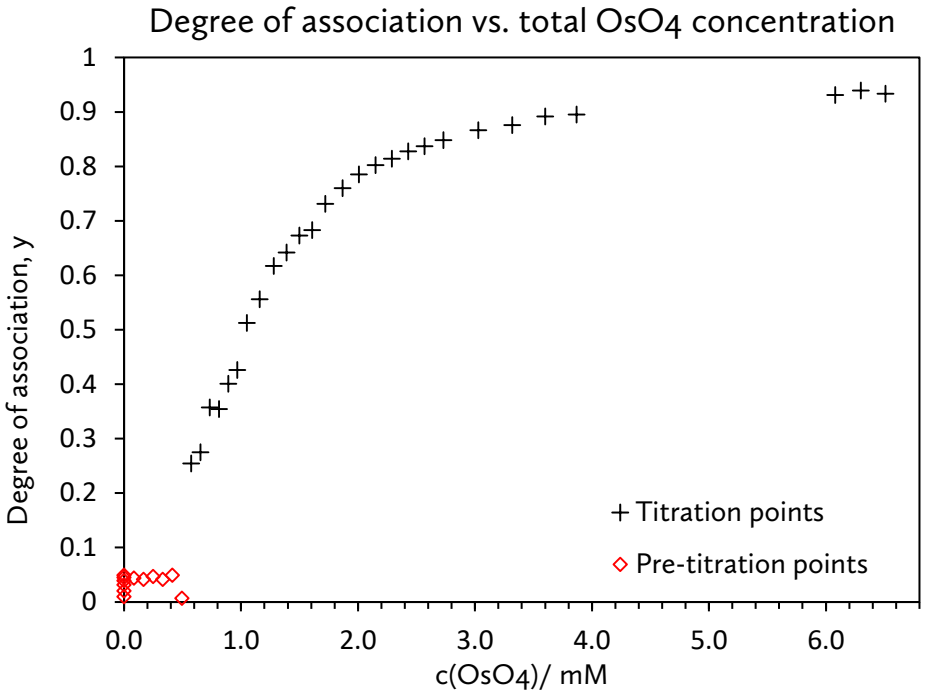

Figure III.9—Plot of the measured degree of association against the total concentration of OsO_4. The red points indicate the measurements made of the blanks (before OsO_4 addition) and after the first addition and 16 h equilibration phase.

Table III.5—Summary of the parameters from 27-point $OsO_4 \subset 1$ titration curve regression.

	Value	Std Error	95% LCL	95% UCL	Dependency	Adj. R^2	DF
x_0 / mM	0.382	0.0149	0.351	0.412	0.53231	0.99071	25
K / mM^{-1}	2.88	0.118	2.64	3.12			

As shown in Table III.5, with 27 points, the value of $\boldsymbol{x_0}$ was determined at (0.38±0.01) mM. Only tubes 5 and 6 had a calculated OsO_4 concentration greater than this. Hence, the first four tubes would not have had enough OsO_4 added pre-titration to prevent further decomposition during the titration.

Notwithstanding, removing those titration points did not improve the fit significantly. The results from this second 23-point regression (see Table and Figures in Appendix Section Chapter VIIB.1.2 for the statistics) show that, even though the quality of fit increased slightly, the dependency of the parameters also increased while not being significantly different at a 95% confidence level. Additionally, the biases in the residual distribution (shown in Figure B.3) are not a great improvement from the previous attempt.

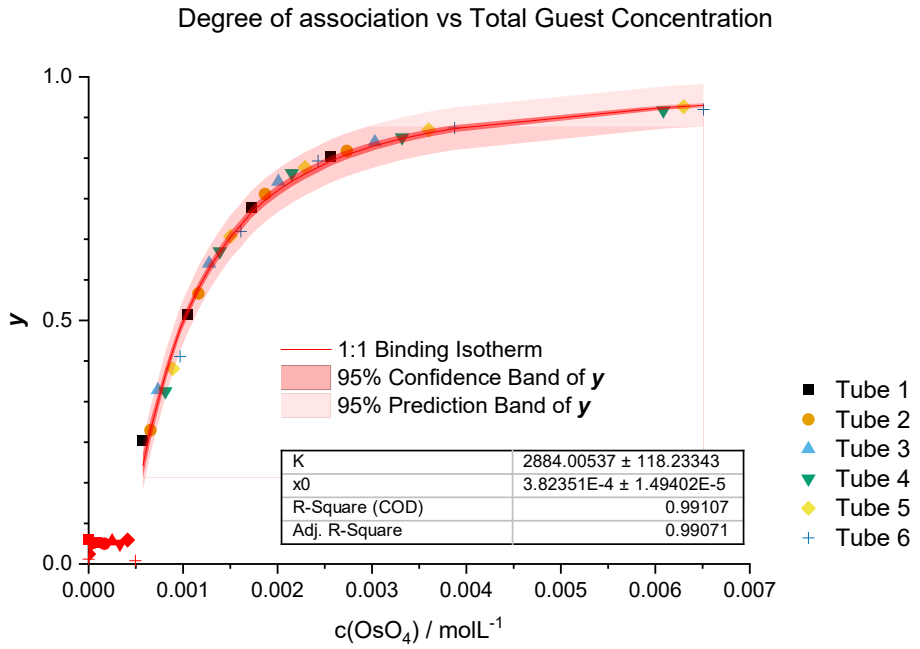

Figure III.10—Plot of the output from Origin's non-linear regression highlighting the different tubes used throughout the titration. Inset table: summary the regression's statistics with the 1:1 Binding Isotherm Model. Red data points not used for regression.

The variances of K and x_0 are not independent, and so the estimators of these parameters have some dependency. There is some confidence, however, that the model used is not overparametrized; the value of the dependency between the parameters is well below 1. Simpler models obtained only lower values for adjusted R^2 with higher errors.

Even though significant trends are observed in the regression's residuals. It's unlikely this is due to unsuitability of the model. The trends may be due to the inherent bias in the calculation of the degree of association from the two H-i signals (which increases with increasing difference in the signals).

III.2.3.a Procedure

6 NMR tubes were filled with 0.60 mL solution of Gdm_4**1** (1 mM and [t-BuOH] = 2.02 mM). After the addition of the first aliquot of titrant ([OsO4] = 25.2 mM and [t-BuOH] = 2.02 mM, the mixture was left at room temperature for 16 h and the ^{1}H NMR spectrum registered. The subsequent additions (according to Table A.1) and spectrum reads were made in the following 2 hours. The data points obtained are plotted in Figure III.10.

III.2.4 $OsO_4 \subset Gdm_4 1$ intake kinetics

Having explored the OsO_4 binding as to the equilibrium thermodynamics, another crucial part of characterizing the host-guest system is evaluating its binding kinetics. More specifically, evaluating the second order intake rate constant ($\boldsymbol{k_{in}}$). From experience with the titration, it was known that the solution reached equilibrium in the time from sample preparation to the first couple of scans (less than 4 min). Thus, a way had to be devised to greatly reduced the time taken between sample preparation and measurement.* The best option was to do a point-by-point study of the intake kinetics, but the doing wet chemistry with OsO_4 in the spectrometer's room was nobody's cup of tea. Hence, Dynamic NMR techniques were attempted first.

EXSY is the technique of choice for slow exchange cases. However, this did not reveal any chemical exchange of signals at any of the timescales studied: 0.3, 0.5, 0.7 and 2 s. Figure III.11 shows an EXSY spectrum obtained with a representative appearance showing the expected NOE cross-peaks amongst a sea of noise. Note that the spectrum was not diagonalized: although there are some signals around areas where cross peaks should be expected, these do not appear symmetrically across the diagonal. Also, observe that the apparent cross-peaks are of opposite sign to the diagonal peak. Chemical exchange peaks would be of opposite when arising from a slow tumbling molecule (e.g. a much bigger cage or protein) which is not the case[125]. The spectra with lower mixing times, naturally, contained less noise but the same overall signals.

Although these experiments were not successful in probing the intake kinetics of this complex, 2D EXSY could still prove useful. Admittedly, the host concentration could have been made higher. Also, some finetuning of acquisition settings will further increase sensitivity. However, if the exchange frequency of the complex is truly too slow for the probing capabilities of EXSY, other techniques must be used, bearing in mind that this particular system is **very** sensitive to heating. Simple line width analysis of the data obtained during titrations did not reveal any consistent results as the signal width seems

* Preferably a way that didn't involve taking an excruciatingly slow elevator nor running down ten flights of stairs holding NMR tubes with OsO_4 in them.

limited mainly by relaxation. The obvious improving step of using a spectrometer with higher field to narrow the lines might enable observation of the effects of chemical exchange. Also, SEXSY and COLSA could be worth the effort.

Nonetheless, a crude minorization can be done from the quickest experiment run. Since equilibrium appeared to have been reached in 4 minutes with 1×10^{-3} M of host and of guest it implies that $k_{in} \gtrapprox 0.6\ M^{-1}s^{-1}$ given that 0.4 was the final degree of association.

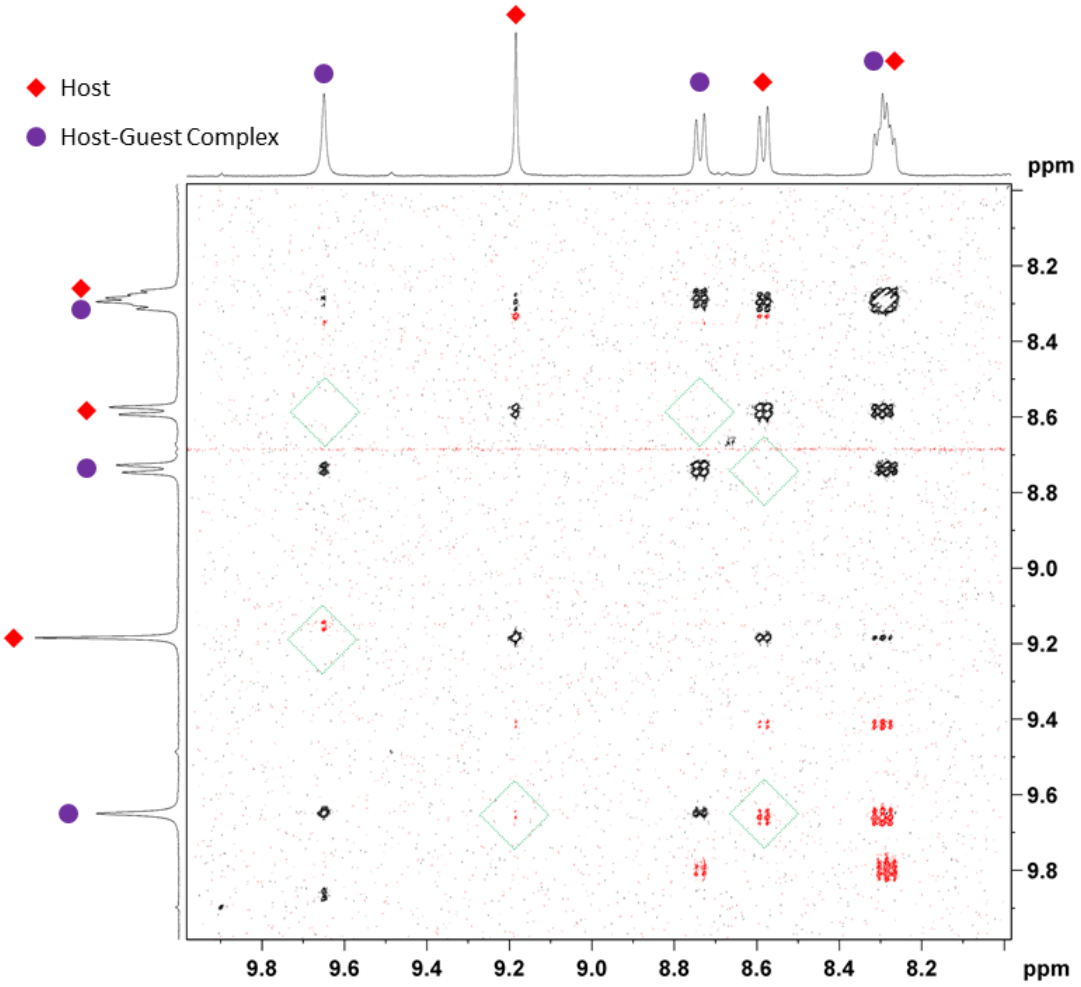

Figure III.11—EXSY spectrum (with 2 s of mixing time, 400 MHz) of a solution containing Gdm$_4$**1** (0.880 mM) and OsO_4 (0.82 mM), resulting in a 52% degree of association. The highlighted regions are those most relevant to the observation of cross-peaks due to chemical exchange.

III.2.5 Discussion

The binding titration curve seems to follow quite closely that of a 1:1 binding model isotherm. With the average concentration of **1** being 0.59 mM, the estimated binding constant at 25°C is (2.9 ± 0.2) mM^{-1}. This is a moderate binding strength like those of other small hydrophobic molecules only slightly soluble in water. For example, cage $(NMe_4)_4$**1** binds chloroform at 1.4 mM^{-1}. However, caution is advised when comparing such results since, as is shown in the next section, the presence of Gdm^+ as counterion changes the binding strength significantly.

Even though the intake rate of OsO_4 is higher than initially expected, it is within what could be expected; it is not odd for such a compact molecule to reach its equilibrium degree of association within **1** on the timescale of a few minutes.

Taking all of this into account, there seems to be enough evidence to show that one molecule of OsO_4 binds inside **1** forming a complex with a structure similar to that shown in Figure III.12.

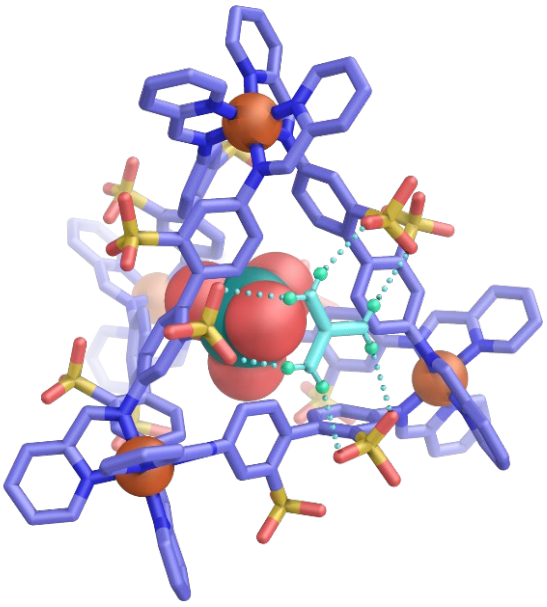

Figure III.12—Model of the hypothesized structure of the $OsO_4 \subset$**1** host-guest complex. One Gdm^+ ion (green) is shown capping one of the faces (with possible H-bonds dashed). The relative orientation of the guest molecule is arbitrary.

III.3 Binding of benzene

The motivation behind the study of the binding of benzene was that of finding a suitable molecule to displace the OsO_4 from the cage's cavity without further interaction. Benzene, being a hydrophobic and relatively small disk shape molecule, had been found to bind with moderate strength to $(NMe_4)_4$**1** ($K = 3.0\times10^3\ M^{-1}$).[89] If successful, the OsO_4/Bzn/**1** (**OB1**) system would provide a way of indirectly manipulating (albeit irreversibly) the catalytic activity of OsO_4 with an alkene.

III.3.1 Bzn⊂Gdm$_4$**1** ^{1}H NMR characterization

The binding of benzene (**Bzn**), similarly to the binding of OsO_4, is observed as a slow exchange interaction at the NMR timescale. The chemical environment itself does not present much change from that observed in the previous work using $(NMe_4)_4$**1**[87] and so the spectrum obtained (in Figure III.13) is quite similar.

Table III.6 shows the signal data extracted from the spectra below. Note that benzene causes overall much larger changes in chemical shift than OsO_4. This change is especially visible in the signals with source nuclides near the vertex part of the cage; the $\Delta\delta$ of H-i is 0.89 ppm, more than ten times that caused by OsO_4. One can conjecture that the wider molecule distorts the coordination at the vertices more than the smaller one thereby further altering polarization of the ligands.

Another interesting feature of the Bzn⊂Gdm$_4$**1** complex is the chemical shift of the protons in the guest itself: it is lowered in frequency by 1.20 ppm. The protons end up more shielded than would be in any solvent. This high shielding is most likely due to the orientation of the benzene molecule relative to the aromatic rings in the ligand's bridge. Even if tumbling, the hydrogen atoms of the guest should mostly be in shielding zones above the middle of the ligand's rings. It does not seem preposterous to imagine the benzene guest molecule in a placement such that perpendicular π-stacking is favoured with some of the ligands' rings.

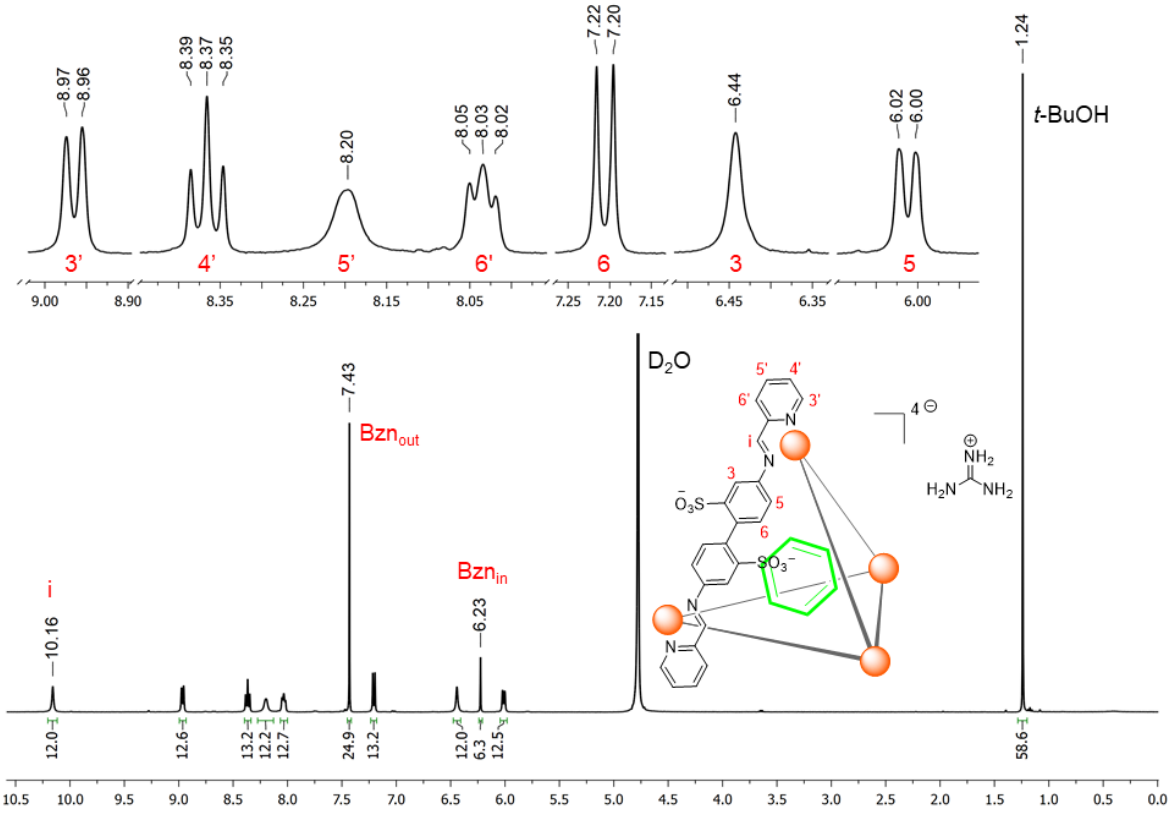

Figure III.13—Labelled ^{1}H NMR spectra of Bzn⊂Gdm$_4$1, with 1.13 mM of total host and 5.79 mM of total benzene and 7.31 mM of *t*-BuOH (400 MHz spectrometer).

Table III.6—Observed ^{1}H NMR signals of Bzn⊂Gdm$_4$1 (400 MHz spectrometer) and variation in δ from the empty cage. [a]Constant found by deconvolution. [b]Relative to free benzene.

^{1}H nuclide	N° nuclides	δ / ppm	Multiplicity	*J* / MHz	Δδ / ppm
3	12	6.44	br s	—	0.02
5	12	6.01	d	8.2	0.22
6	12	7.21	d	8.0	0.10
3'	12	8.96	d	7.6	0.29
4'	12	8.37	t	7.8	-0.02
5'	12	8.20	br s	—	0.45
6'	12	8.03	t	6.5 [a]	0.52
i	12	10.16	s	—	0.89
Bzn$_{in}$	6	6.23	s	—	-1.20 [b]

III.3.2 Bzn⊂Gdm$_4$1 binding titration

With the greater imine proton shift, the titration of a solution of Gdm$_4$**1** with benzene was even easier to follow than that with OsO_4 (see Figure III.14), with the advantage that there is no reactivity between host and guest. Additionally, benzene can be monitored directly by ^{1}H NMR. The execution of a titration as planned, however, turned out to be a bit more difficult than expected due to two factors: the relatively slow kinetics of benzene intake and its volatility.

To save time to anyone attempting a similar procedure, the author strongly recommends the use of NMR tubes of uniform length. As it turns out, the headspace in the tube greatly influences the equilibrium benzene concentration in the solution, with this changing significantly with temperature. This causes the nicely planned progression along a titration curve to end up in shambles with irregular spacing between points. Also, since the equilibrium of guest intake is reached much more slowly, big changes in temperature take the system out of equilibrium as more benzene either evaporates or condenses in the headspace above the solution.

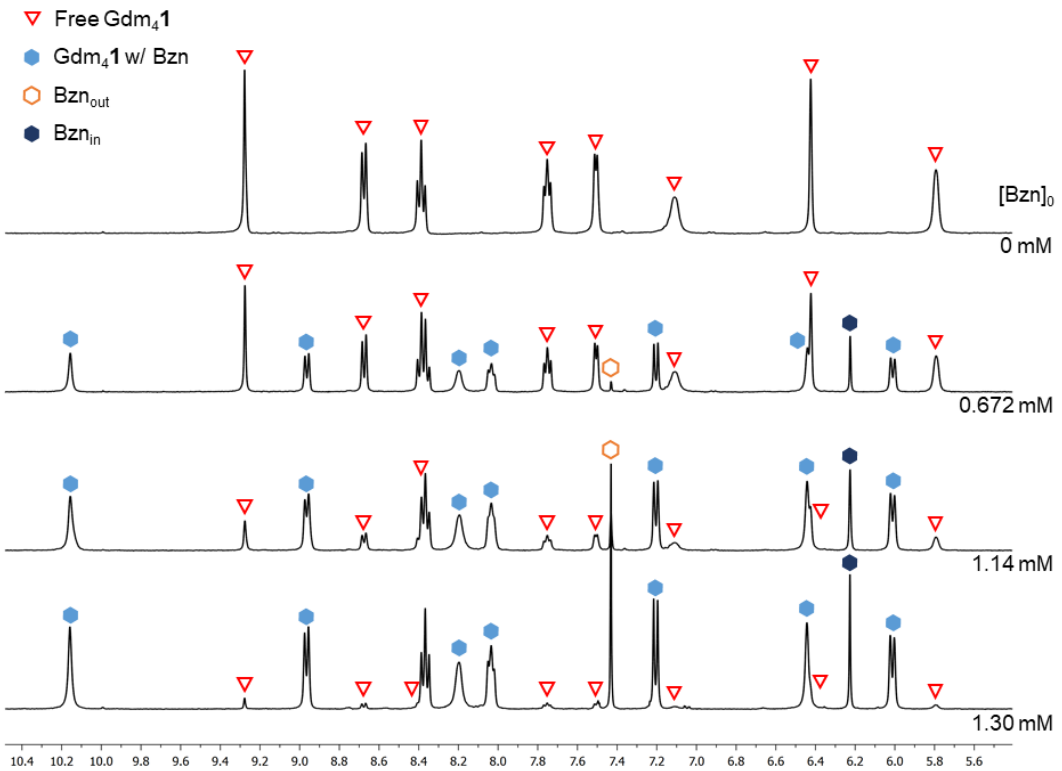

Figure III.14—^{1}H NMR spectra representative of the progress of a titration of Gdm$_4$1 with benzene.

Moreover, using a greater number of tubes helps in the throughput since the equilibration takes half a day. Mind that heating will not help! From experience, the presence of big guests tends decrease the cage's stability which only degrades with increasing temperature. Besides, upon cooling, the solution would again be out of equilibrium.

As to the model used in this case, it should be possible to use a simpler binding isotherm model, namely the hyperbolic model. Nonetheless, the complete isotherm binding model still showed better results due to it accounting for total concentration variations in the system.

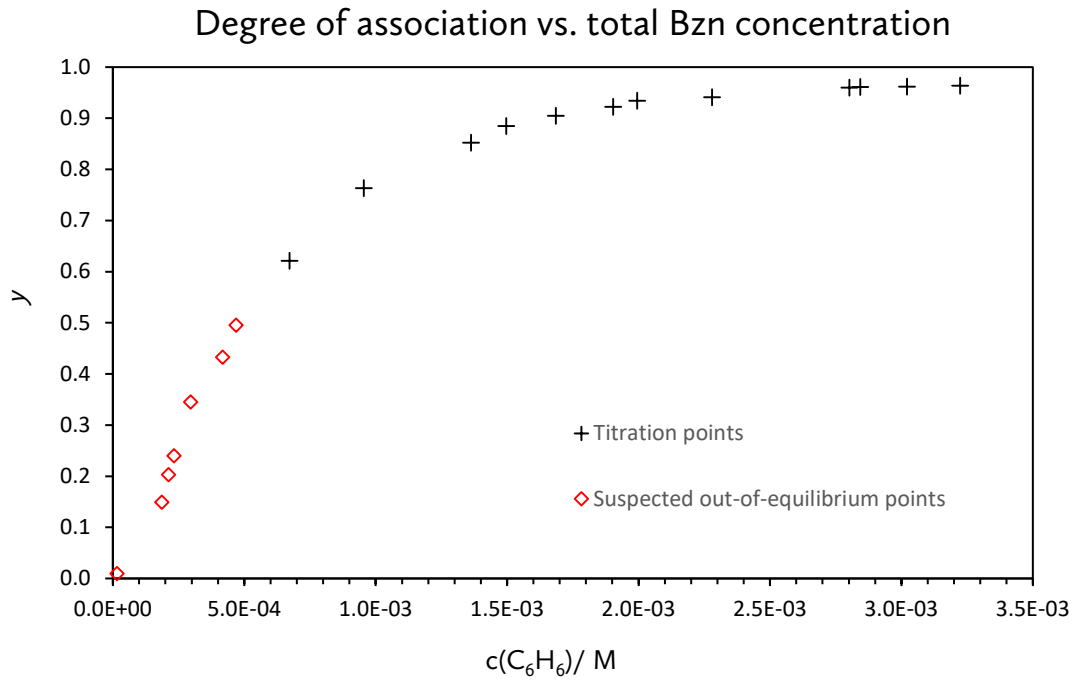

Figure III.15—Plot of the measured degree of association against the total concentration of benzene as measured by NMR. The red diamonds indicate the points which were found to be out of equilibrium. These were not used in the final regression.

Table III.7—Summary of the parameters from 13-point Bzn⊂1 titration curve regression.

	Value	Std Error	95% LCL	95% UCL	Adj. R^2	DF
K / mM^{-1}	14.80	0.407	13.91	15.68	0.99798	12

The data points obtained in the best run are plotted in Figure III.15. A first trial at fitting lead to a regression with severe biases in its residuals with a poor fitting (see Chapter VIIB.2.1 for statistics). By analysing the trends in the data points, it was possible to conclude that the first 7 solutions measured were likely out of equilibrium (with more benzene in solution that that evidenced by the measured degree of association). Removing the points sequentially resulted in a gradual improvement of the fitting. Removal of the sixth point deteriorated the fit. The final regression therefore used 13 points and its parameters are presented in Table III.7 with the isotherm plotted in Figure III.16.

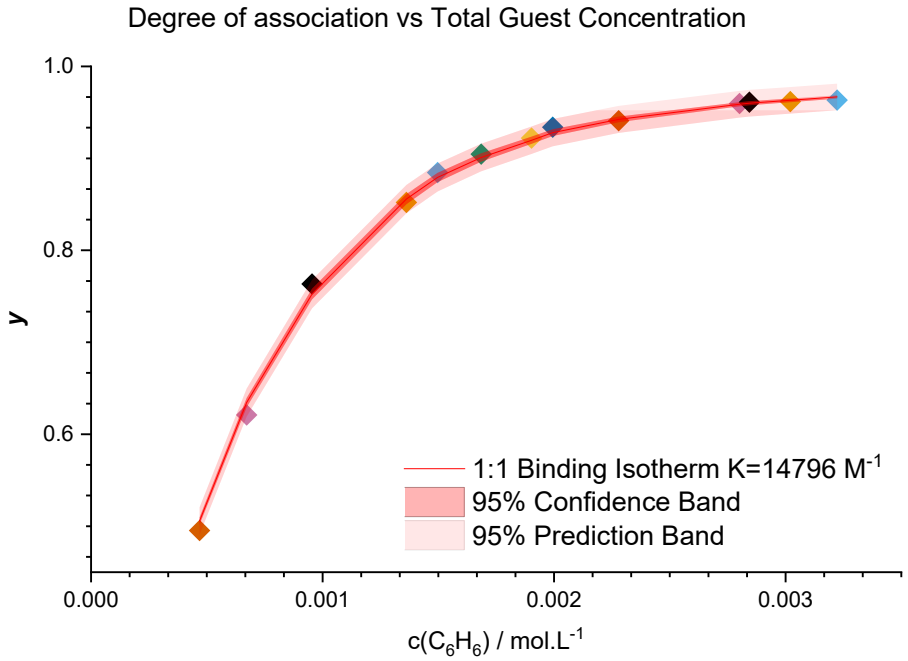

Figure III.16—Plot of the output from Origin's non-linear regression. Points of the same colour are measured from the same tube with different amounts of titrant.

The final regression shows a good adjusted coefficient of determination, quite low error and well distributed residuals. Therefore, there is a high confidence in the result obtained.

III.3.2.a Procedure

The titrant was prepared by saturating a solution of Gdm_4**1** 1 mM with a droplet of benzene overnight. 500 µL aliquots of a stock solution of Gdm_4**1** 1 mM, the titrate, were transferred into 13 NMR tubes. After a first series of spectra was registered, aliquots of guest were added to each tube aiming at steps of 0.2 equivalents of guest (see Table B.3

in Section Chapter VIIB.2 for solution data) . Evaporation led to the range of degree of association covered being shorter than planned and so a second aliquot was added to the 6 tubes with greater amounts of benzene. After each addition the tubes were left tumbling at room temperature for at least 12 hours before measurements.

III.3.3 Bzn⊂Gdm$_4$**1** intake kinetics

Measuring the intake constant of Bzn⊂**1** was straightforward since the rate is slow enough to allow for a point-by-point measurement. Figure III.17 shows the acquired data points plotted in order to visualize the variations of the species concentration. Note that the first point in the concentration of benzene is an outlier. This is probably due poor initial mixing of the solution. Also, as field shimming was far from perfect throughout the experiment, initial distortion due to bubbles forming can be the cause. Anyway, the measured concentration quickly stabilised afterwards. Owing to this, only the following seven points were used in the regression for estimating the intake rate constant.

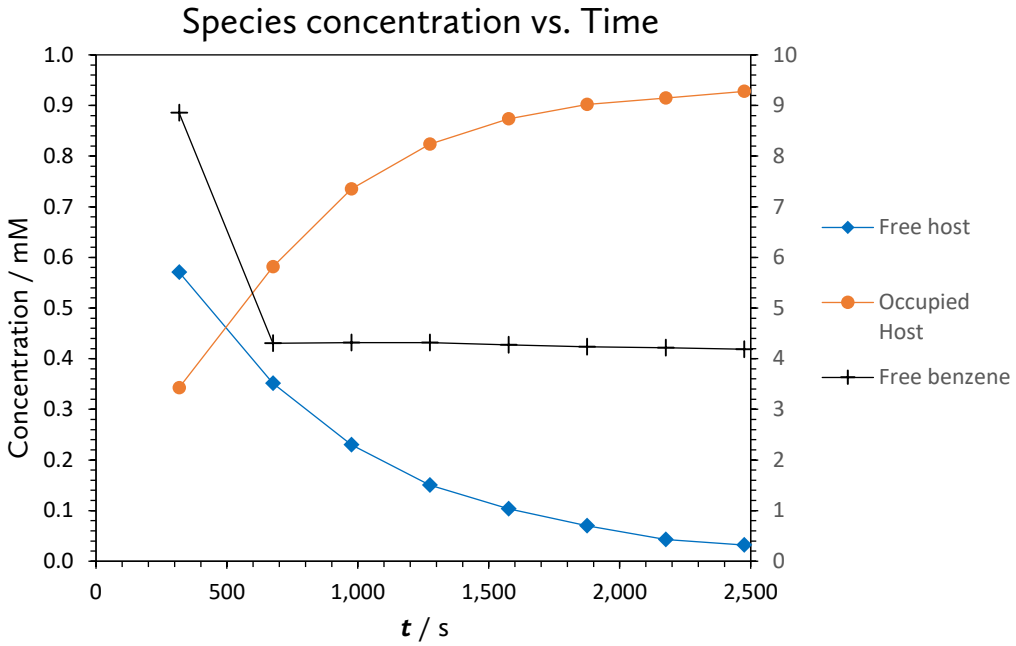

Figure III.17—Plot of the concentration of the species present in a benzene intakes kinetics experiment (see Table B.5 for data). Free benzene concentration (crosses) plotted on secondary scale.

For the regression, using the fraction of free cage (1-*y*) as the dependent variable is much more convenient as its initial value is 1 (by definition). With the data imported into

Origin, the regression was done using the inbuilt exponential decay function with a life-time constant $t_1 = k_{app}^{-1}$; The amplitude was fixed at 1 and the offset at 0. The resulting decay curve is plotted in Figure III.18. The regression parameters are summarized in Table III.8.

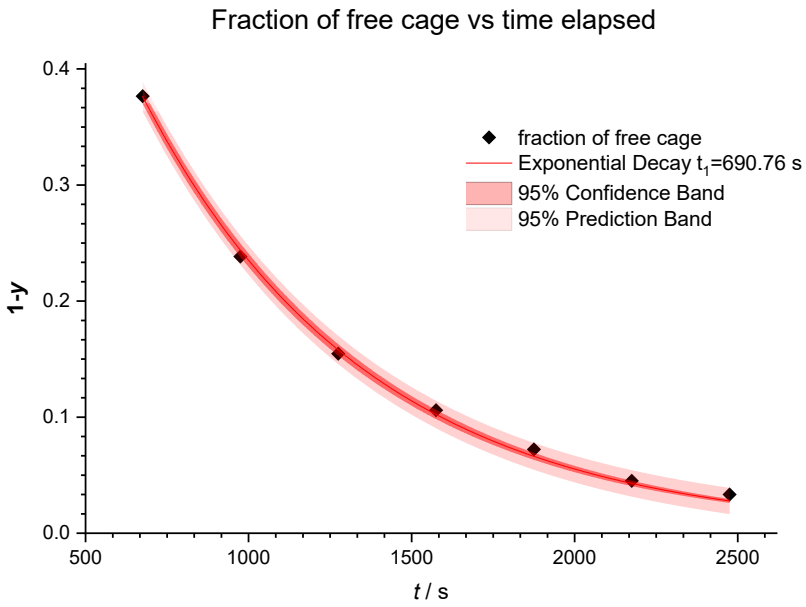

Figure III.18—Plot of the exponential decay curve fitted to the experimental data of benzene entering Gdm$_4$**1** with corresponding confidence and prediction bands.

Table III.8—Summary of regression parameters of Bzn⊂Gdm$_4$**1** intake.

	Value	Std Error	95% LCL	95% UCL	Adj. R^2
t_1 / s	690.76	4.69	679.27	702.24	0.99863
k_{app} / $s^{-1} \cdot 10^3$	1.4477	0.00984	1.4240	1.4722	

With an excess of guest, the initial rate allows to estimate the second order intake reaction constant from the apparent decay constant. Writing the rate law as

$r = k_{in}[G]_0[H]_0$, with $r = k_{app}[H]_0$, then $k_{app} = k_{in}[G]_0$.

It is assumed that the initial guest concentration is equal to average guest concentration measured over the fitted points.

$$\therefore\ k_{in} = \frac{k_{app}}{[G]_0} = \frac{1.4477\times10^{-3}}{4.264\times10^{-3}} = 0.3395\ \mathrm{M^{-1}s^{-1}}$$

Duly propagating the standard errors:

$$\frac{SE(k_{in})}{k_{in}} = \sqrt{\left(\frac{SE(k_{app})}{k_{app}}\right)^2 + \left(\frac{SE([G]_0)}{[G]_0}\right)^2} = \sqrt{\left(\frac{9.84 \times 10^{-6}}{1.4477 \times 10^{-3}}\right)^2 + \left(\frac{19.4 \times 10^{-5}}{4.264 \times 10^{-3}}\right)^2}$$

$$\Leftrightarrow SE(k_{in}) = 0.0460 \times 0.3395 = 0.0156\ \mathrm{M^{-1}s^{-1}}$$

III.3.3.a Procedure

A 1.0 mL aliquot of Gdm$_4$**1** (0.96 mM) was introduced into an NMR tube. The tube was sealed with a rubber septum and the condition of the solution verified with a preliminary NMR scan. 1.6 µL of benzene were injected and the solution gently stirred. An initial spectrum ^{1}H NMR was measured at 317 s after injection, spectra were then measured at 300 s intervals as a pseudo-2D NMR experiment for accurate timing. The data obtained are presented in Table B.5 and in Figure III.7.

III.3.4 Discussion

The binding of benzene, as expected due to previous work in a similar host, bound to Gdm$_4$**1** in a 1:1 ratio with the titration curve agreeing quite well with a 1:1 binding model isotherm and satisfactory regression statistics leading to a high confidence in the results. With an average concentration of host of (1.16 ± 0.04) mM, the estimated binding constant at 25°C is (14.8 ± 0.4) mM^{-1}. On that account, benzene is a strong binding guest of Gdm$_4$**1**. It is noteworthy that the binding constant of Bzn⊂Gdm$_4$**1** is almost three times as that of Bzn⊂(NMe$_4$)$_4$**1**[87]. This is probably due to the enhancement of the hydrophobic effect caused by the guanidinium ions. As more Gdm$^+$ ions bind to the faces of **1**, the contribution of the the non-classical hydrophobic effect to the binding event increases (see section I.3.6.a). Thus, the Gdm$^+$ ions may be considered as modulators of the cavity's 'effective curvature' from the perspective of solvent interactions. This hypothesis could be tested with calorimetric titration experiments.

The intake rate of Bzn⊂Gdm$_4$**1** was expected to be slow and the experimental results agree. The second order rate constant for the intake reaction was determined as

(0.34 ± 0.02) $M^{-1}s^{-1}$ which is, surprisingly, significantly higher than that reported by *Smulders et al.*: (0.158 ± 0.01) $M^{-1}s^{-1}$ for the Bzn⊂$(NMe_4)_4$**1** complex.[87]

The contrary was expected as the Gdm^+ ions should hinder the entrance of the guest. The author argues, however, that the value reported could well be inaccurate. This is because the value of k_{app} reported for that complex, (0.362 ± 0.02) $\times 10^{-3}$ $M^{-1}s^{-1}$ is slightly higher than that obtained in this work, which is anticipated. But, the striking difference is in the initial guest concentration with that assumed by *Smulders et al.* being the saturation concentration of benzene in solution. Unless the authors used a vast excess of benzene to ensure saturation (which prevents homogeneity of the solution), it seems unreasonable to assume that state. However, if the difference in values came to be confirmed its causes would be quite interesting to investigate.

III.4 Binding of DHF

One of the objectives of the work leading to this dissertation was to explore the dynamics of a system in which two reactive guests (one of them a catalyst, OsO_4) would compete for the same host. Hence, a suitable compound had to be found that had the following properties: reasonable solubility in water, reactivity towards OsO_4 and would bind to **1**.

A search for such a compound previously done in the research group led do the finding of 2,5-dihydrofuran (**DHF**). It is hydrophilic enough to be soluble in water in the 100 mM range but still displayed a binding interaction with Gdm_4**1** (as previous work with the NMe_4^+ salt, furan and tetrahydrofuran would indicate through). Most importantly, DHF possesses a double bond capable of reacting with OsO_4. Secondly, but no less important, the molecule is symmetric as is the product of its dihydroxylation, (3*R*,4*S*)-tetrahydrofuran-3,4-diol (**DHOF**). This greatly simplifies the NMR spectra. The reference spectra for these compounds can be found in the appended Sections Chapter VIIA.3 and Chapter VIIA.4. Lastly, DHOF is too polar to bind to **1**, which further simplifies the OsO_4/DHF/**1** (**OD1**) system.

To understand interactions in a more complex system, one must first characterize the more elementary host-guest interactions in the DHF⊂Gdm_4**1** complex. The results are presented in the following sections.

III.4.1 DHF⊂Gdm$_4$1 ^{1}H NMR characterization

As with the other guests, DHF exhibited a binding interaction with **1** on a slow exchange regime in the NMR timescale. The ^{1}H NMR spectrum of DHF⊂Gdm$_4$**1** can be seen labelled in Figure III.19. As can be observed, some signals overlap in this particular spectrum. Nevertheless, it is possible to discriminate them by monitoring their change throughout the titration with the guest (see Figure III.20). The interpretation of the spectra is only made more difficult with the presence of some free host and excess guest. As expected, the changes in chemical shift upon DHF intake (showed in Table III.9) are intermediate between those of OsO_4 and benzene.

Concerning the signals of DHF inside the cage, similarly to benzene, it seems the cage shields the nuclides from the bulk field. While there is reasonable certainty as to the signal from H-β_{in} due to its clear isolation and relative integration, the signal from H-α_{in} is harder to assign. Surely, it should be at a lower chemical shift that H-α_{out} (4.62 ppm).

There is but one significant group of signals in that region. Then the signal at 3.45-3.66 ppm is quite close do double that of H-β_{in} (counting with a possible ethanol contamination that was found in the Gdm$_4$1 stock and integrated to around 0.9 across all samples). While signal broadening makes it quite likely, the pattern is not what was expected given that H-β_{in} appears as a singlet. Nonetheless, it could be that the cage's cavity restricts the conversion between DHF conformers breaking the ring's pseudo-symmetry in the NMR timescale. This would explain the complex pattern since the nuclides in the ring would form an ABX spin system.

Notice in Figure III.19, that the free DHF's H-β signal overlaps with the complex's H-5 signal. Initially, using the sum of those signals seemed like the best possibility. The compound concentrations would be easily calculated without having a nearby signal biasing the result. Yet, it was found that, if the shimming quality were closely controlled, the concentration of free DHF could be monitored directly through the H-α signal without degrading accuracy while increasing precision (since uncertainties would not accumulate).

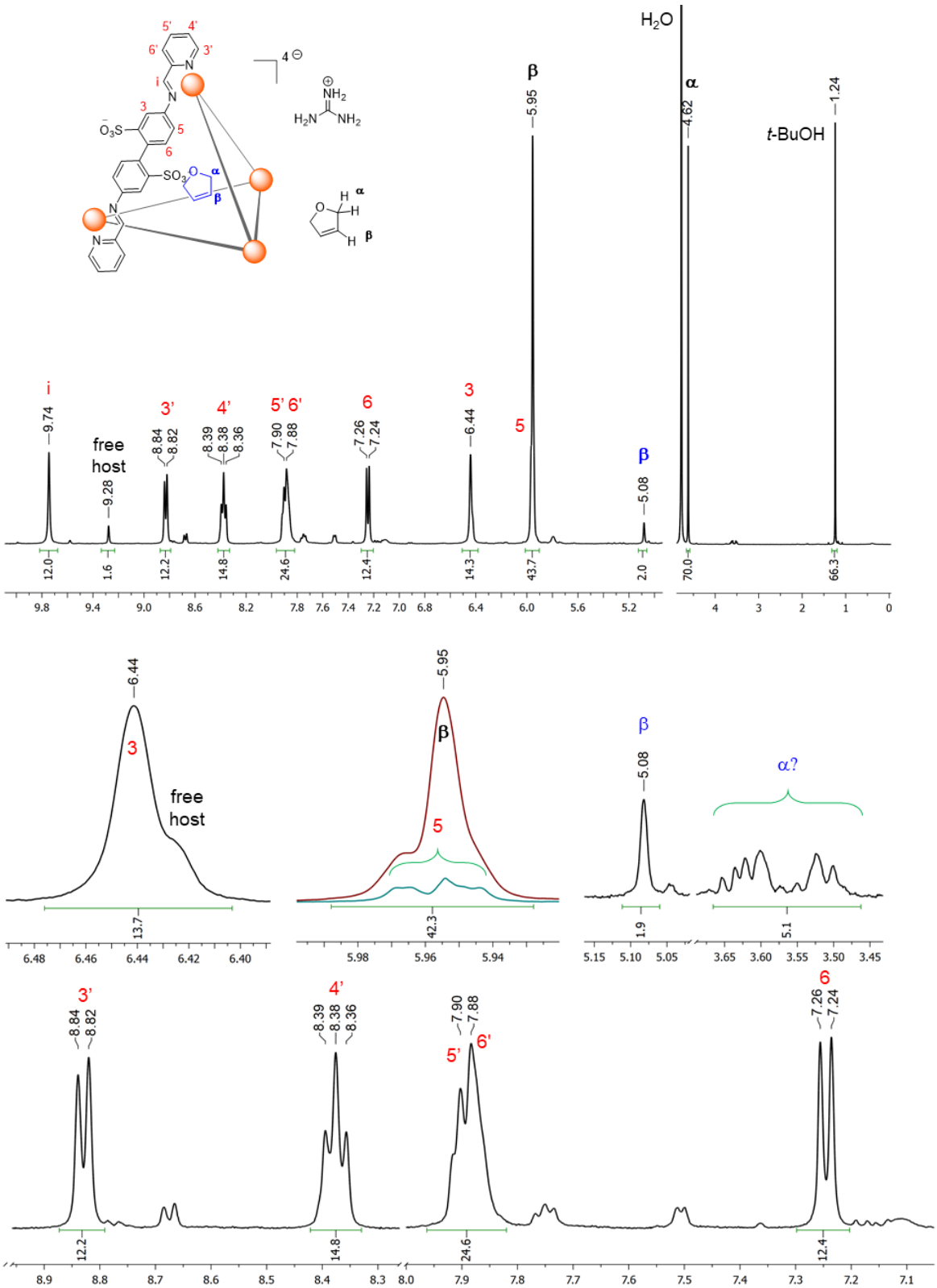

Figure III.19—Top: labelled ^{1}H NMR spectrum of DHF⊂Gdm$_4$1, with 0.96 mM of total host, 5.79 mM of total DHF and 15.4 mM of *t*-BuOH (400 MHz spectrometer). Bottom: zoom of the same spectrum; to evidence the H-5 multiplet, the section around 5.95 ppm is overlayed with a spectrum from a mixture with 1.75 mM of DHF (in blue). Mind that vertical scale different between sections.

Table III.9— Observed ^{1}H NMR signals of DHF⊂Gdm$_4$1 and variation in δ from the empty cage. [a]Relative to free DHF.

^{1}H nuclide	Nº nuclides	δ / ppm	Multiplicity	*J* / MHz	*Δδ* / ppm
3	12	6.44	s	—	-0.67
5	12	5.95	m	—	-0.47
6	12	7.25	d	8	1.46
3'	12	8.83	d	7.7	0.16
4'	12	8.37	t	7.5	-0.02
5'	12	7.90	m	—	0.15
6'	12	7.87	m	—	0.36
i	12	9.74	s	—	0.47
β	2	5.08	s	—	-0.87[a]

III.4.2 DHF⊂Gdm$_4$1 binding titration

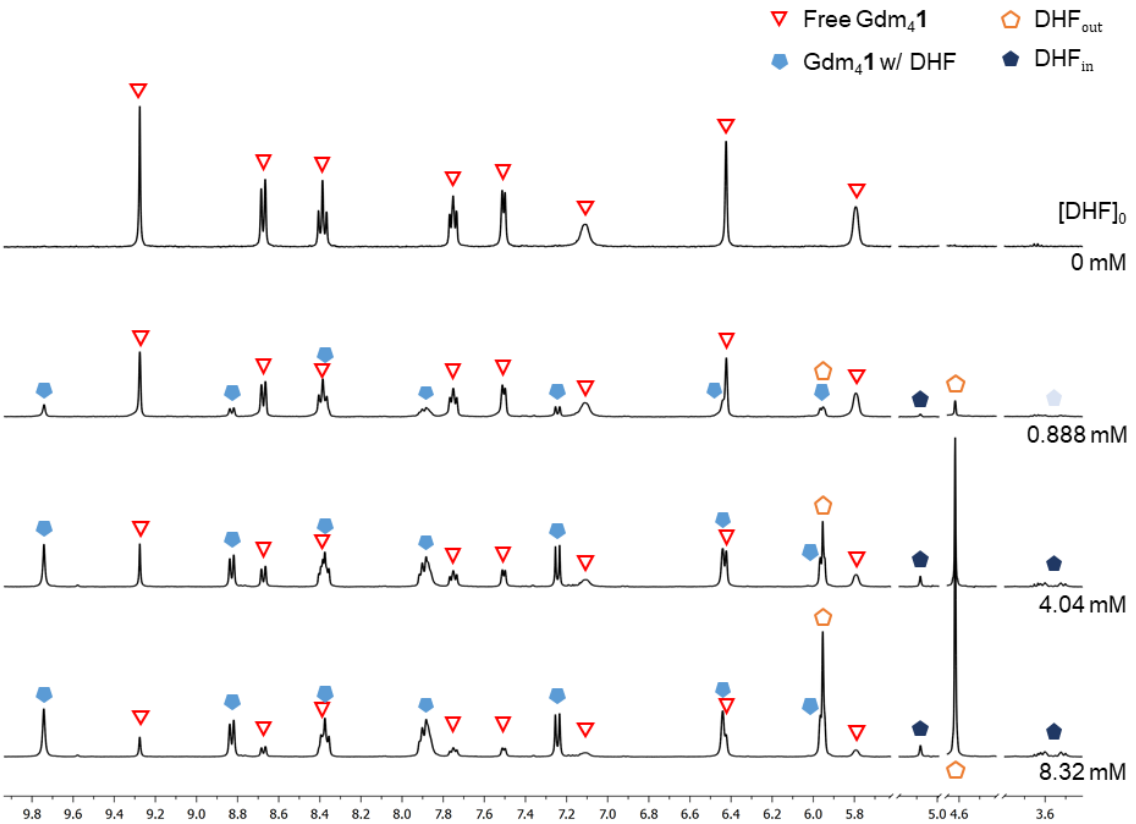

Figure III.20—Representative ^{1}H NMR spectra of the progress of a titration of Gdm$_4$1 with DHF (400 MHz spectrometer).

As with benzene, DHF is quite volatile. Fortunately, also like benzene, DHF can be directly monitored by NMR eliminating the need for careful concentration control. The method for binding constant determination was thus quite similar.

Being a bigger issue than expected, spectra that presented unacceptable line shapes (due to bad shimming) were immediately discarded. The small steps in guest addition enable removal of several data points that present a large deviation without compromising the coverage of the titration curve range. The isotherm model to be used was the same as for the benzene titration and for the same reasons.

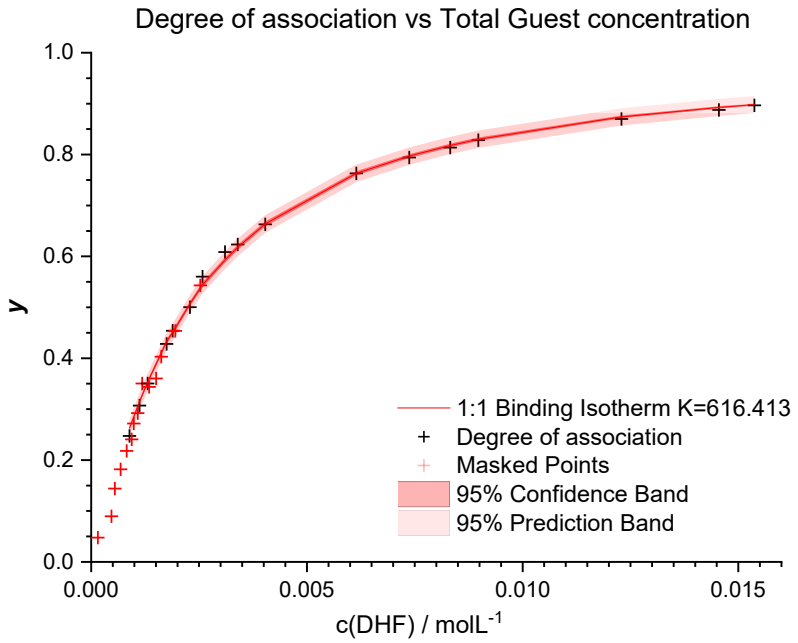

Figure III.21—Plot of the measured degree of association against the total concentration of DHF along with the output from *Origin*'s non-linear regression.

Table III.10—Summary of the parameters from DHF⊂Gdm$_4$**1** titration curve regression.

	Value	Std Error	95% LCL	95% UCL	Adj. R^2	DF
K / mM^{-1}	0.61641	0.00685	0.60190	0.63093	0.99866	16

After processing the data points, the final regression used 17 of them. The coefficient of determination is reasonable as is the distribution of residuals, albeit with a detectable trend (these are plotted in Figure B.7).

III.4.2.a Procedure

The titrant, a stock solution of guest, was prepared by dissolving 20.0 µL of DHF in D_2O in a 2 mL volumetric flask, the DHF concentration was 130 mM. 600 µL aliquots of Gdm_4FC stock solution (1 mM) were put in five different NMR tubes. A first series of spectra was registered before addition of any guest. The additions to the tubes aimed at intervals of 0.2 eq of guest in between data points until at least 90% degree of association. An equilibration period of at least 1 h was allowed (shaking the tubes occasionally) before taking any measurement. The solution data are presented in Table B.6. The points obtained are plotted in Figure III.21.

Bad signal line shape (due to poor shimming quality) was a unexpected issue with several initial samples. Noting that DHF solutions appeared cloudy for several minutes after preparation, it was decided to extend the equilibration period to 6 h.

III.4.3 DHF⊂Gdm_4**1** binding intake kinetics

The kinetics of DHF was another challenge to follow and the work here forth presented should not be regarded as final. Homogeneity of DHF solutions had already proved an issue since the study of the equilibrium behaviour with Gdm_4**1**. The worst was yet to come at the hands of the experiments on intake kinetics!

On the one hand, the best way to obtain a homogenous solution is to add everything in a small vial with a magnetic stir bar and let it stir for a few seconds. The reactants however, eternally impatient, do not wait for one to inject their mixture into the NMR tube and the cage might be saturated by the time the first measurement is done. On the other hand, runs in which the addition was done directly into the NMR tube besides the spectrometer achieve poor homogeneity and poor shimming due to all bubbles trapped due to vigorous agitation* with changes in concentration being overwhelmed by changes in signal quality.

* Both the problem of bubbles sticking to the tube's wall and the problem of homogeneity, to a certain extent, are easily solvable with the placement of a small sonicator bath nearby the spectrometer.

The data points obtained during the best run are plotted in Figure III.22. As evidenced, both the number of points and the range of variables covered are low. A non-linear regression of an exponential decay model would need two parameters (to estimate the initial amplitude due to uncertainty on the true "start" of the reaction); 4 points allow for only 2 degrees of freedom with a high dependency between parameters. Those points can give, nonetheless, an approximation of the reaction rate over a small period through a linear regression (of the form $1-y=a+bt$).

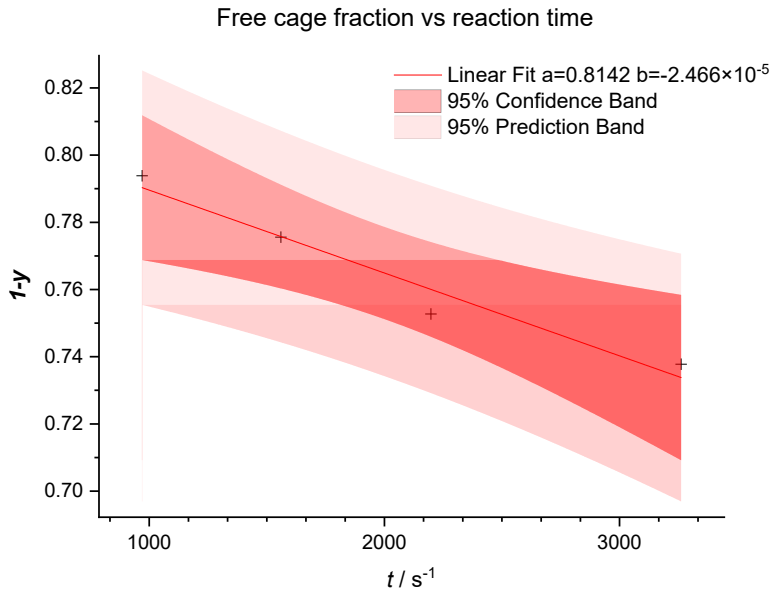

Figure III.22—Plot of a linear regression fitted to the experimental data of DHF entering $Gdm_4\mathbf{1}$ with corresponding confidence and prediction bands.

Table III.11—Summary of $1-y=a+bt$ regression parameters of DHF⊂$Gdm_4\mathbf{1}$ intake.

	Value	Std Error	95% LCL	95% UCL	Adj. R^2	DF
a	0.81423	0.00815	0.77916	0.84931	0.93349	2
b / s^{-1}	-2.466×10^{-5}	3.76×10^{-6}	-4.082×10^{-5}	-8.499×10^{-6}		

From Table III.11, the conclusion is that the fit is quite poor, but an estimate of the rate constant can still be obtained to guide future work. Using the average species concentration and average rate over the monitored time:

$$r = -[H]_0 b = k_{in}[G]_0[H]_0 \therefore k_{in} = -\frac{-2.466\times10^{-5}}{1.638\times10^{-2}} = 1.505\times10^{-3}\ M^{-1}s^{-1}$$

Using the corresponding mean standard deviations and propagating the variables' uncertainties:

$$\frac{SE(k_{in})}{k_{in}} = \sqrt{\left(\frac{SE(b)}{|b|}\right)^2 + \left(\frac{SE([G]_0)}{|[G]_0|}\right)^2} = \sqrt{\left(\frac{3.76 \times 10^{-6}}{2.466 \times 10^{-5}}\right)^2 + \left(\frac{7.34 \times 10^{-5}}{1.614 \times 10^{-2}}\right)^2}$$

$$\Leftrightarrow SE(k_{in}) = 0.153 \times 1.505 \times 10^{-3} = 2.30 \times 10^{-4}\ \mathrm{M^{-1}s^{-1}}$$

III.4.3.a Procedure

A 600 μL aliquot of Gdm$_4$**1** (1 mM, [*t*-BuOH] = 4.40) was introduced into a 1 mL vial with a small stir bar. Then 1.0 μL of DHF were measured into the vial with fast stirring. After 10 s the solution was transferred into an NMR tube. An initial spectrum ^{1}H NMR was measured at 317 s after injection, individual ^{1}H NMR spectra were then measured at approximate 10 min intervals. The data obtained are presented in Table B.7.

III.4.4 Discussion

The binding strength of DHF⊂Gdm$_4$**1** is moderate and the weakest of all studied, with an association equilibrium constant of (6.16 ± 0.07) × 10^2 M^{-1}. This value is in the range expected for this kind of molecule in this kind of cage. Previous work *Smulders et al.* on (Me$_4$N)$_4$**1** found the association constants of THF and furan to be (5.7 ± 0.1) × 10^2 M^{-1} and (5.7 ± 0.1) × 10^3 M^{-1} respectively.[87] Despite the initial trouble in obtaining good quality data, the final results yielded a very good agreement with a one-to-one binding isotherm model with a very low error.

As with the binding strength, the second order rate constant for the intake reaction of DHF was expected to be between those of THF and furan for (Me$_4$N)$_4$**1**. The values of the latter are reported *Smulders et al.* as (8.3 ± 0.1) × 10^{-3} s^{-1}M^{-1} and (2.1 ± 0.3) s^{-1}M^{-1} respectively.[87] The value of k_{in} discovered for DHF⊂Gdm$_4$**1** is (1.5 ± 0.2) × 10^{-3} s^{-1}M^{-1}. This indicates, as anticipated, that the behaviour of DHF is much closer to that of THF than furan.

Chapter IV

Entertaining the guests

IV.1 The OsO_4/$Gdm_4$1+pentenol system

The simplest chemical system with OsO_4 functioning as a guest and as a catalyst is one were both the reactants and reactions products have no interaction with the cage. The idea behind such a system is to emulate the activation of an enzyme as the substrate becomes available, a possible signalling pathway in biochemical systems. With a reaction 'occupying' the catalyst is should gradually get out and, if reuptake is slow enough, it should be available until all the substrate is spent. At the end of the reaction, the OsO_4 would then return to its 'reservoir', simulating the self-inhibition that some bio-catalytical systems exhibit.

A suitable reactant had been found prior to this work. Pent-4-en-1-ol (**Pent**; reference ^{1}H NMR spectrum in Figure A.11) has all the desired properties: high solubility in water, does not present any observable interactions with **1** does its reaction product (see Figure A.12 and Figure A.14 for control experiments), is simple enough to monitor through ^{1}H NMR and should react well with OsO_4 to form pentane-1,2,5-triol (**DHOP**; reference spectrum in Figure A.13).[*]

Consequently, the catalysis' kinetics of the $Gdm_4$1/OsO_4/pentenol (**O1+P**) system was the first to be studied thus. Given the information gathered on the reactivity of OsO_4 towards alkenes (see section I.9), it was decided to use a bicarbonate buffer to prevent disproportionation of the Os(VI) species and to promote cycloaddition step.[†]

As for the final oxidizer, serving effectively as an Os re-oxidizer, the initial choice was obvious: trimethylamine *N*-oxide (**TMAO**); it is shown to be successful as re-oxidizer for the di-hydroxylation of alkenes while being perfect for NMR analysis since its signal is a single singlet. The same is true of its reduction product: trimethylamine (**TMA**).

---

[*] Pentenol, has the pesky tendency to oxidize and polymerize so care should be taken in stock preservation or else precious time could be wasted in preparing samples that will have abhorrent spectra.

[†] It was only after several experiments had been done that I realized, after concluding the research on the subject, that the low pH could actually be slowing down the catalyst turnover, however this actually proved useful in stabilizing the system and enhancing the dip in free OsO_4 concentration.

Yet, the formation of TMA is a major flaw: it forms adducts with OsO_4 by ligating to the Os atom. This is what makes it a good promotor of the catalyst, but it is an impediment to the use of TMAO in a supramolecular system if the goal is free OsO_4 at the end of the catalytic cycle. Trying to troubleshoot the system several experiments had been done with TMAO without observing the reuptake of OsO_4;* Unfortunately, it was only after those that TMA's behaviour was revealed and control experiments executed (see Section Chapter VIIA.9 for description).

The best alternative to TMAO as OsO_4 re-oxidizer is N-methylmorpholine N-oxide (NMMO, reference ^{1}H NMR spectrum in Figure A.16). The compound had only been excluded initially due to the added complexity of its ^{1}H NMR spectrum. Due to steric hindrance, it has a much lower constant for binding to the Os atom. Additionally, it did not show any interaction with the cage by NMR.

Still, alternative re-oxidizers were searched for. Ferric cyanide was unsuccessful, showing no hydroxylation of pentenol in the alkaline medium. A quite interesting alternative would have been the periodate ion. With an excess of periodate, the vicinal diol made by dihydroxylation can be cleaved into two aldehydes. The aldehyde can then participate in dynamic covalent bonding to form supramolecular structures enabling the design of systems with very interesting signal flows. As brilliant as the concept is, the presence of periodate proved too much even for such a sturdy cage as Gdm_4**1**; the cages NMR signals quickly start to broaden with presence of free ligand being noticeable in a couple of hours. Nevertheless, that idea could be useful in the development of other supramolecular/catalytic systems.

Subsequently, the investigation of the kinetics of the **O1+P** system and others that followed used NMMO as OsO_4 re-oxidant. To ease preparation of the solutions for experiments and increase consistency, it is recommended that the stock solutions of NMMO contain also the appropriate excess of $NaHCO_3$ (besides the *t*-BuOH standard).

In Figure IV.1 the concentrations of the host species are plotted against the reaction time in an experiment with the O1+P system. This was the best run executed both in terms of

* The phrase 'a day reading saves you a month in lab' never seemed more right.

data quality (they are typically much noisier) and in terms of the observation of a reuptake of OsO_4. As is shown, the dip in concentration of $OsO_4 \subset Gdm_4\mathbf{1}$ is quite small; the maximum variation was of just 0.05 mM with an average total host amount of (1.701 ± 0.007) mM. The degree of association shows a maximum variation of 0.02 which correlates to a maximum variation in concentration of free OsO_4 of 0.04 mM.

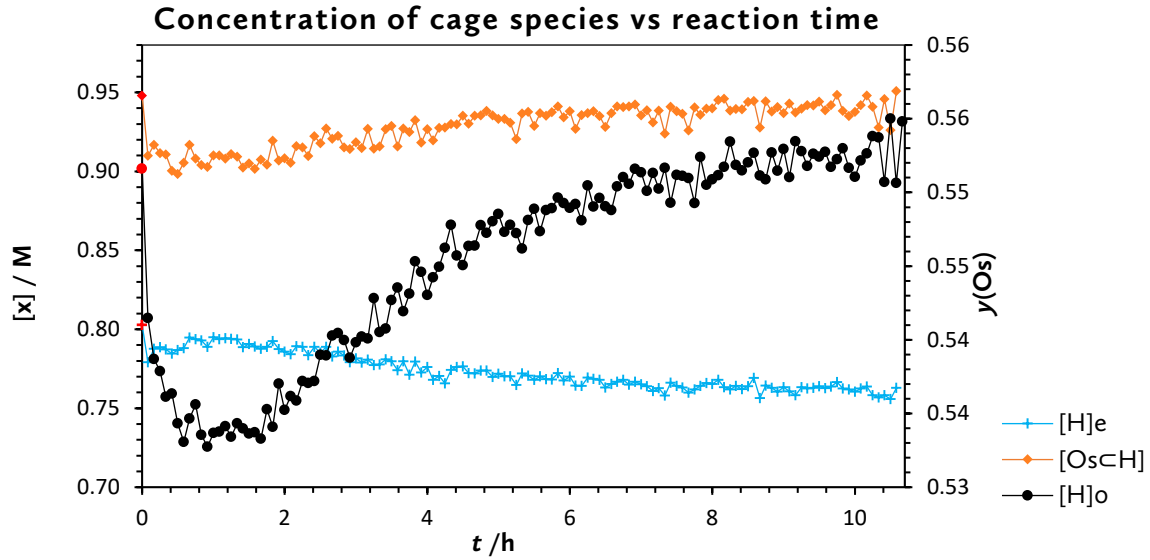

Figure IV.1—Speciation of $Gdm_4\mathbf{1}$ during a dihydroxylation reaction of the O1+P system as estimated by ^{1}H NMR. Degree of association, *y*(Os) concentration is plotted the secondary scale. The points highlighted in red concern the state before the addition of the pentenol solution.

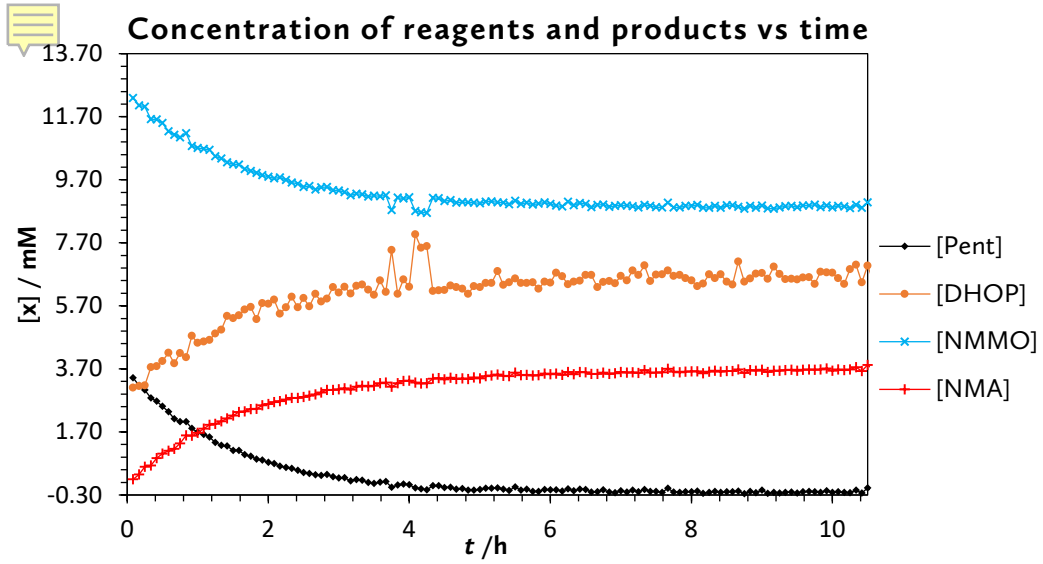

Figure IV.2—Concentration of dihydroxylation reagents and products in the O1+P system plotted against reaction time. Notice that the points at around 4 h that are anomalies of unknown origin.

IV.1.1 Procedure

A 1.00 mL aliquot of Gdm$_4$**1** stock (0.721 mM, [*t*-BuOH] = 3.896 mM) was introduced into an NMR tube. Then 2.90 mg of $NaHCO_3$ (34.5 nmol) along with 0.70 mg of NMMO (6.0 nmol) were added to the tube. Then 30.0 μL of OsO_4 stock (36.1 mM, [*t*-BuOH] = 3.896 mM) were added. A spectrum was registered to assure good condition of the solution. To start the reaction, 3.0 μL of pentenol stock (475 mM, [*t*-BuOH] = 2.021 mM) were quickly injected through the rubber lid and mixed with minimum air incorporation.

The first spectrum was acquired 300 s after injection and the following 127 spectra were acquired and a pseudo 2D experiment at 300 s intervals.

IV.1.2 Discussion

Attempts attain higher dips in degree of association resulted in very poor data. The limited solubility of the cage prevents trapping of a greater fraction of OsO_4 and quality of the data degrades quickly as cage concentration increases. An alternative would be to greatly increase the pentenol to OsO_4 ratio. However, the inefficiency of the terminal oxidizer starts to be significant as does the degradation of catalyst. Additionally, greater amounts of pentenol, NMMO and $NaHCO_3$ seriously degrade the quality of the spectra obtained. This is critical as many of the signals are close to each other.

Figure IV.2 shows the overall change in concentration of reagents. As can be seen, the estimated concentration of pentenol falls to very small negative values, this is a consequence of the automatic baselining algorithm used. No form was found to avoid this that was practical to apply in batch processing. Still, the change in pentenol concentration, along with the change of NMMO concentration are the most reliable, least noisy signals and the best estimators for the progression of the dihydroxylation.

Analysing the variations in reagent concentrations, it was found that they fit well to an exponential decay model of the form $y = y0 + Ae^{-tk}$. The regressions' statistics are shown in and the data points are plotted in the figures of Section Chapter VIIB.6. The simple exponential decay makes it appear as the kinetics is of first order. The most important observation, though, is that the k_{app} of pentenol is significantly higher than that

of NMMO. At the same time, the k_{app} of NMMO is not significantly different from that of DHOP. This is indicative that the rate limiting step in this system is the re-oxidation of the Os center.

Table IV.1—Summary of the regression statistics on the concentrations of dihydroxylation reagents and diol product in the OP+1 system.

parameter	Value	Std Error	95% LCL	95% UCL	Dependency	Adj. R^2	DF
pentenol concentration							
y0 / mM	-0.21245	0.00519	-0.22272	-0.20217	0.52567	0.99763	125
A / mM	3.8544	0.0209	3.8131	3.8956	0.52978		
k / h^{-1}	0.70718	0.00654	0.69423	0.72012	0.69635		
NMMO concentration							
y0 / mM	8.8429	0.00602	8.8310	8.8548	0.55490	0.99699	118
A / mM	3.6152	0.0222	3.5712	3.6591	0.52201		
k / h^{-1}	0.65624	0.00707	0.64225	0.67023	0.70252		
DHOP concentration							
y0 / mM	6.6127	0.0245	6.56418	6.66123	0.55484	0.95632	121
A / mM	-3.7998	0.0904	-3.9787	-3.6209	0.53260		
k / h^{-1}	0.6520	0.0274	0.5978	0.7062	0.70783		

From the information obtained, it is possible to assume that diol release follows immediately from oxidation. It seems reasonable to further assume that the OsO_4 is in fast equilibrium with the cage and that the cycloaddition of OsO_4 to the pentenol is irreversible. So, it seems as if the observed reaction can be modelled by a sequential addition mechanism as shown in the following scheme.

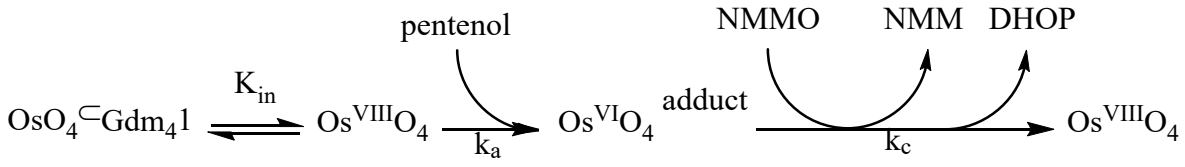

Figure IV.3—Scheme of the model dihydroxylation reaction in the conditions of performed experiment in the O1+P system.

With this model, the difference, at any point in time, between the consumption of pentenol and that of NMMO should be equal to the concentration of adduct. In this manner, considering the mass balance for OsO_4, the following expression should hold:

$$[OsO_4 \subset 1] + [OsO_4] + (\Delta[alkene] - \Delta[NMMO]) = c(Os)_0 \qquad \textbf{(VI.1)}$$

Using the knowledge of the binding constant of $OsO_4 \subset Gdm_4 1$ the concentrations can be estimated from the data. From the sum in the expression VI.1, subtracting the initial estimated amount of osmium in solution, $c(Os)_0$, results a 'mass balance residual' that is plotted against reaction time in Figure IV.4.

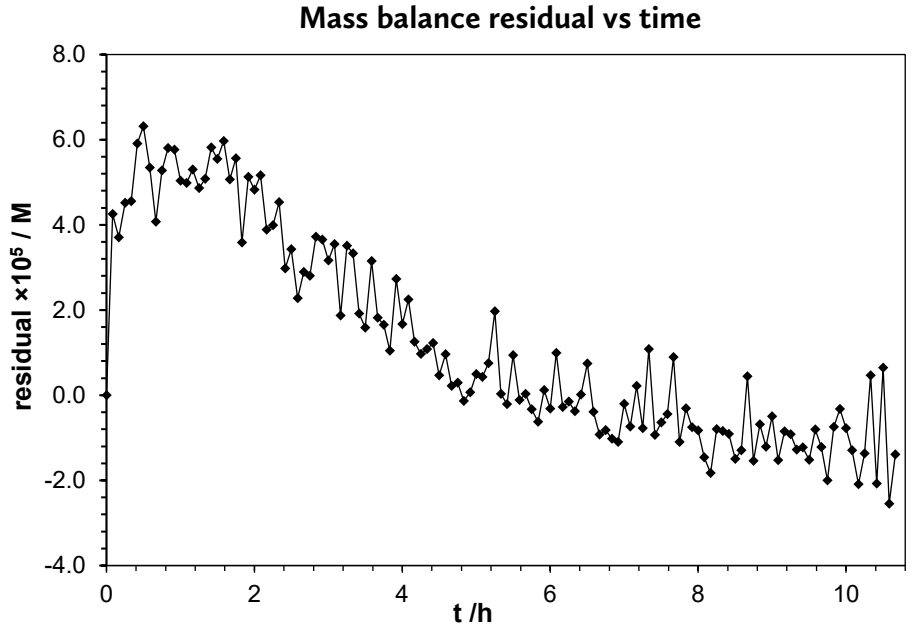

Figure IV.4—Residual of the mass balance from the equation VI.1 plotted against reaction time.

As can be seen from the plot above, the supposedly null mass balance residual presents a trend typical of the concentration of a catalytic intermediary. There are several ways the proposed model could be wrong. There could be a limitation of the reaction rate by the

pentenol addition step that cannot be ignored as the reactions comes to an end. However, the fact that it remains pseudo-first-order might have to do with the ability of the cage to effectively buffer the OsO_4 concentration. Furthermore, and most likely, the assumption of fast equilibration of OsO_4 does not hold for this turnover rate. This would cause the 'sensing' of free OsO_4 by the cage to essentially lag behind. Nevertheless, these are all but educated guesses. Without further experiments with carefully planned variations initial conditions, few conclusions can be drawn except that the proposed model presented is not an accurate representation.

It appears that the fast intake kinetics of $OsO_4 \subset Gdm_4$**1** does not result in a trapping effect as hoped; the effect is akin to an inhibitor, albeit an unusual one: we are used to observing a big catalyst being inhibited by a smaller moiety often bounded covalently. In this system, the smaller catalyst in bound within the inhibitor which appears to effectively compete for the 'binding' to the catalyst cycle (which might be reversible)

IV.2 The OsO_4/benzene/$Gdm_4$1+pentenol system

As further complication to the O1+P system is to add another inert guest into the mixture. The OB1+P systems achieves that with benzene. As referred before, the goal of experimenting with this system was to demonstrate the ability of a host-guest system being used to regulate a catalytic system with a 'orthogonal signal' (not chemical interfering with the catalyst nor reagents).

The experiment was performed with four tubes with different amounts of benzene added. Since the conditions turned out to be slightly different between tubes, Figure IV.5 shows the fraction of total pentenol plotted against time as a better way of comparison.

It is obvious that the amount of benzene added influenced the reaction rate; the greater the amount of total benzene in solution the faster the reaction. Although, the run with the highest amount of benzene seems to have been slightly slower and there is no apparent reason for this. A control experiment was done and showed that there is no influence of benzene in the dihydroxylation kinetics if no cage is present.

While the trend can be noted, quantitative analysis of the results cannot be done. The OB1 system was out of equilibrium due to the slow kinetics of benzene intake. This

makes the concentration of available host highly variable during the experiment and, consequently, that of the available catalyst. Further characterization of the system should be done, with higher temporal resolution and the execution of true replicate essays. Detailed investigation of the initial reaction rate period should detect an induction period where there is an acceleration as the amount of free guest increases as benzene slowly occupies the cage. With more good quality data, differential analysis would be a powerful tool to extract more information on the system.

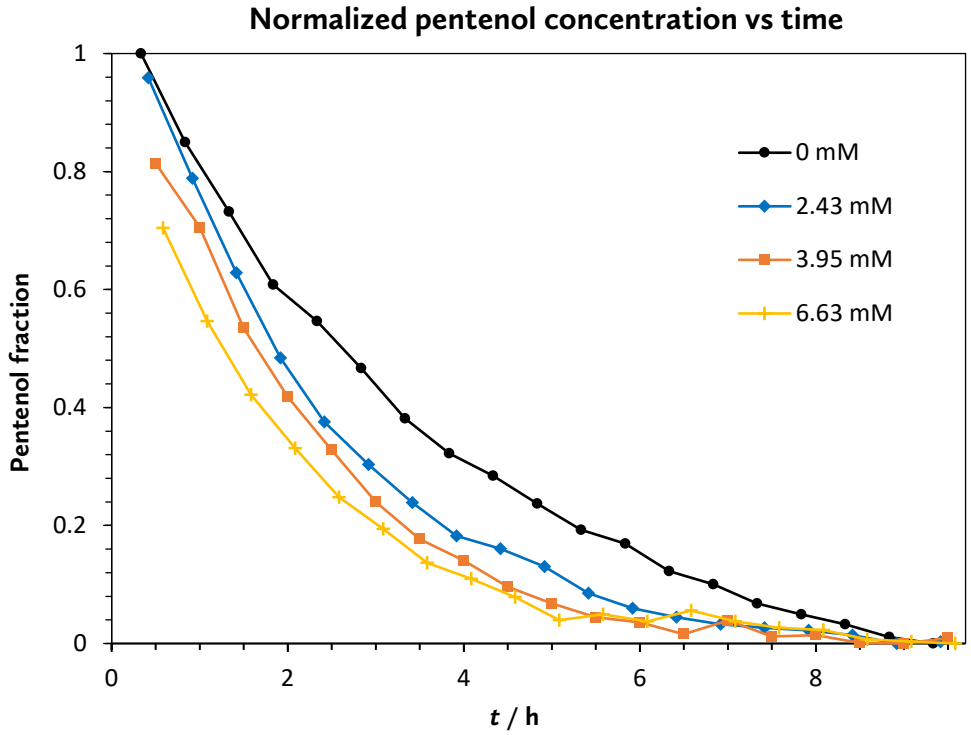

Figure IV.5—Plot of the pentenol concentration, normalized against the maximum measured, against time since injection for each tube with the indicated initial total benzene concentrations.

IV.2.1 Procedure

To four NMR tubes were added the following: 1.00 mL of Gdm_4**1** solution (0.981 mM), 110 µL of NMMO solution (105.9 mM, with [$NaHCO_3$] = 116.3 mM) and 35 µL of OsO_4 solution (25.5 mM). The condition of the solutions was verified by the acquisition of a first series of spectra. Then, the 2nd (**b**), 3rd (**c**) and 4th (**d**) tubes were added 0.5 µL, 0.8 µL, 1.2 µL of benzene respectively; the 1st tube (**a**) contained no benzene. Then, 3 minutes later, 50 µL of pentenol solution (95.7 mM) were added, starting the reaction.

The first spectrum was taken from the first tube 10 minutes after injection. The sampling rate was 30 minutes with an offset of 5 minutes between tube sampling. The reactions were monitored for approximately 10 hours.

IV.3 The OsO_4/DHF/Gdm_4**1** system

Having proven the influence of an inert guest in the catalytic activity of OsO_4, the next step in increasing complexity of the system was to experiment on a system with an additional guest that was itself reactive. The OsO_4/DHF/$Gdm_4$1 (**OD1**) system achieves just that: DHF is both an alkene reactive towards OsO_4 and a guest. If the influence of DHF in the dihydroxylation kinetics is enough, the reaction should initially be self-promoting with the rate accelerating as DHF enters the cage.

Besides the issues already faced during the DHF⊂Gdm_4**1** titration, the data processing in the experiments on the OD1 system involves some arithmetic on the NMR signals to derive the reagents' concentrations. The most reliable signals in the presented case were those of NMMO and DHOF.

The data points of the best experiment are presented in Figure IV.6 and Figure IV.7 , the temporal resolution is course since various tubes were being monitored at the time of acquisition. For unknown reasons, it is also lacking three sampling moments at around 2 h, a critical moment in the dynamics. It is presented, nonetheless, as an example of the typical data quality obtained along the several experiments done trying to obtain some OsO_4 reuptake. Although other trials were done simultaneously with other concentrations, the data was even poorer with no additional information provided by them.

Figure IV.6 also shows very clearly a variation in the guest complex concentrations whose shape is slightly different from that found in the O1+P and OB1+P systems; the reuptake of Os seems almost linear. Still, from this one experiment very little insight is gained into the unique dynamics of this system. The reagent decay is still approximately exponential in the range observed. The additional influence of substrate on the rate of catalysis is not observed.

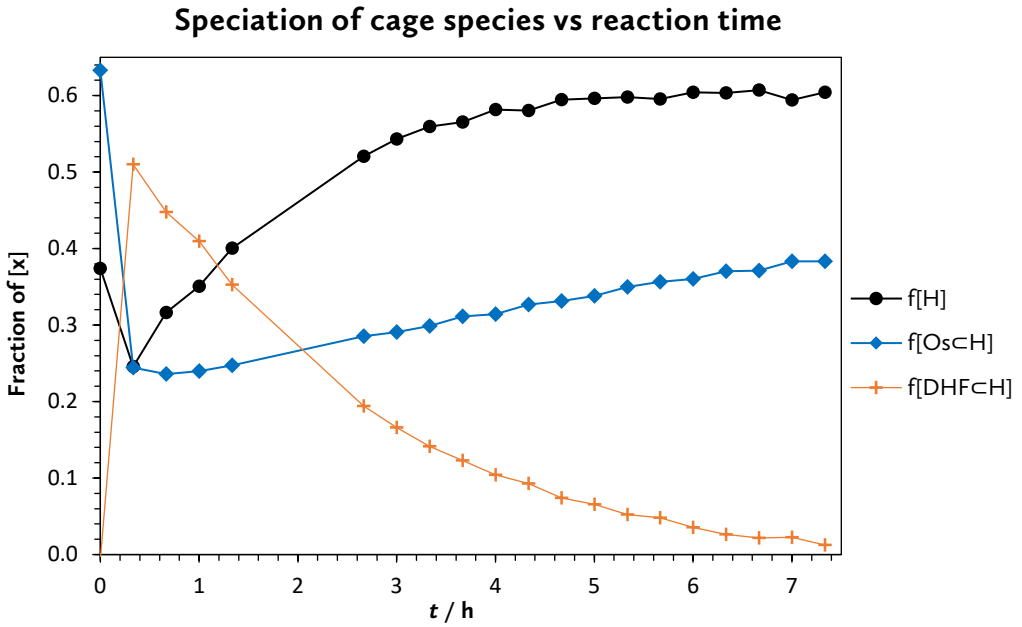

Figure IV.6—Fraction of $Gdm_4\mathbf{1}$ species plotted against reaction time for experiment A on the OD1 system.

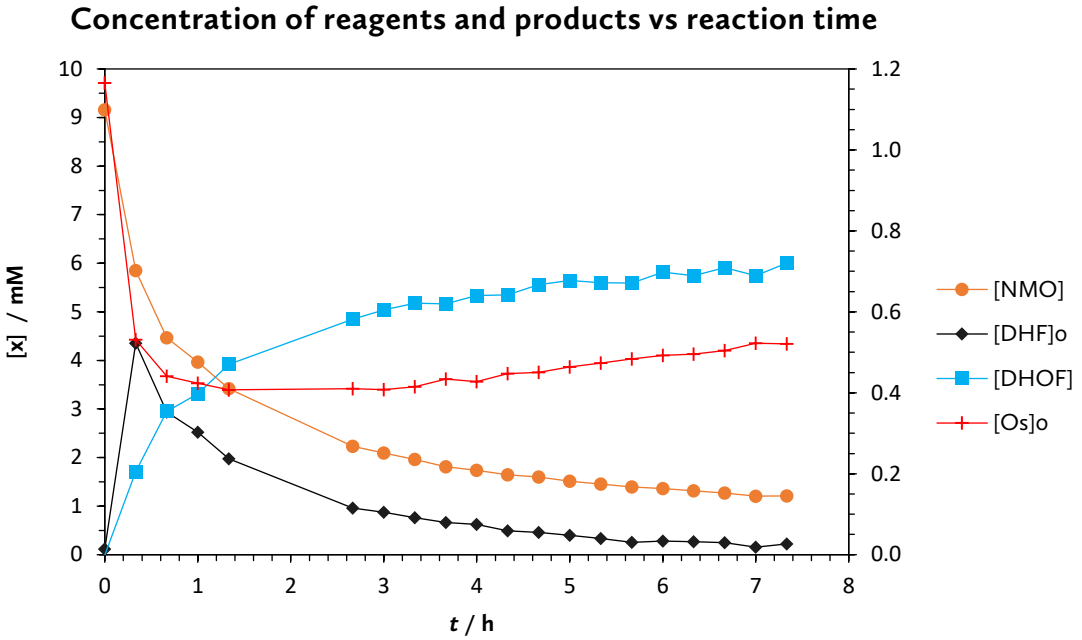

Figure IV.7—Total reagent, product and catalyst concentration plotted against reaction time for an experiment on the OD1 system. $[Os]_0$ is plotted in the secondary scale.

IV.3.1 Procedure

The procedure was essentially the same as presented in Section IV.2.1. The added volume of DHF solution (95.7 mM) was 70.0 µL—replacing pentenol. The volume of OsO_4 solution (27.7 mM) was 80.0 µL.

Chapter V

Digressions

This short chapter is dedicated to some of the experiments that were done 'on the side' to explore possible research pathways. All of the following were thrown together without much worry on the accuracy of preparation just to 'see what would happen'. All of the conclusions of these experiments should be taken with a pinch of salt, but could be valuable to guide future work.

V.1 OsO_4/cyclohexene/$Gdm_4$1 system

An attempt was made with a OsO_4/cyclohexene/$Gdm_4$1 system. The extremely slow association kinetics of cyclohexene and very strong binding[87] was appealing; it could enable the observation of a long 'induction period' as more OsO_4 was gradually displaced. However, the excess of cyclohexene used was clearly too great as the was cage quickly saturated with it. Consequently, the reaction rate observed was very fast at first as the free cyclohexene reacted. It was then very much linear as the slow dissociation rate of the complex limits the reaction.

The reuptake of OsO_4 was never observed and the cyclohexene never completely consumed. The very long reaction time (5 days) gives way for an appreciable decomposition of OsO_4. However, the competition for binding of OsO_4 could be used to probe the validity of dihydroxylation mechanisms at very low substrate concentration; the very slow kinetics can be used to measure the extent to each the cycloaddition step is reversible.

V.2 MS of $OsO_4 \subset Gdm_4$1

Mass spectrometry characterization of the $OsO_4 \subset Gdm_4$1 complex was tried as a way to confirm encapsulation of guest (as an alternative to XRD). However this particular cage was known in the research group to be difficult to observe in ESI-MS spectra. Ionization in water is quite difficult and the use of harsher ESI conditions leads to high fragmentation. The ions $[Gdm_2 1]^{2-}$ and $[Gnd1]^{3-}$ have been observed but in a methanol/water mixtures.[89] Several co-solvents were tried with water (methanol, ethanol, acetone, MeCN, DMSO) but all of them either crashed the cage out of solution or turned the assembly too unstable to resist the addition of OsO_4.

V.3 $OsO_4 \subset Gdm_4$1 in the solid state

To evaluate the ability of $Gdm_4$1 to acts as a storage medium for OsO_4 in the solid state the following was executed.

To 1 mL of solution of cage (1 mM) were added approximately 2 eq of OsO_4. Then, GdmCl was added until precipitation of the cage and a clear solution was observed. The suspension was filtered through a membrane filter with a 1 mL syringe. Through the same filter were passed 3 mL of GdmCl and NaS_2O_3 solution (2 mM), next 1 mL of ice cold water. Afterwards, 1 mL of D_2O with *t*-BuOH 1.25 mM was passed very slowly to dissolve all the solid.

The ^{1}H NMR spectrum revealed the following concentrations: [H] as 0.457 mM, [HG] as 0.247 mM, so the $[G]_0/[H]_0$ turns out as 0.62. The degree of association before precipitation was 0.714. Although further experiments would need to be done, this already give some indication that OsO_4 is at least stable and probably encapsulated in the solid state (as opposed to just occluded).

Chapter VI

Conclusion & Prospects

The main goal of characterization of the new $OsO_4 \subset Gdm_4$**1** complex has been partially fulfilled. Full ^{1}H and ^{13}C NMR characterization was achieved as well as improving the cage's synthesis. The stability of the complex has been successfully assessed as well as the binding equilibrium constant contrary to the binding kinetics. The trapping of OsO_4 in the solid state was crudely demonstrated, but its stability was not evaluated.

The stability of the supramolecular system $OsO_4 \subset Gdm_4$**1**, along with the relatively fast kinetics and moderately strong binding, enable it to be used for *in situ* monitoring of the free OsO_4 in solution (through ^{1}H NMR). This has been demonstrated in principle. Its limitations must, nonetheless, be recognized: sensitivity to pH, solubility limits, and inherent competitive inhibition of the catalyst (granting this would useful for competitive binding studies).

The dynamics of two other host-guest complexes were fully characterized, motivated by the search for more complex systems. Bzn$\subset Gdm_4$**1** has been found to have a strong binding with slow intake kinetics. A contribution of the non-classical hydrophobic effect due to the Gdm^+ counterion has been proposed as the cause of increasing binding strength by comparison to Bzn$\subset (NMe_4)_4$**1**. DHF$\subset Gdm_4$**1** has also been fully characterized and has the lowest binding constant of the three complexes studied. Its intake kinetics has been studied but the results should not be regarded as quantitative for future work; the range studied was quite small and is the result with the lowest confidence of all. Table VI.1 summarizes the results.

Table VI.1—Summary of equilibrium and intake rate constants for the studied complexes.

	$OsO_4 \subset Gdm_4$**1**	Bzn$\subset Gdm_4$**1**	DHF$\subset Gdm_4$**1**
K_a / mM^{-1}	2.9 ± 0.2	14.8 ± 0.4	0.616 ± 0.007
k_{in} / $M^{-1}s^{-1}$	not determined	0.34 ± 0.02	(1.5 ± 0.2) × 10^{-3}

The goal of demonstrating orthogonal regulation has been attained even if not quantitatively. The presence of benzene in the OB1+P system acts has an 'inhibitor's inhibitor', increasing the rate of OsO_4 catalysis without interfering directly with the dihydroxylation reaction itself.

Accomplishing the demonstration of higher order rate regulation by DHF in the OD1 will require further work. The analysis done shows it as not being significantly different from that of benzene. The design of a system with a self-signalled on/off reaction switch has not been accomplished.

Future work can take several paths. Firstly, improvement of the $OsO_4 \subset Gdm_4$**1** binding strength and stability could allow a similar supramolecular system to be used in the future as a means to handle more safely OsO_4. Reduction of the imine moiety to amine should be tested to attain this (the reduced ligand should be less susceptible to oxidation). Other metal ions could also be used to try and alter the pore and cavity size and lability of the vertices, thereby manipulating intake kinetics and equilibrium.

The OsO_4+Gdm_4**1** system as is could already has its uses. Detailed study of the speciation of the oxoanions of Os is simplified by the absence of further reagents. Measuring the variations of the degree of association as a function of ionic strength, pH and redox potential could be provide valuable information for designing of Os(VIII) catalysts. On this last subject, this system has the potential to simplify the evaluation of ligand binding to OsO_4 whenever the ligand is silent or otherwise difficult to analyse.

Secondly, the investigation of peculiar out-of-equilibrium dynamics in the studied supramolecular systems could be worthwhile and serve as a base to the discovery of more useful systems. To better study the host-guest dynamics along the reaction, future work should focus on monitoring one tube at a time as a pseudo-2D NMR experiment.

The lesson learned from this work is that monitoring several tubes saves spectrometer time but sacrifices time resolution and spectra quality. However, even the monitorization of several tubes could be improved with faster equipment (namely the autosampler).

Higher concentration of both substrates and cage should enable observation of the different catalysis dynamics. Reaction in these conditions could be explored in more detail by end-point studies.

With kinetic essays in the 10 mL range, aliquots can be extracted in much shorter time periods than NMR sampling would provide with decent accuracy. The aliquots would be mixed immediately into $Na_2S_2O_3$ solutions, reducing the Os(VIII) to inactive forms and stopping the reaction. At the end, timely analysis of dihydroxylation products by GC would easily reveal the dynamics without much complication. This kind of essay could work in the mol/L concentration regime with a sampling resolution of a few seconds.

Chapter VII

References

1. CLERK-MAXWELL, J. Over de contimiiteit van den gas- en vloeistofiocstand Academisch proefschrift. *Nature* **10,** 477–480 (1874).

2. Lichtenthaler, F. W. 100 Years "Schlüssel-Schloss-Prinzip": What Made Emil Fischer Use this Analogy? *Angew. Chemie Int. Ed. English* **33,** 2364–2374 (1995).

3. Muller, P. in *Pure and Applied Chemistry* **66,** 1077–1184 (1994).

4. Martinez, C. R. & Iverson, B. L. Rethinking the term "pi-stacking". *Chem. Sci.* **3,** 2191 (2012).

5. Matta, C. F., Castillo, N. & Boyd, R. J. Extended weak bonding interactions in DNA: π-stacking (base-base), base-backbone, and backbone-backbone interactions. *J. Phys. Chem. B* **110,** 563–578 (2006).

6. Waller, M. P., Robertazzi, A., Platts, J. A., Hibbs, D. E. & Williams, P. A. Hybrid density functional theory for π-stacking interactions: Application to benzenes, pyridines, and DNA bases. *J. Comput. Chem.* **27,** 491–504 (2006).

7. Burattini, S. *et al.* A healable supramolecular polymer blend based on aromatic π-π Stacking and hydrogen-bonding interactions. *J. Am. Chem. Soc.* **132,** 12051–12058 (2010).

8. Goff, A. Le *et al.* Facile and tunable functionalization of carbon nanotube electrodes with ferrocene by covalent coupling and π-stacking interactions and their relevance to glucose bio-sensing. *J. Electroanal. Chem.* **641,** 57–63 (2010).

9. Thomas III, S. W., Amara, J. P., Bjork, R. E. & Swager, T. M. Amplifying fluorescent polymer sensors for the explosives taggant 2,3-dimethyl-2,3-dinitrobutane (DMNB). *Chem. Commun.* 4572 (2005).

10. Tidmarsh, I. S. *et al.* Octanuclear cubic coordination cages. *J. Am. Chem. Soc.* **130,** 15167–15175 (2008).

11. Giese, M., Albrecht, M. & Rissanen, K. Anion-π interactions with fluoroarenes. *Chemical Reviews* **115,** 8867–8895 (2015).

12. Patrick, C. R. & Prosser, G. S. A Molecular Complex of Benzene and Hexafluorobenzene. *Nature* **187,** 1021 (1960).

13. Wheeler, S. E. & Houk, K. N. Substituent effects in cation/π interactions and electrostatic potentials above the centers of substituted benzenes are due primarily to through-space effects of the substituents. *J. Am. Chem. Soc.* **131,** 3126–3127 (2009).

14. Zhong, W. From ab initio quantum mechanics to molecular neurobiology : A cation – binding site in the nicotinic receptor. *Proc. Natl. Acad. Sci.* **95,** 12088–12093 (1998).

15. Quiñonero, D. *et al.* Anion-π interactions: Do they exist? *Angew. Chemie Int. Ed.* **41,** 3389–3392 (2002).

16. De Hoog, P., Gamez, P., Mutikainen, I., Turpeinen, U. & Reedijk, J. An aromatic anion receptor: Anion-π interactions do exist. *Angew. Chemie - Int. Ed.* **43,** 5815–5817 (2004).

17. Claessens, C. G. & Stoddart, J. F. π-Interactions in Self-Assembly. *J. Phys. Org. Chem.* **10,** 254–272 (1997).

18. Schwalbe, C. H. June Sutor and the C–H ··· O hydrogen bonding controversy. *Cryst. Rev.* **18,** 191–206 (2014).

19. Markovitch, O. & Agmon, N. The distribution of acceptor and donor hydrogen-bonds in bulk liquid water. *Mol. Phys.* **106,** 485–495 (2008).

20. Meot-Ner, M. The ionic hydrogen bond. *Chemical Reviews* **105,** 213–284 (2005).

21. Cordier, F., Rogowski, M., Grzesiek, S. & Bax, A. Observation of Through-Hydrogen-Bond $^{2h}J_{HC'}$ in a Perdeuterated Protein. *J. Magn. Reson.* **140,** 510–512 (1999).

22. Desiraju, G. R. & Steiner, T. in *The Weak Hydrogen Bond: In Structural Chemistry and Biology* **9,** 1–28 (Oxford University Press, 1999).

23. Brammer, L. Metals and hydrogen bonds. *Dalt. Trans.* 3145 (2003).

24. Legon, A. C. & Millen, D. J. Angular geometries and other properties of hydrogen-bonded dimers: a simple electrostatic interpretation of the success of the electron-pair model. *Chem. Soc. Rev.* **16,** 467 (1987).

25. Hamon, L. *et al.* Molecular insight into the adsorption of H_2S in the flexible MIL-53(Cr) and rigid MIL-47(V) MOFs: Infrared spectroscopy combined to molecular simulations. *J. Phys. Chem. C* **115,** 2047–2056 (2011).

26. Seo, P. W., Khan, N. A., Hasan, Z. & Jhung, S. H. Adsorptive Removal of Artificial Sweeteners from Water Using Metal-Organic Frameworks Functionalized with Urea or Melamine. *ACS Appl. Mater. Interfaces* **8,** 29799–29807 (2016).

27. Arunan, E. *et al.* Defining the hydrogen bond: An account (IUPAC Technical Report). *Pure Appl. Chem.* **83,** 1619–1636 (2011).

28. Arunan, E. *et al.* Definition of the hydrogen bond (IUPAC Recommendations 2011). *Pure Appl. Chem.* **83,** 1637–1641 (2011).

29. Echeverría, J., Aullón, G., Danovich, D., Shaik, S. & Alvarez, S. Dihydrogen contacts in alkanes are subtle but not faint. *Nat. Chem.* **3,** 323–330 (2011).

30. Mikheev, Y. a., Guseva, L. N., Davydov, E. Y. & Ershov, Y. a. The hydration of hydrophobic substances. *Russ. J. Phys. Chem. A* **81,** 1897–1913 (2007).

31. Yaminsky, V. V & Vogler, E. A. Hydrophobic hydration. *Curr. Opin. Colloid Interface Sci.* **6,** 342–349 (2001).

32. Silverstein, T. P. The Real Reason Why Oil and Water Don't Mix. *J. Chem. Educ.* **75,** 116 (1998).

33. Haselmeier, R., Holz, M. & Marbach, W. Water Dynamics near a Dissolved Noble Gas. First Direct Experimental Evidence for a Retardation Effect. *J. Phys. Chem.* **99,** 2243–2246 (1995).

34. Silverstein, T. P. Hydrophobic Solvation NOT via Clathrate Water Cages. *J. Chem. Educ.* **85,** 917 (2008).

35. Rezus, Y. L. A. & Bakker, H. J. Observation of immobilized water molecules around hydrophobic groups. *Phys. Rev. Lett.* **99,** (2007).

36. Hillyer, M. B. & Gibb, B. C. Molecular Shape and the Hydrophobic Effect. *Annu. Rev. Phys. Chem.* **67,** 307–329 (2016).

37. Furlan, R. L. E., Otto, S. & Sanders, J. K. M. Supramolecular templating in thermodynamically controlled synthesis. *Proc. Natl. Acad. Sci.* **99,** 4801–4804 (2002).

38. Otto, S. & Engberts, J. B. F. N. Hydrophobic interactions and chemical reactivity. *Society* **44,** 2809–2820 (2003).

39. Chandler, D. Interfaces and the driving force of hydrophobic assembly. *Nature* **437,** 640–647 (2005).

40. Wittenberg, J. B. & Isaacs, L. in *Supramolecular Chemistry* (John Wiley & Sons, Ltd, 2012). doi:10.1002/9780470661345.smc004

41. Whitesides, G. M. Self-Assembly at All Scales. *Science (80-.).* **295,** 2418–2421 (2002).

42. Hunter, C. A. & Anderson, H. L. What is cooperativity? *Angew. Chemie - Int. Ed.* **48,** 7488–7499 (2009).

43. von Krbek, L. K. S., Schalley, C. A. & Thordarson, P. Assessing cooperativity in supramolecular systems. *Chem. Soc. Rev.* **46,** 2622–2637 (2017).

44. Whitty, A. Cooperativity and biological complexity. *Nat. Chem. Biol.* **4,** 435–9 (2008).

45. Delgado, R. *Coordination Chemistry of Macrocyclic Compounds*. *Rev. Port. Quim. (Lisbon)* **2,** (1979).

46. Robert D. Hancock & Arthur E. Martell. The Chelate, Cryptate and Macrocyclic Effects. *Comments Inorg. Chem.* **6,** 237–284 (1988).

47. Chen, Q., Cannell, K., Nicoll, J. & Dearden, D. V. The macrobyciclic cryptate effect in the gas phase. *J. Am. Chem. Soc.* **27,** 3635–3644 (1996).

48. Brachvogel, R.-C., Maid, H. & von Delius, M. NMR Studies on Li^+, Na^+ and K^+ Complexes of Orthoester Cryptand o-Me_2-1.1.1. *Int. J. Mol. Sci.* **16,** 20641–56 (2015).

49. Hinz, F. P. & Margerum, D. W. Effect of Ligand Solvation on the Stability of Metal Complexes in Solution. An Explanation of the Macrocyclic Effect. *Journal of the American Chemical Society* **96,** 4993–4994 (1974).

50. Chekhlov, A. N. Synthesis and crystal structure of aqua(2.2.2-cryptand)(perchlorato-O)lead(II) diaqua(2.2.2-cryptand)lead(II) tris(perchlorate). *Russ. J. Coord. Chem.* **32,** 552–558 (2006).

51. Dvir, H., Silman, I., Harel, M., Rosenberry, T. L. & Sussman, J. L. Acetylcholinesterase: From 3D structure to function. *Chem. Biol. Interact.* **187,** 10–22 (2010).

52. Buller, A. R. & Townsend, C. A. Intrinsic evolutionary constraints on protease structure, enzyme acylation, and the identity of the catalytic triad. *Proc. Natl. Acad. Sci.* **110,** E653–E661 (2013).

53. Chapman, R. G. & Sherman, J. C. Templation and encapsulation in supramolecular chemistry. *Tetrahedron* **53,** 15911–15945 (1997).

54. Hoss, R. & Vögtle, F. Template Syntheses. *Angew. Chemie Int. Ed. English* **33,** 375–384 (1994).

55. Marks, T. J. & Stojakovic, D. R. Large Metal Ion-Centered Template Reactions. Chemical and Spectral Studies of the "Superphthalocyanine" Dioxocyclopentakis (1-Iminoisoindolinato) Uranium (Vl) and its Derivatives. *J. Am. Chem. Soc.* **100,** 1695–1705 (1978).

56. Ercolani, G., Mandolini, L. & Masci, B. Template Effects . 3 . The Quantitative Determination of the Catalytic Effects of Alkali and Alkaline Earth Cations in the Formation of Benzo-18-crown-6 in Methanol Solution. **6,** 2780–2782 (1981).

57. Lehn, J.-M. From supramolecular chemistry towards constitutional dynamic chemistry and adaptive chemistry. *Chem. Soc. Rev.* **36,** 151–60 (2007).

58. Caulder, D. L. & Raymond, K. N. The rational design of high symmetry coordination clusters. *J. Chem. Soc. Dalt. Trans.* 1185–1200 (1999). doi:10.1039/a808370c

59. Hasenknopf, B. *et al.* Self-Assembly of Tetra- and Hexanuclear Circular Helicates.

60. Ronson, T. K. *et al.* Size-selective encapsulation of hydrophobic guests by self-assembled M_4L_6 cobalt and nickel cages. *Chem. - A Eur. J.* **19,** 3374–3382 (2013).

61. Lincoln, S. F., Richens, D. T. & Sykes, A. G. Metal Aqua Ions in *Comprehensive Coordination Chemistry.* **1,** 515–555 (Elsevier, 2004).

62. He, Q.-T. *et al.* Copper(I) Cuboctahedral Coordination Cages: Host-Guest Dependent Redox Activity. *Angew. Chemie Int. Ed.* **48,** 6156–6159 (2009).

63. Minkenberg, C. B. *et al.* Responsive vesicles from dynamic covalent surfactants. *Angew. Chemie Int. Ed.* **50,** 3421–3424 (2011).

64. Diemer, S. L., Kristensen, M., Rasmussen, B., Beeren, S. R. & Pittelkow, M. Simultaneous disulfide and boronic acid ester exchange in dynamic combinatorial libraries. *Int. J. Mol. Sci.* **16,** 21858–21872 (2015).

65. Rocard, L., Berezin, A., De Leo, F. & Bonifazi, D. Templated Chromophore Assembly by Dynamic Covalent Bonds. *Angew. Chemie Int. Ed.* **54,** 15739–15743 (2015).

66. Jin, Y., Wang, Q., Taynton, P. & Zhang, W. Dynamic covalent chemistry approaches toward macrocycles, molecular cages, and polymers. *Acc. Chem. Res.* **47,** 1575–1586 (2014).

67. Belowich, M. E. & Stoddart, J. F. Dynamic imine chemistry. *Chem. Soc. Rev.* **41,** 2003 (2012).

68. Godoy-Alcántar, C., Yatsimirsky, A. K. & Lehn, J. M. Structure-stability correlations for imine formation in aqueous solution. *J. Phys. Org. Chem.* **18,** 979–985 (2005).

69. Nitschke, J. R. Construction, substitution, and sorting of metallo-organic structures via subcomponent self-assembly. *Acc. Chem. Res.* **40,** 103–112 (2007).

70. Mastalerz, M. One-pot synthesis of a shape-persistent endo-functionalised nano-sized adamantoid compound. *Chem. Commun.* 4756 (2008).

71. Liu, W. X. *et al.* Oxime-Based and Catalyst-Free Dynamic Covalent Polyurethanes. *J. Am. Chem. Soc.* **139,** 8678–8684 (2017).

72. Dirksen, A., Dirksen, S., Hackeng, T. M. & Dawson, P. E. Nucleophilic catalysis of hydrazone formation and transimination: Implications for dynamic covalent chemistry. *J. Am. Chem. Soc.* **128,** 15602–15603 (2006).

73. Gil-Ramírez, G., Leigh, D. A. & Stephens, A. J. Catenanes: Fifty years of molecular links. *Angewandte Chemie International Edition* **54,** 6110–6150 (2015).

74. Dietrich-Buchecker, C. O., Sauvage, J. P. & Kern, J. M. Templated synthesis of interlocked macrocyclic ligands: the catenands. *J. Am. Chem. Soc.* **106,** 3043–3045 (1984).

75. Diederich, F., Dietrich-Buchecker, C., Nierengarten, J.-F. & Sauvage, J.-P. A Copper(I)-complexed Rotaxane with Two Fullerene Stoppers. *J. Chem. Soc., Chem. Commun.* (1995).

76. Albrecht-Gary, A. M., Saad, Z., Dietrich-Buchecker, C. O. & Sauvage, J. P. Interlocked Macrocyclic Ligands: A Kinetic Catenand Effect in Copper(I) Complexes. *J. Am. Chem. Soc.* **107,** 3205–3209 (1985).

77. Cantrill, S. J. *et al.* A new protocol for rotaxane synthesis. *Tetrahedron Lett.* **40,** 3669–3672 (1999).

78. Nobel Media AB 2014. The 2016 Nobel Prize in Chemistry - Press Release. (2017). Available at: https://www.nobelprize.org/nobel_prizes/chemistry/laureates/2016/press.html. (Accessed: 10th October 2017)

79. Philp, D. & Stoddart, J. F. Self-Assembly in Natural and Unnatural Systems. *Angew. Chemie Int. Ed. English* **35,** 1154–1196 (1996).

80. Browne, W. R. & Feringa, B. L. Making molecular machines work. *Nat. Nanotechnol.* **1,** 25 (2006).

81. Johnson, J. R. *et al.* Squaraine rotaxanes: Superior substitutes for Cy-5 in molecular probes for near-infrared fluorescence cell imaging. *Angew. Chemie Int. Ed.* **46,** 5528–5531 (2007).

82. Arunkumar, E., Forbes, C. C., Noll, B. C. & Smith, B. D. Squaraine-derived rotaxanes: Sterically protected fluorescent near-IR dyes. *J. Am. Chem. Soc.* **127,** 3288–3289 (2005).

83. Stoddart, J. F. The chemistry of the mechanical bond. *Chem. Soc. Rev.* **38,** 1802 (2009).

84. Pavel, F. M. Microemulsion Polymerization. *J. Dispers. Sci. Technol.* **25,** 1–16 (2004).

85. Breiner, B., Clegg, J. K. & Nitschke, J. R. Reactivity modulation in container molecules. *Chem. Sci.* **2,** 51–56 (2011).

86. Mal, P., Schultz, D., Beyeh, K., Rissanen, K. & Nitschke, J. R. An unlockable-relockable iron cage by subcomponent self-assembly. *Angew. Chemie - Int. Ed.* **47,** 8297–8301 (2008).

87. Smulders, M. M. J., Zarra, S. & Nitschke, J. R. Quantitative understanding of guest binding enables the design of complex host-guest behavior. *J. Am. Chem. Soc.* **135,** 7039–7046 (2013).

88. Mal, P., Breiner, B., Rissanen, K. & Nitschke, J. R. White phosphorus is air-stable within a self-assembled tetrahedral capsule. *Science* **324,** 1697–9 (2009).

89. Zarra, S., Smulders, M. M. J., Lefebvre, Q., Clegg, J. K. & Nitschke, J. R. Guanidinium binding modulates guest exchange within an $[M_4L_6]$ capsule. *Angew. Chemie Int. Ed.* **51,** 6882–6885 (2012).

90. Lehn, J.-M. Toward Self-Organization and Complex Matter. *Science* **295,** 2400–2403 (2002).

91. New York Daily News. Ford's assembly line turns 100: How it changed society - NY Daily News. 1 (2013). Available at: http://www.nydailynews.com/autos/ford-assembly-line-turns-100-changed-society-article-1.1478331. (Accessed: 17th October 2017)

92. Salles, A. G., Zarra, S., Turner, R. M. & Nitschke, J. R. A self-organizing chemical assembly line. *J. Am. Chem. Soc.* **135,** 19143–19146 (2013).

93. Smulders, M. M. J. & Nitschke, J. R. Supramolecular control over Diels-Alder reactivity by encapsulation and competitive displacement. *Chem. Sci.* **3,** 785–788 (2012).

94. Ogawa, E. Vapour Pressure, Surface Tension and Density of Osmium Tetroxide. *Bull. Chem. Soc. Jpn.* **6,** 302–317 (1931).

95. Krebs, B. & Hasse, K. D. Refinements of the crystal structures of $KTcO_4$, $KReO_4$ and OsO4. The bond lengths in tetrahedral oxoanions and oxides of d0 transition metals. *Acta Crystallogr. Sect. B Struct. Crystallogr. Cryst. Chem.* **32,** 1334–1337 (1976).

96. Di Scipio, F., Raimondo, S., Tos, P. & Geuna, S. A simple protocol for paraffin-embedded myelin sheath staining with osmium tetroxide for light microscope observation. *Microsc. Res. Tech.* **71,** 497–502 (2008).

97. Bailey, A. J. *et al.* Oxo osmium(VIII) complexes in oxidation: crystal structures of OsO_4·nmo (nmo = N-methylmorpholine N-oxide) and OsO_4·nmm (nmm = N-methylmorpholine), and use of cis-$[OsO_4(OH)_2]^{2-}$ as an oxidation catalyst. *Dalt. Trans.* **4,** 3245–3250 (1997).

98. Kosiorek-Rupińska, A., Święcicka-Füchsel, E. & Balcerzak, M. Speciation analysis of osmium(VIII) and osmium(IV) by UV-VIS spectrophotometry using quercetin as the reagent. *Anal. Lett.* **39,** 589–602 (2006).

99. Sauerbrunn, R. D. & Sandell, E. B. The Ionization Constants of Osmic(VIII) Acid. *J. Am. Chem. Soc.* **75,** 4170–4172 (1953).

100. Malin, J. M. Potassium tetrahydroxodioxoosmate(VI) and trans-bis(ethylenediamine) dioxoosmium (VI) chloride. *Inorg. Synth.* **XX,** 61–63 (1978).

101. Griffith, W. P. TMC Literature Highlights- 22 Organic oxidations by osmium and ruthenium oxo complexes. *Transit. Met. Chem* **15,** 251–256 (1990).

102. Kobs, S. F. & Behrman, E. J. Complexation of osmium tetroxide with tertiary amines. *Inorganica Chim. Acta* **128,** 21–26 (1987).

103. DelMonte, A. J. *et al.* Experimental and theoretical kinetic isotope effects for asymmetric dihydroxylation. Evidence supporting a rate-limiting '(3+2)' cycloaddition. *J. Am. Chem. Soc.* **119,** 9907–9908 (1997).

104. Erdik, E. Kinetic Role of Tert -Amines in the Osmium Tetroxide Catalyzed Trimethylamine N -Oxide Dihydroxylation of. 12–14 (1996).

105. Dupau, P., Epple, R., Thomas, A. A., Fokin, V. V & Sharpless, K. B. Osmium-Catalyzed Dihydroxylation of Olefins in Acidic Media: Old Process, New Tricks. *Adv. Synth. Catal.* **344,** 421–433 (2002).

106. Norrby, P.-O. & Gable, K. P. 098. Kinetic constraints on possible reaction pathways for osmium-catalysed asymmetric dihydroxylation. *J. Chem. Soc., Perkin Trans. 2* 171 (1996).

107. Tse, M. K., Schröder, K. & Beller, M. in *Modern Oxidation Methods* **1,** 1–36 (2005).

108. Jacobsen, E. N., Marko, I., France, M. B., Svendsen, J. S. & Sharpless, K. B. Kinetic role of the alkaloid ligands in asymmetric catalytic dihydroxylation. *J. Am. Chem. Soc.* **111,** 737–739 (1989).

109. Zseduai, A. The Acidic Behaviour of Osmium (VIII) and Osmium (VI). *Transit. Met. Chem* **332,** 328–332 (1983).

110. Cantrill, S. J., Fyfe, M. C. T., Raymo, F. M. & Stoddart, J. F. in *NMR in Supramolecular Chemistry* (ed. Pons, M.) 1–18 (Springer Netherlands, 1999).

111. Čuperlović-Culf, M. Experimental methodology. *NMR Metabolomics Cancer Res.* **39,** 139–213 (2013).

112. Kost, D., Carlson, E. H. & Raban, M. The validity of approximate equations for k_c in dynamic nuclear magnetic resonance. *J. Chem. Soc. D Chem. Commun.* 656–657 (1971).

113. Gutowsky, H. S. & Holm, C. H. Rate processes and nuclear magnetic resonance spectra. II. Hindered internal rotation of amides. *J. Chem. Phys.* **25,** 1228–1234 (1956).

114. Feeney, J., Batchelor, J. G., Albrand, J. P. & Roberts, G. C. K. The Effects of Intermediate Exchange Processes on the Estimation of Equilibrium Constants by NMR. *J. Magn. Reson.* **33,** 519–529 (1979).

115. Perrin, C. L. & Dwyer, T. J. Application of Two-Dimensional NMR to Kinetics of Chemical Exchange. *Chem. Rev.* **90,** 935–967 (1990).

116. Vassilev, N. G. & Dimitrov, V. S. Dynamic NMR: Combined use of 1D selective EXSY and complete lineshape analysis of spectra subjected to reference deconvolution and linear prediction or the maximum entropy method. *Magn. Reson. Chem.* **39,** 607–614 (2001).

117. Thordarson, P. Determining association constants from titration experiments in supramolecular chemistry. *Chem. Soc. Rev.* **40,** 1305–1323 (2011).

118. Angermüller, S. & Fahimi, H. D. Imidazole-buffered osmium tetroxide: an excellent stain for visualization of lipids in transmission electron microscopy. *Histochem. J.* **14,** 823–835 (1982).

119. Huber, M. L., Laesecke, A. & Friend, D. G. The Vapor Pressure of Mercury NISTIR 6643. *Mon. Weather Rev.* **32,** 566–566 (1904).

120. Occupational Safety and Health Administration. OSHA Occupational Chemical Database | Osmium Tetroxide. Available at: https://www.osha.gov/chemicaldata/chemResult.html?RecNo=308. (Accessed: 21st May 2018)

121. Occupational Safety and Health Administration. Chemical Sampling Information | Mercury (organo) Alkyl Compounds (as Hg). Available at: https://www.osha.gov/dts/chemicalsampling/data/CH_250500.html. (Accessed: 21st May 2018)

122. Mecozzi, S. & Rebek, J. The 55% solution: A formula for molecular recognition in the liquid state. *Chem. - A Eur. J.* **4,** 1016–1022 (1998).

123. Hristova, Y. R., Smulders, M. M. J., Clegg, J. K., Breiner, B. & Nitschke, J. R. Selective anion binding by a 'Chameleon' capsule with a dynamically reconfigurable exterior. *Chem. Sci.* **2,** 638–641 (2011).

124. Center for Disease Control and Prevention. CDC - NIOSH Pocket Guide to Chemical Hazards - Osmium Tetroxide. *National Institute of Occupational Safety and Health* (2016).

125. Steed, J. W., Atwood, J. L. & Gale, P. A. *Definition and Emergence of Supramolecular Chemistry*. *Supramolecular Chemistry* (2012).

Appendix A

NMR Spectra

A.1 Gdm4l NMR spectra

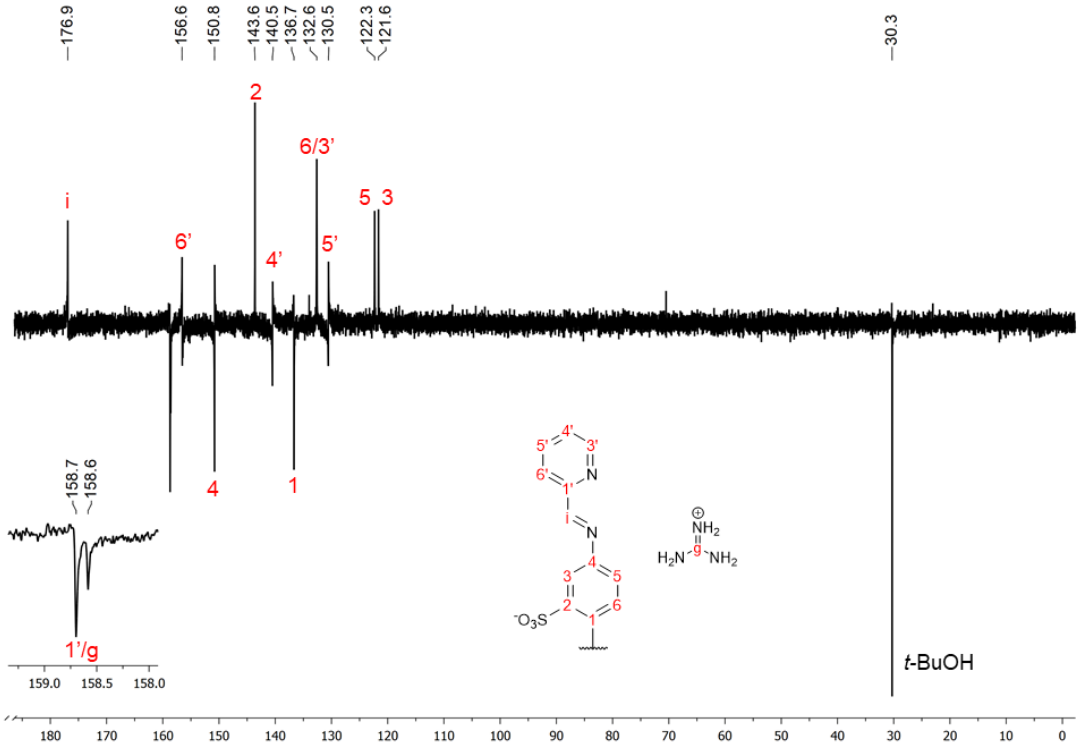

Figure A.1—^{13}C APT NMR spectrum of Gdm4l 2.42 mM.

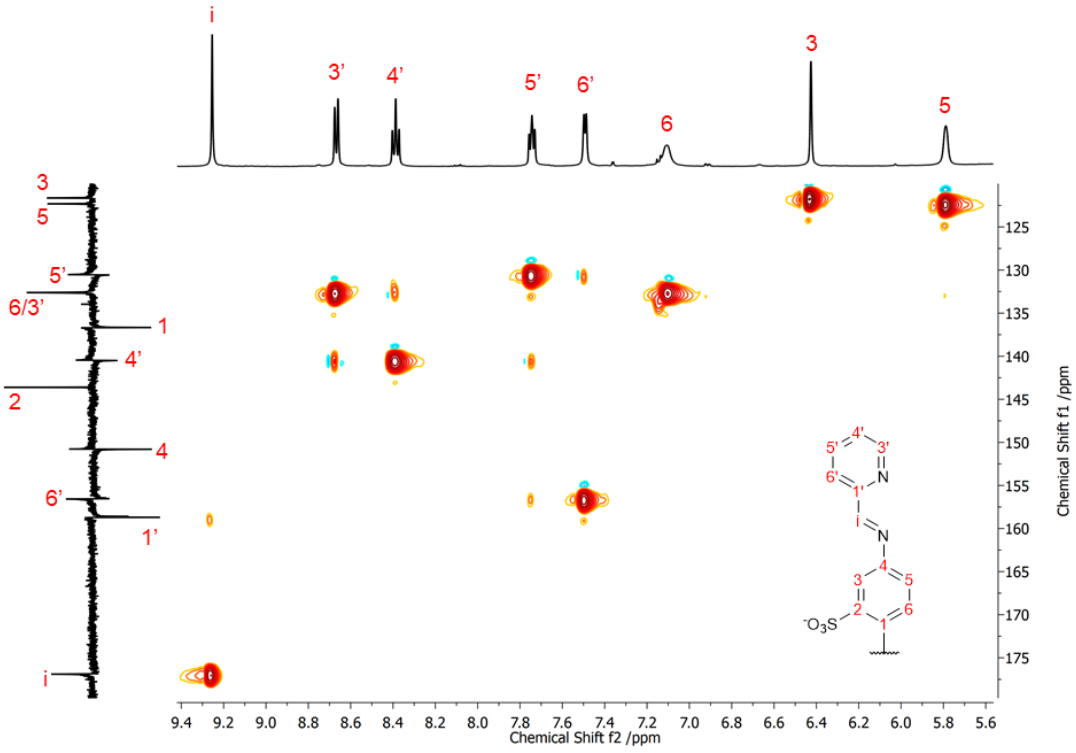

Figure A.2— HSQC NMR spectrum of Gdm4l 2.42 mM.

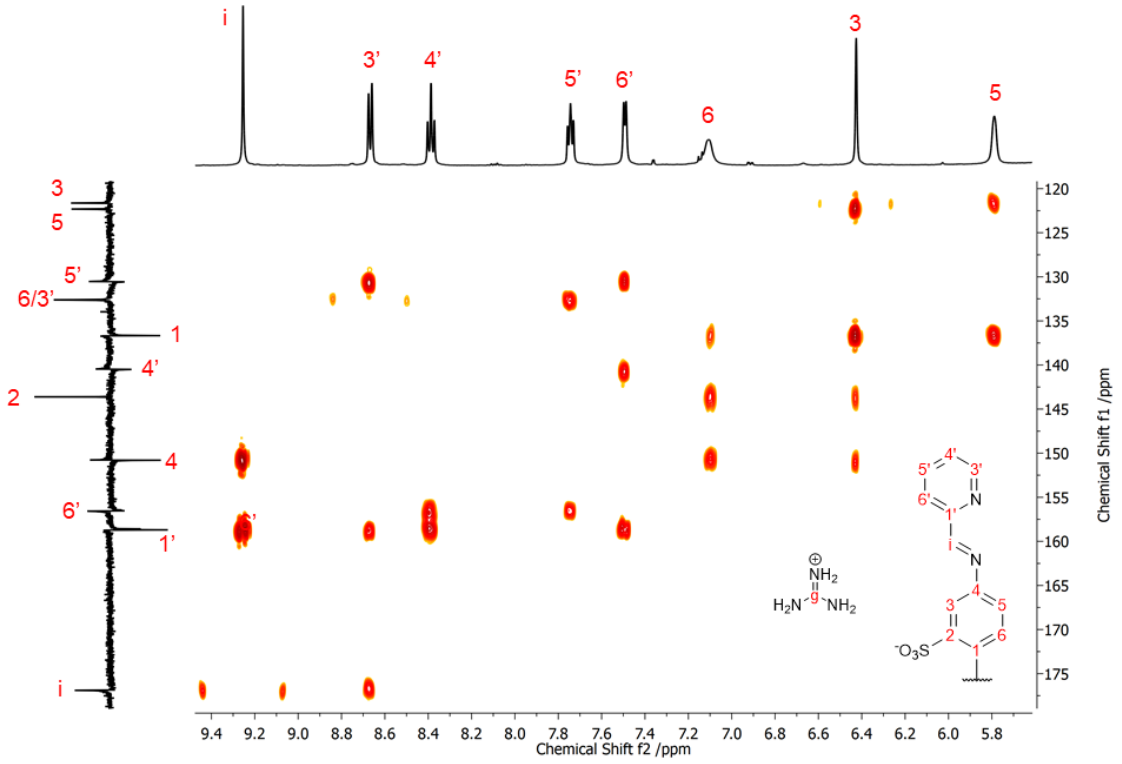

Figure A.3—HMBC NMR spectrum of $Gdm_4$1 2.42 mM.

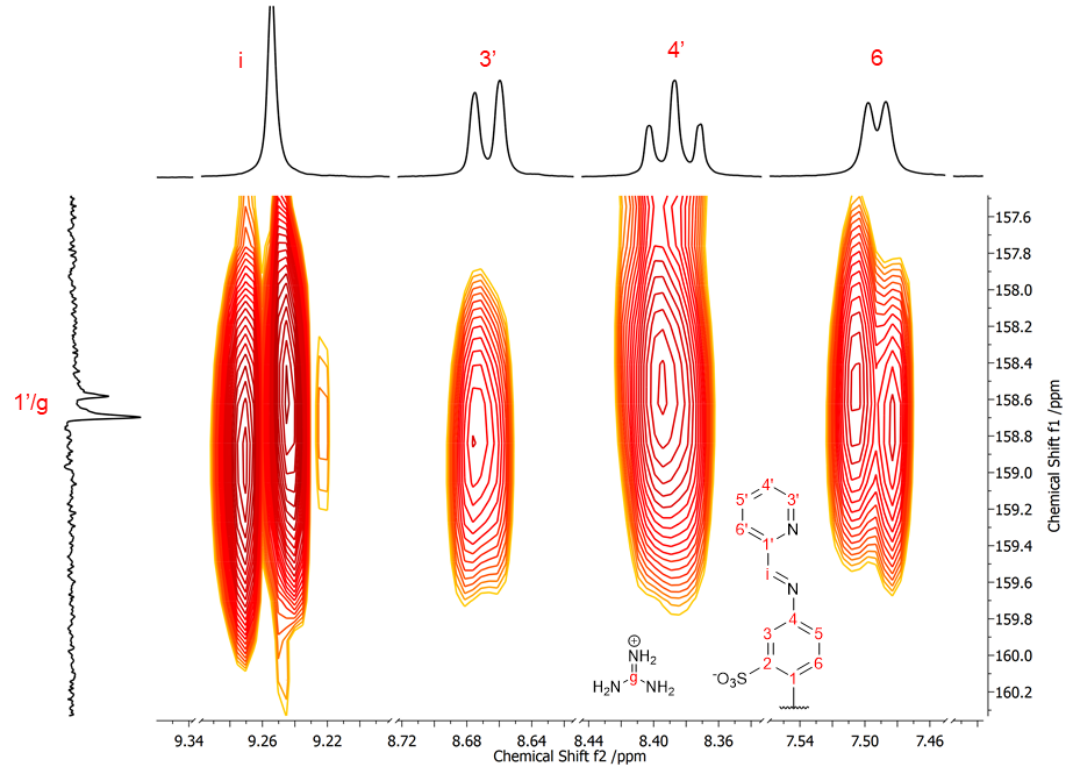

Figure A.4—Magnification of HMBC NMR spectrum above, $Gdm_4$1 2.42 mM.

A.2 OsO_4⊂$Gdm_4$1 NMR spectra

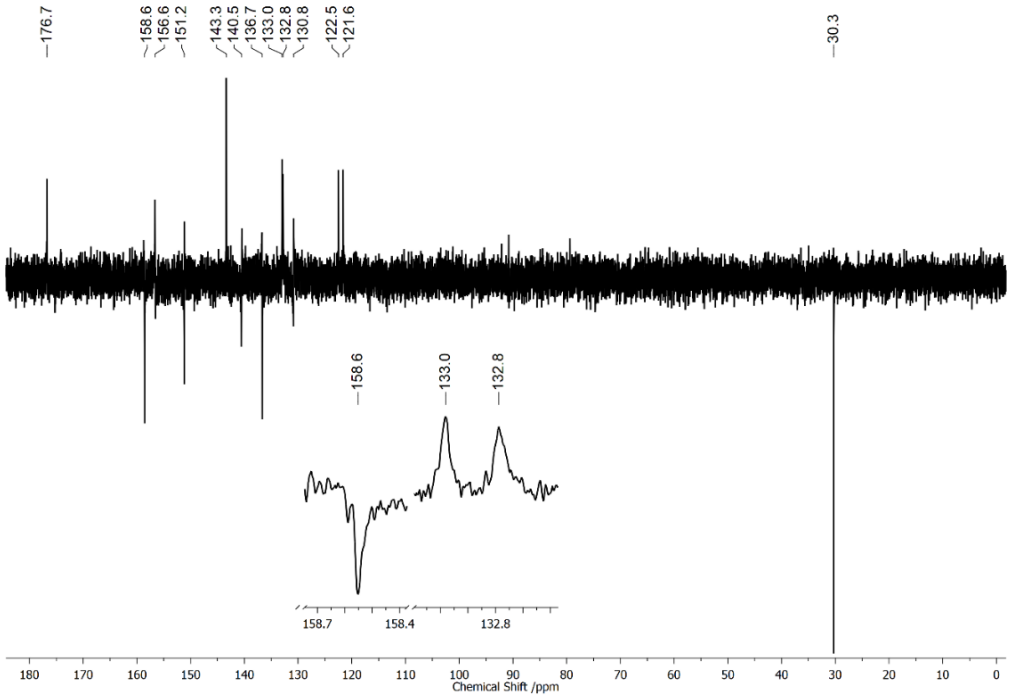

Figure A.5—^{13}C NMR spectra of OsO_4⊂$Gdm_4$1, 1.48 mM of total host and 8.6 mM of total guest.

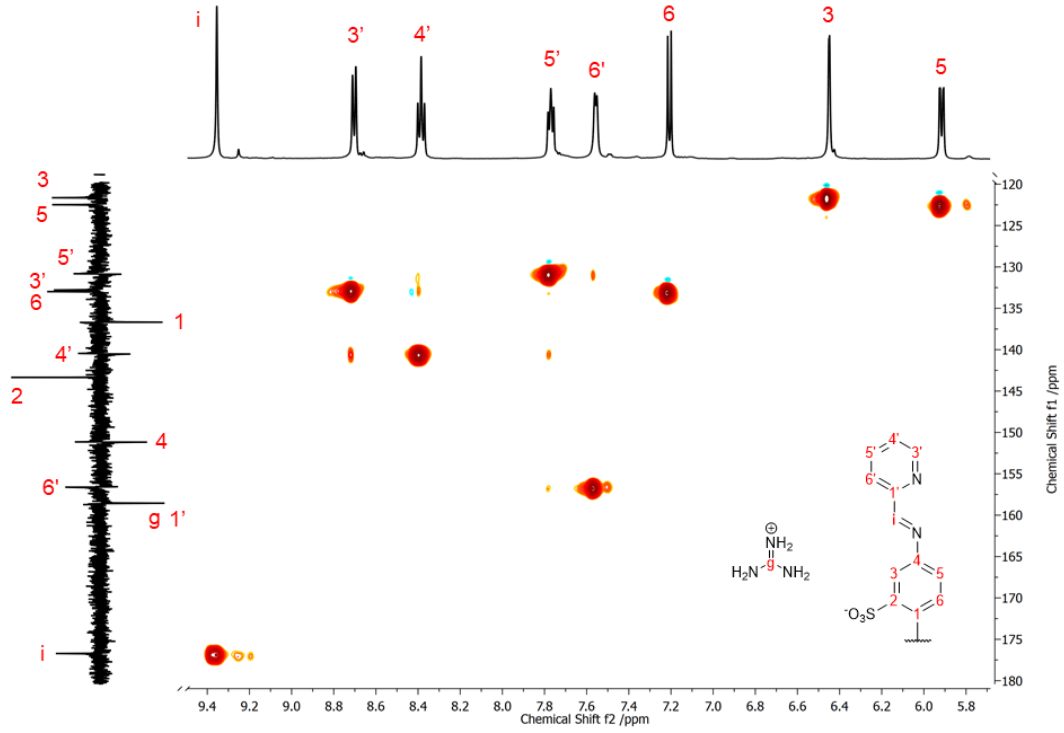

Figure A.6—HSQC NMR spectra of OsO_4⊂$Gdm_4$1, 1.48 mM of total host and 8.6 mM of total guest.

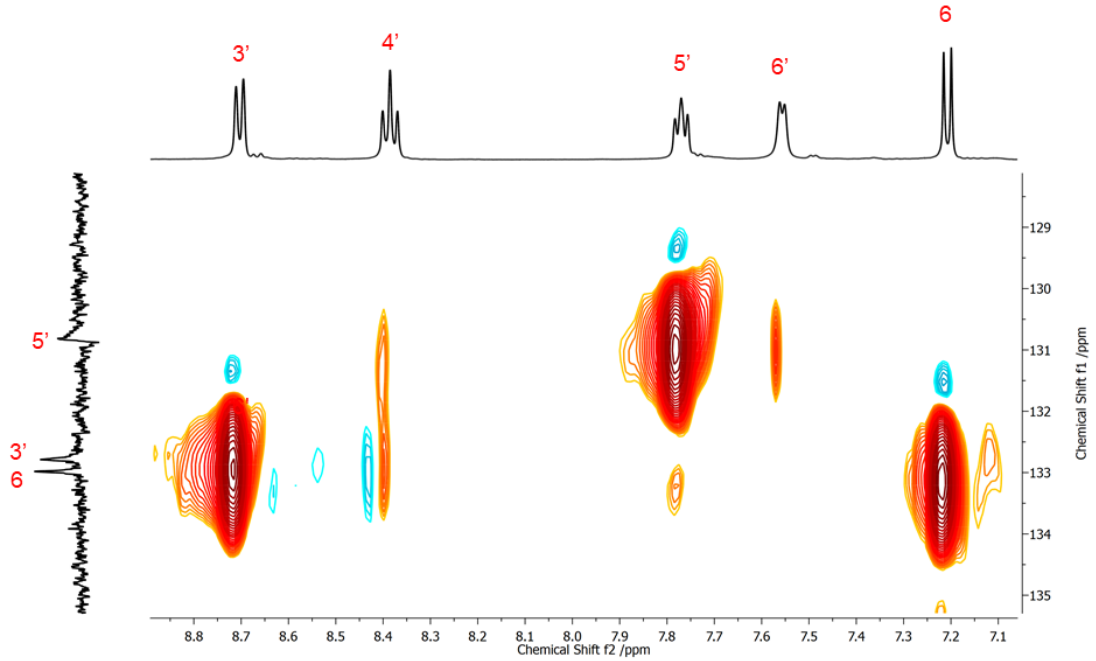

Figure A.7—Magnification of the HSQC NMR spectra above of $OsO_4 \subset Gdm_4 1$.

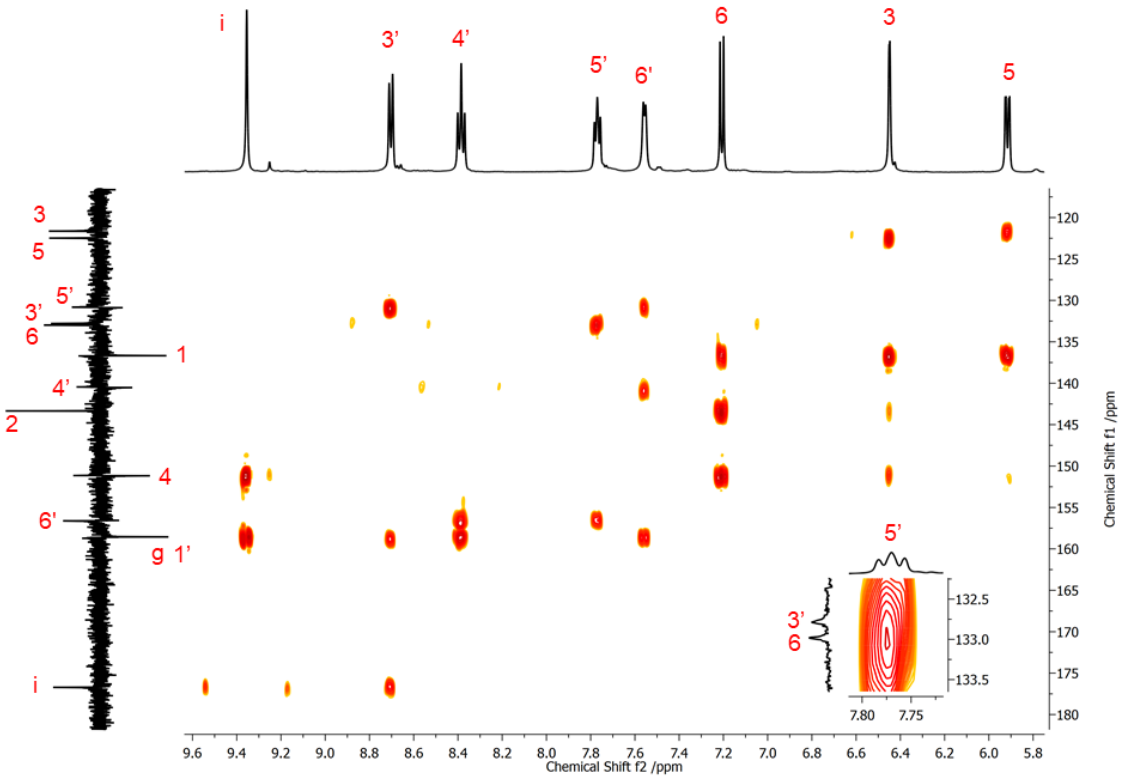

Figure A.8—HSQC NMR spectra of $OsO_4 \subset Gdm_4 1$, 1.48 mM of total host and 8.6 mM of total guest (500 MHz spectrometer).

A.3 2,3-dihydrofuran reference ^{1}H NMR spectrum

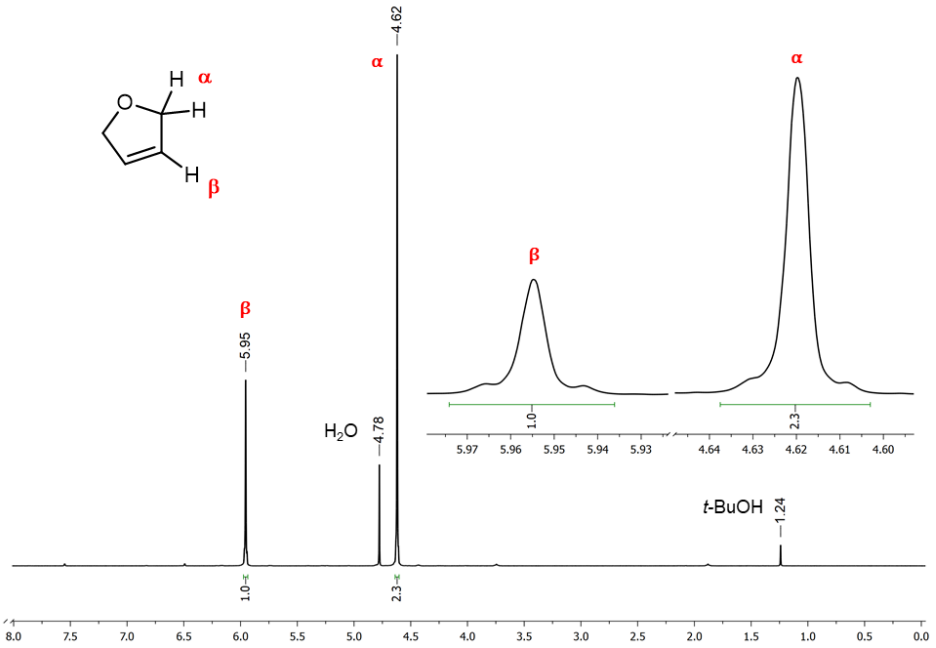

Figure A.9—Reference ^{1}H NMR spectrum of the 2,5-dihydrofuran with corresponding labelling of signals. There are few signals adding to 3% of the total signal, this is due to typical manufacturing impurities namely: THF, 2,3-dihydrofuran and furan.

A.4 Tetrahydrofuran-3,4-diol reference ^{1}H NMR spectrum

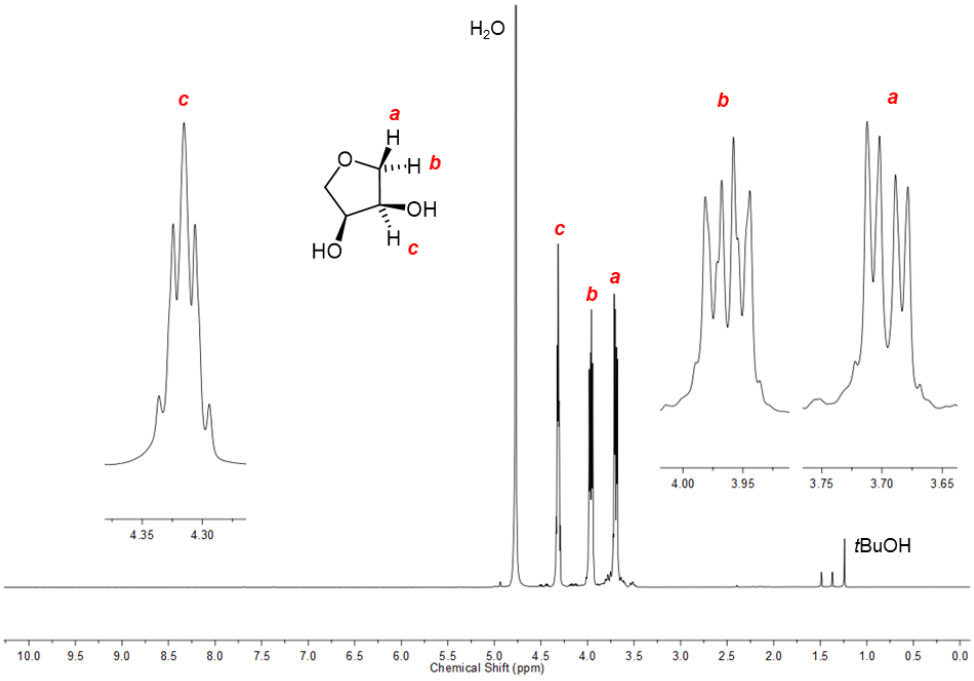

Figure A.10—Reference ^{1}H NMR spectrum of the tetrahydrofuran-3,4-diol with corresponding labelling of signals. The impurities here seem to be DHOF still in the osmate adduct at the end of the catalytic cycle.

A.5 Pent-4-en-1-ol ^{1}H NMR reference spectrum

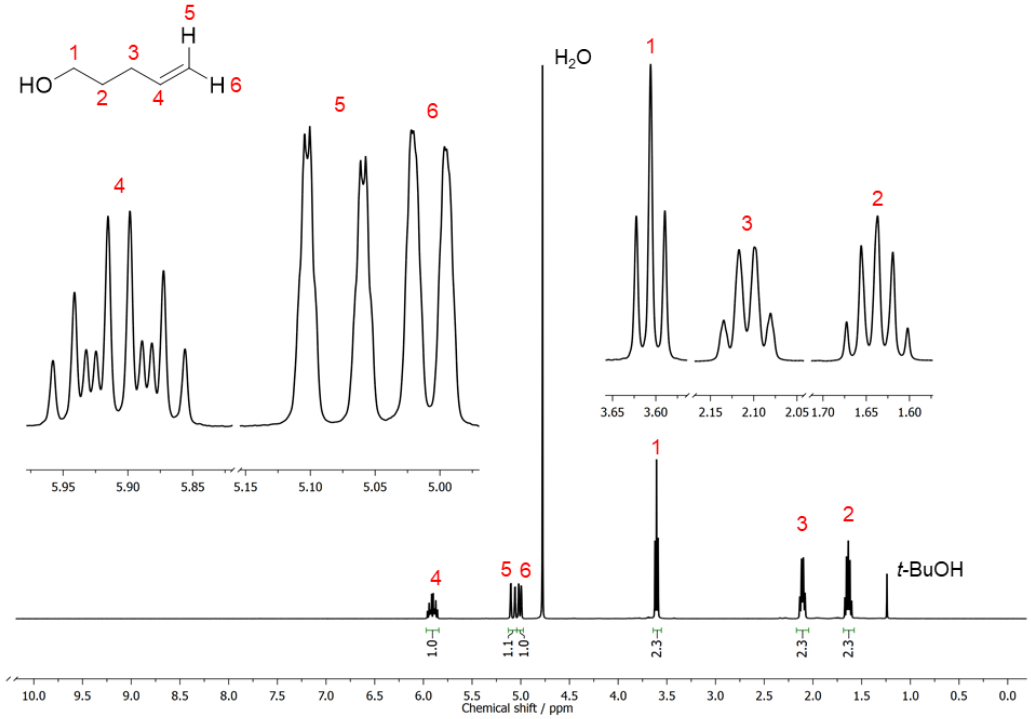

Figure A.11—Labelled reference ^{1}H NMR spectrum of the pent-4-en-1-ol. There are signals adding to less than 4% of the total signal; likely due to isomeric alcohols and even oligomers.

A.6 Pent-4-en-1-ol with Gdm$_4$1 ^{1}H NMR reference spectrum

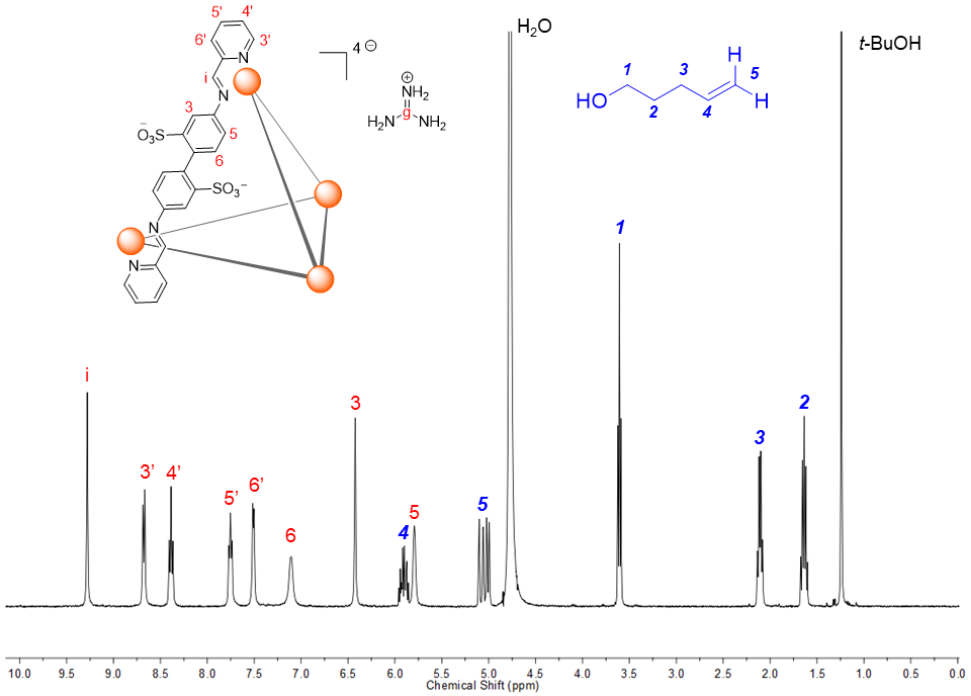

Figure A.12—^{1}H NMR spectrum of a mixture of pent-4-en-1-ol and Gdm$_4$1 as a control experiment to assess their interaction.

A.7 Pentan-1,2,5-triol ^{1}H NMR reference spectrum

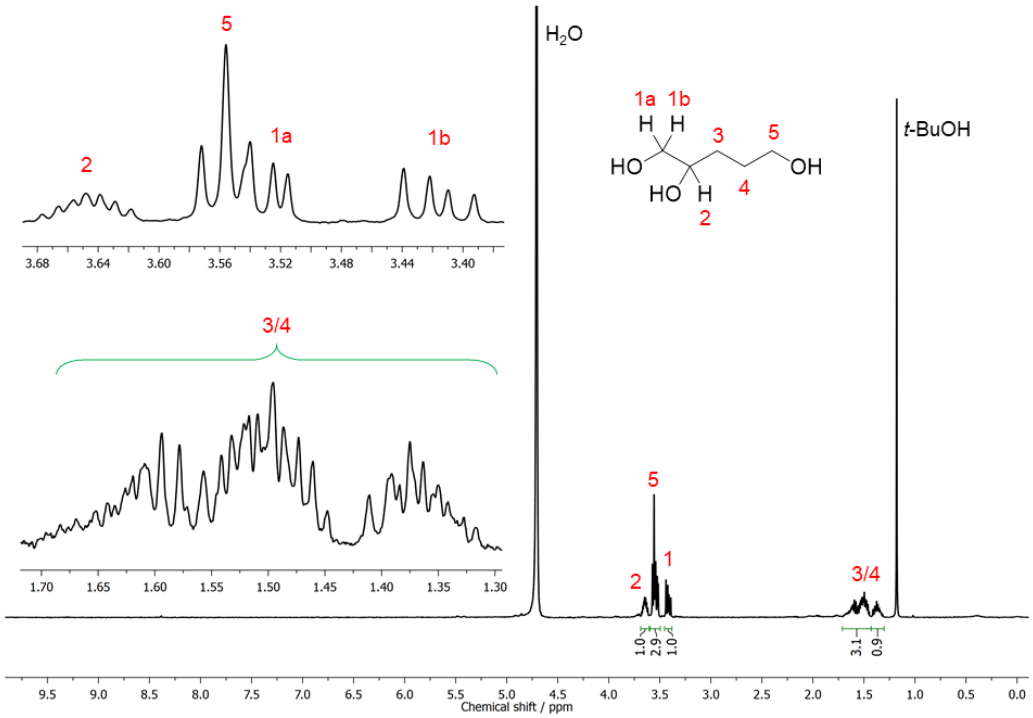

Figure A.13—Reference ^{1}H NMR spectrum of the pentan-1,2,5-triol with corresponding labelling of signals. The complex signals are due to triol still in the form of osmate adduct.

A.8 Pentan-1,2,5-triol with $Gdm_4$1 ^{1}H NMR spectrum

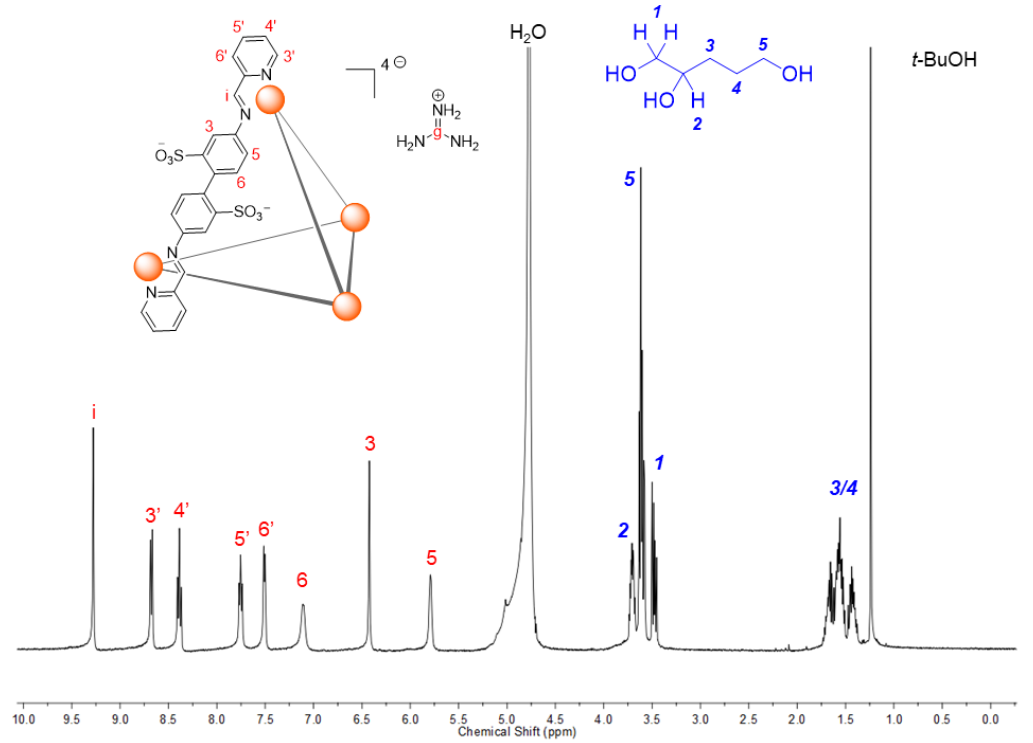

Figure A.14—^{1}H NMR spectrum of a mixture of pentan-1,2,5-triol and $Gdm_4$1 as a control experiment to confirm their lack of interaction.

A.9 TMA and OsO_4 reactivity experiment

The solutions giving rise to the spectra in Figure A.15 below were prepared by adding an aqueous solution of TMA 25% to a solution of Gdm_4 and OsO_4. The reader might notice that the chemical shift of the TMA signal changed quite significantly. This is because of a change in pH that causes a fast exchange of chemical environment in the nuclides.

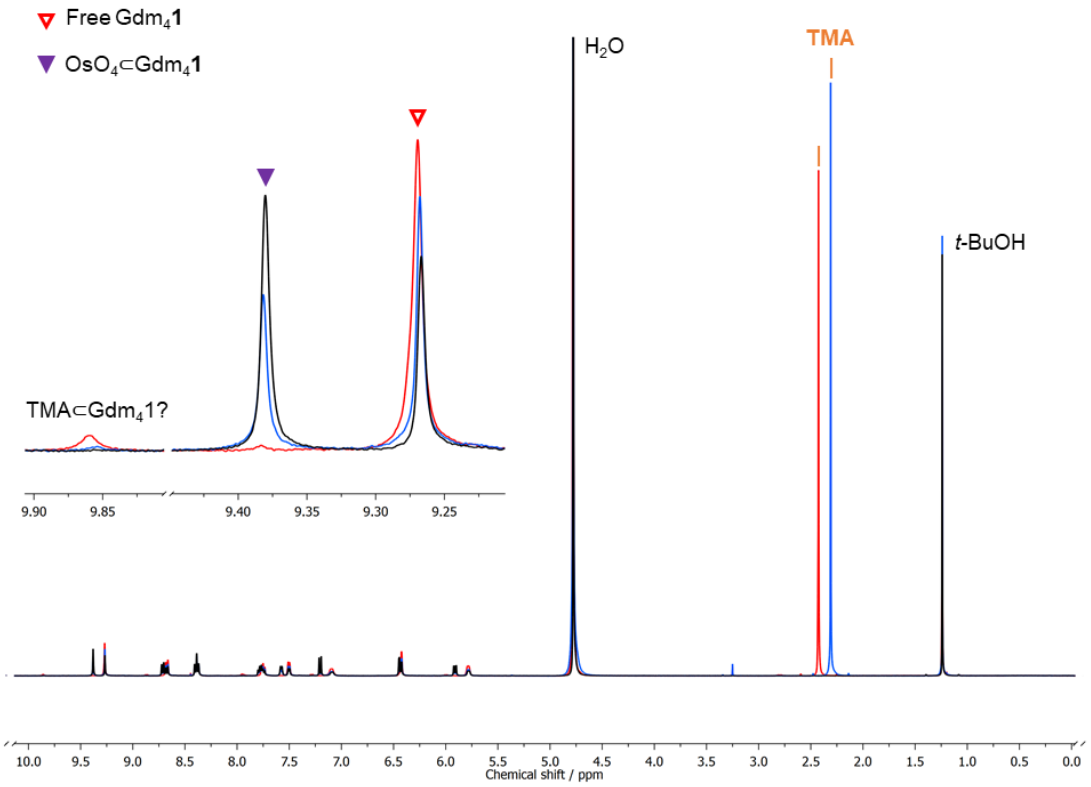

Figure A.15—Superimposition of three ^1H NMR spectra of a solution of OsO_4 (0.540 mM) and $Gdm_4$1 (0.853 mM) with increasing amounts of free TMA and varying degrees of association: black—no TMA, y = 59.3%, blue—6.63 mM, y = 40.3%, red—7.15 mM, y = 6.26%.

A.10 NMMO NMR reference spectrum

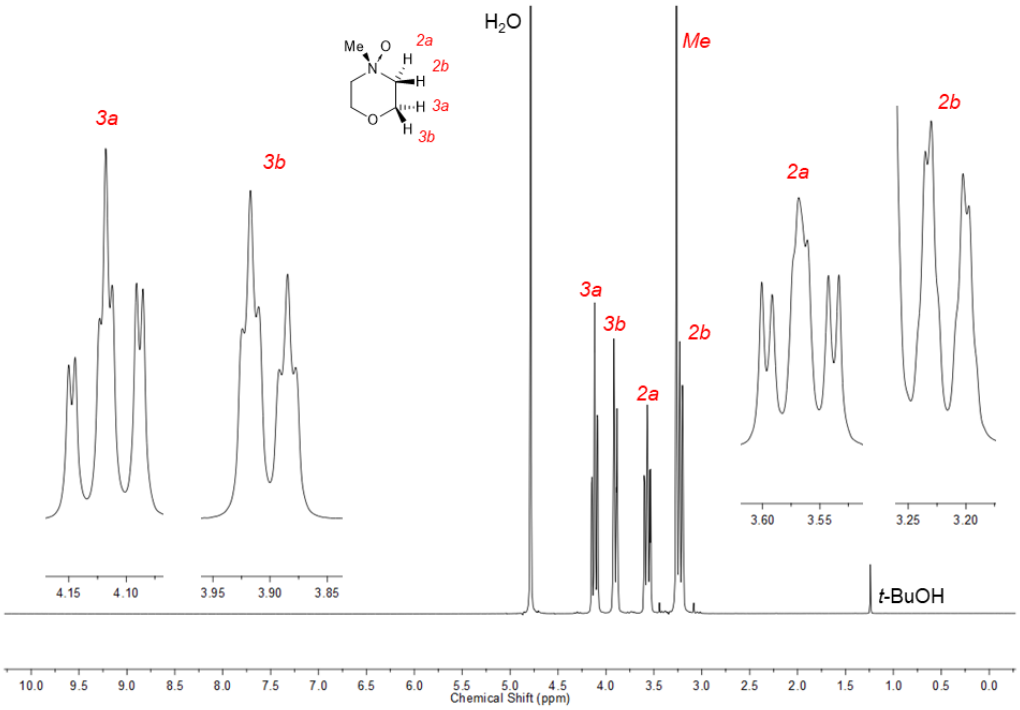

Figure A.16—Reference ^{1}H NMR spectrum of *N*-methylmorpholine *N*-oxide and corresponding labelling of signals.

A.11 NMMO with Gdm$_4$l ^{1}H NMR spectrum

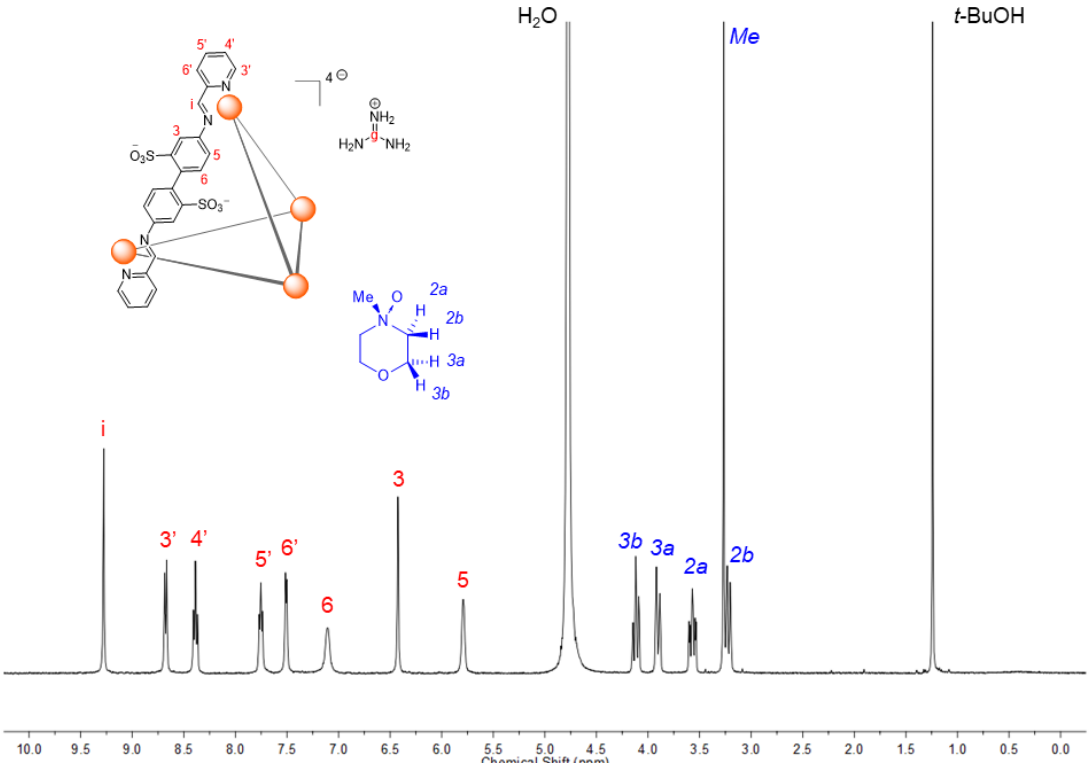

Figure A.17—^{1}H NMR spectrum of a mixture of NMMO and Gdm$_4$l as a control experiment to confirm their lack of interaction.

Appendix B

Regression

Data & Statistics

B.1 OsO_4 titration data

Table B.1—Total titrant volumes and estimated total concentrations of OsO_4 for each NMR tube used in the $OsO_4 \subset \mathbf{1}$ titration (from Section III.2.3).

Tube	V(titrant) / µL	c(OsO_4) / mM	Tube	V(titrant) / µL	c(OsO_4) / mM	Tube	V(titrant) / µL	c(OsO_4) / mM
	0.00	0.00		0.00	0.00		0.00	0.00
	2.00	0.0837		4.00	0.167		6.00	0.250
1	14.0	0.575	***2***	16.0	0.655	***3***	18.0	0.734
	26.0	1.05		29.0	1.16		32.0	1.28
	44.0	1.72		48.0	1.87		52.0	2.01
	68.0	2.57		73.0	2.73		82.0	3.03
	0.00	0.00		0.00	0.00		0.00	0.00
	8.00	0.332		10.0	0.413		12.0	0.494
	20.0	0.813		22.0	0.891		24.0	0.969
4	35.0	1.39	***5***	38.0	1.50	***6***	41.0	1.61
	56.0	2.15		60.0	2.29		64.0	2.43
	91.0	3.32		100	3.60		109	3.87
	191	6.08		200	6.30		209	6.51

B.1.1 27-point regression statistics

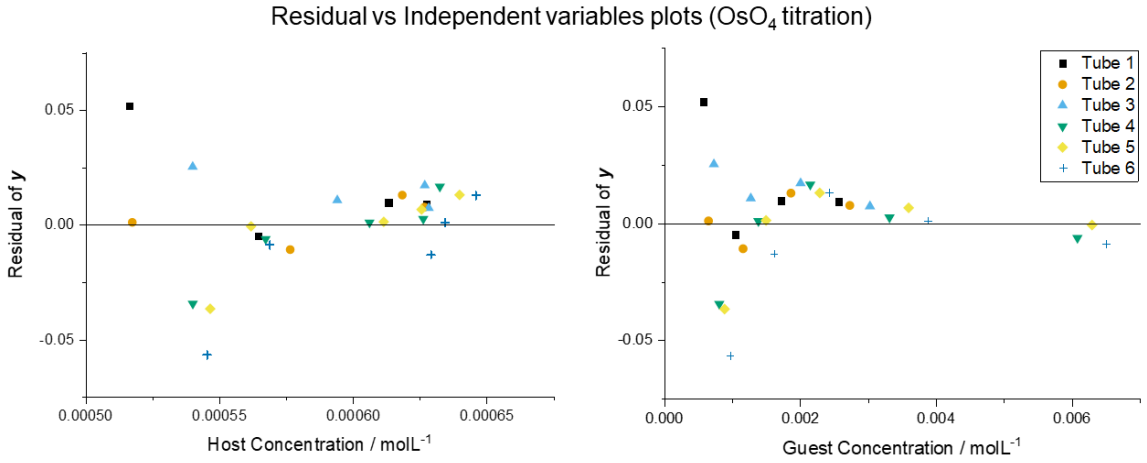

Figure B.1— **27 point regression** residual values plotted against guest concentration and host concentration (left and right, respectively).

B.1.2 23-point regression statistics

Table B.2—Summary of the parameters from 23-point $OsO_4 \subset 1$ titration curve regression.

	Value	Std Error	95% LCL	95% UCL	Dependency	Adj. R^2
x_0 / mM	0.469	0.0132	0.441	0.496	0.67313	0.99562
K / mM^{-1}	3.30	0.0928	3.11	3.49		

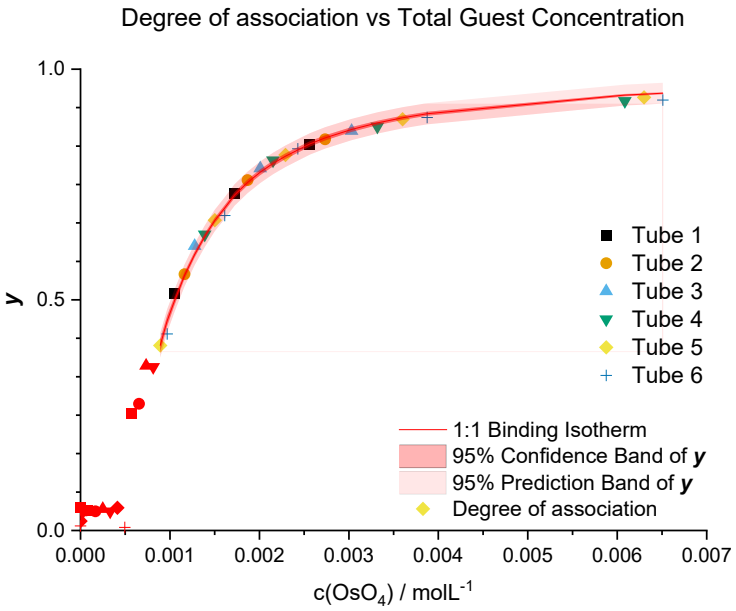

Figure B.2—Plot of the output from Origin's **23-point** non-linear regression. Red data points not used for regression.

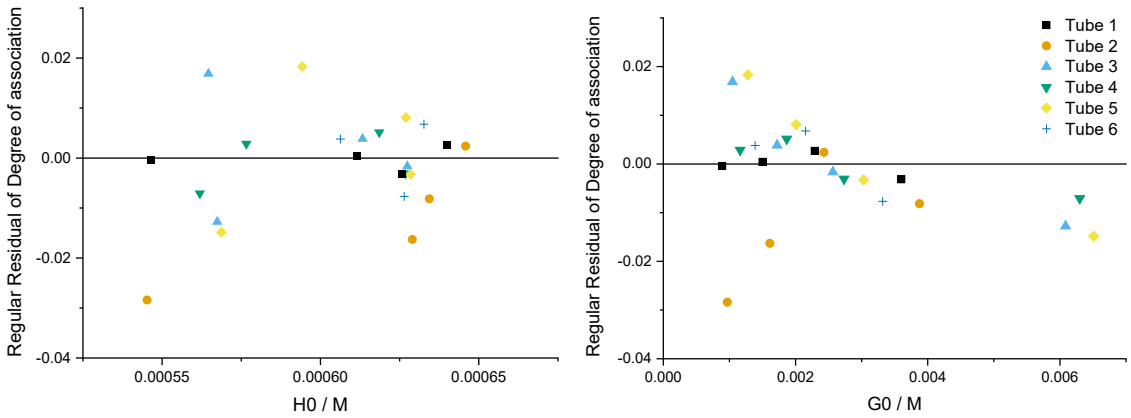

Figure B.3—**23 point regression** residual values plotted against guest concentration and host concentration (left and right, respectively).

B.2 Benzene titration data

Table B.3—Solution volumes and estimated concentrations of *t*-BuOH standard for each NMR tube solution prepared (from Section III.3.2).

	V(titrant) / μL	V(total) / μL	estimated c(t-BuOH) / mmol·L^{-1}
	0.00	500	1.77
	6.00	506	1.84
	9.00	509	1.87
	12.0	512	1.90
	15.0	515	1.93
	18.0	518	1.96
	21.0	521	1.99
	28.0	528	2.06
	38.0	538	2.16
	48.0	548	2.26
	60.0	560	2.36
	70.0	570	2.45
	80.0	580	2.53
	98.0	598	2.68
	108	608	2.75
	128	628	2.90
	140	640	2.98
	150	650	3.05
	160	660	3.11
Titrant*	500	500	7.31

B.2.1 20-point regression statistics

Table B 4—Summary of the parameters from 20-point Bzn⊂**1** titration curve regression.

	Value	Std Error	95% LCL	95% UCL	Adj. R^2
K / mM^{-1}	12.4	1.59	9.04	15.7	0.98500

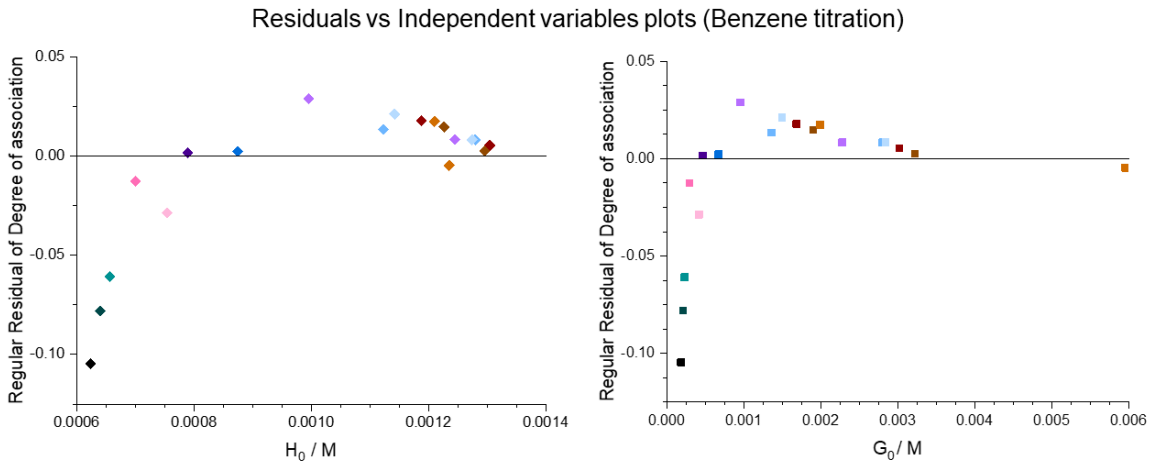

Figure B.4—Bzn⊂Gdm$_4$**1** **20-point regression** residual values plotted against total guest concentration and total host concentration (left and right, respectively).

Note in the figure above that the first seven points seem to be quite distant from those that follow, with the first five clearly having unacceptable residuals.

B.2.2 13-point regression statistics

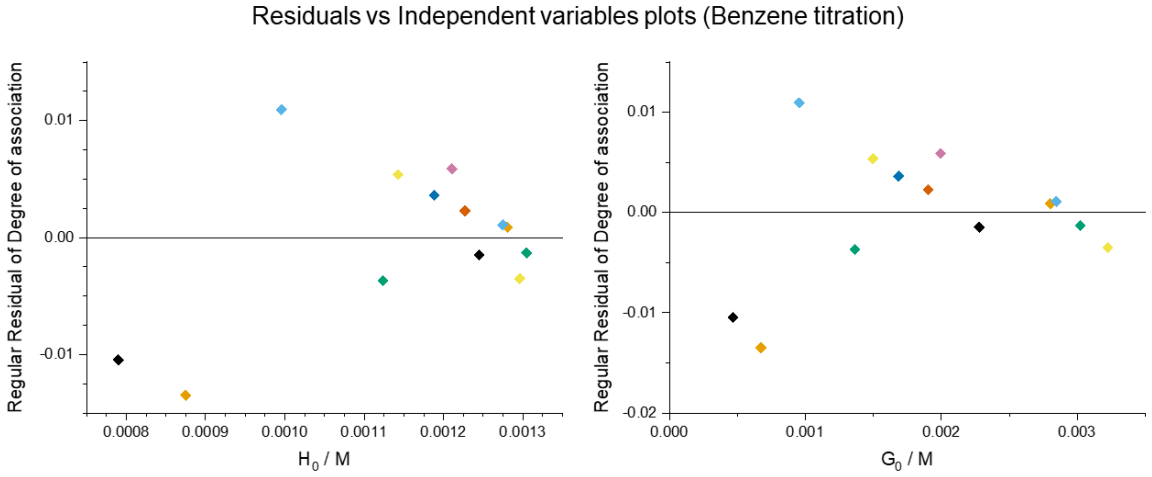

Figure B.5—Bzn⊂Gdm$_4$**1** **13-point regression** residual values plotted against total guest concentration and total host concentration (left and right, respectively).

B.3 Benzene intake kinetics data

The *t*-BuOH concentration was 2.25 mM.

Table B.5—Solution data for of the benzene intake kinetics experiment discussed in Section III.3.3.

	$[Gdm_41]_0$ / mM	$[Gdm_41]$ / mM	[Bzn⊂H] / mM	[Bzn] / mM	*y*	*t* /s
	0.999*	0.999	0	0*	0	—
	0.913	0.571	0.342	8.86*	0.375	317
	0.932	0.351	0.582	4.30	0.624	675
	0.965	0.230	0.735	4.32	0.762	975
	0.974	0.151	0.823	4.31	0.845	1275
	0.977	0.104	0.874	4.27	0.894	1575
	0.972	0.0703	0.902	4.24	0.928	1875
	0.958	0.0432	0.915	4.22	0.955	2175
	0.959	0.0320	0.928	4.19	0.967	2475
mean	0.963			4.264		
SE of mean	0.00572			0.0194		

B.3.1 Benzene intake regression statistics

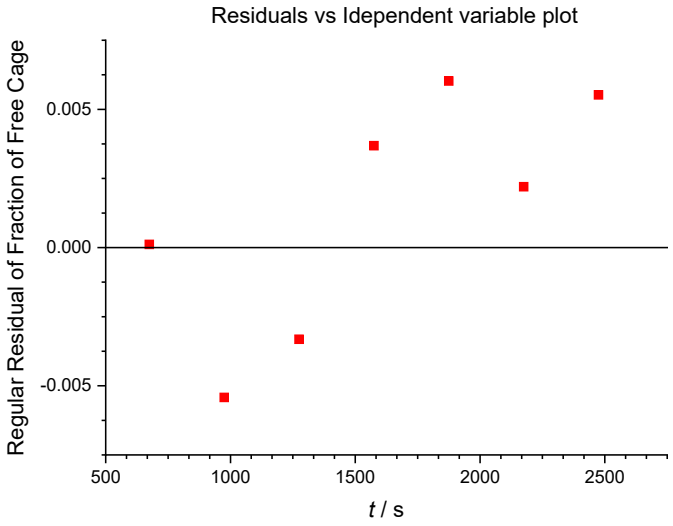

Figure B.6—Bzn⊂Gdm_41 intake regression residual values plotted against elapsed reaction time.

B.4 DHF titration data and regression statistics

Table B.6—Solution volumes and estimated concentrations for each NMR solution prepared (from Section 0).

V(titrant) / µL	V(total) / µL	estimated c(*t*-BuOH) / mmol·L^{-1}	$[Gdm_41]_0$ / mmol·L^{-1}	$[DHF]_0$ / mmol·L^{-1}
0.00	600.0	7.312	1.267	0.000
0.60	600.6	7.305	1.266	0.130
3.60	603.6	7.268	1.259	0.777
3.60	603.6	7.268	1.259	0.777
10.6	610.6	7.185	1.245	2.260
20.6	620.6	7.069	1.225	4.322
50.6	650.6	6.743	1.168	10.13
1.20	601.2	7.297	1.264	0.260
4.20	604.2	7.261	1.258	0.905
4.20	604.2	7.261	1.258	0.905
7.20	607.2	7.225	1.252	1.544
12.2	612.2	7.166	1.242	2.595
1.80	601.8	7.290	1.263	0.389
4.80	604.8	7.254	1.257	1.033
4.80	604.8	7.254	1.257	1.033
7.80	607.8	7.218	1.251	1.671
13.8	613.8	7.148	1.239	2.927
33.8	633.8	6.922	1.199	6.943
73.8	673.8	6.511	1.128	14.26
2.40	602.4	7.283	1.262	0.519
5.40	605.4	7.247	1.256	1.161
8.40	608.4	7.211	1.250	1.798
15.4	615.4	7.129	1.235	3.258
40.4	640.4	6.851	1.187	8.214
90.4	690.4	6.355	1.101	17.05
3.00	603	7.276	1.261	0.648
6.00	606	7.240	1.254	1.289
6.00	606	7.240	1.254	1.289
9.00	609	7.204	1.248	1.924
17.0	617	7.111	1.232	3.587
47.0	647	6.781	1.175	9.458
107	707	6.205	1.075	19.71

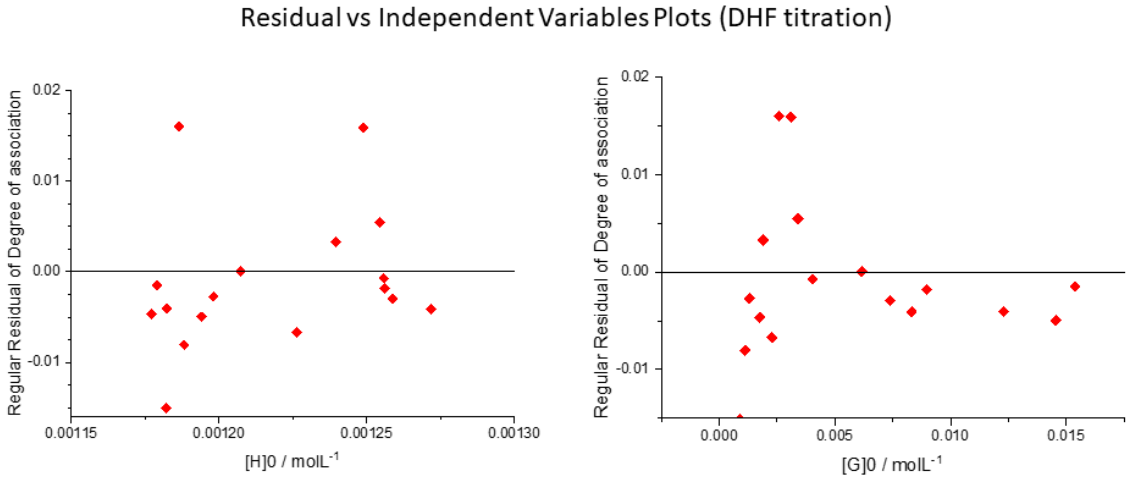

Figure B.7—Regression residual values plotted against guest concentration and host concentration (left and right respectively).

B.5 DHF intake kinetics data

Table B.7—Solution data for of the DHF intake kinetics experiment discussed in Section III.4.3.

t / s	$[H]_0$ / mmol·L^{-1}	$[G]_e$ / mol·L^{-1}	y
970	0.830	16.4	0.7938
1560	0.820	16.4	0.7756
2198	0.824	1.65E-02	0.7527
3262	8.34	1.62E-02	0.7378
mean	8.287	16.136	
SE of mean	0.00217	0.0601	

B.6 O1+P dihydroxylation regression data

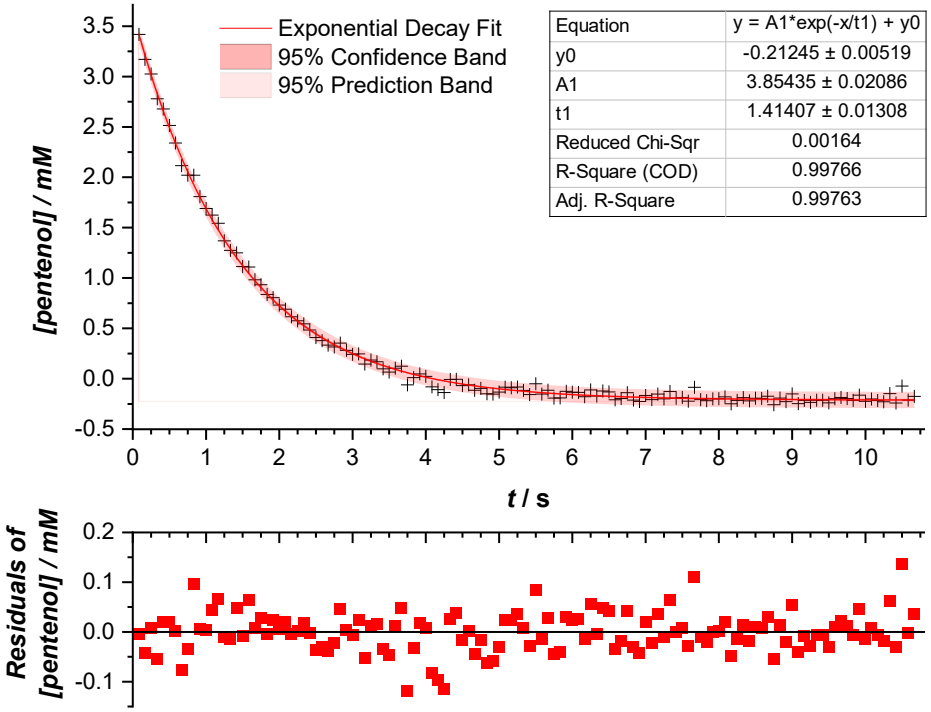

Figure B.8— Plot of the measured concentration of pentenol against reaction time in the O1+P system stacked with the regular residual plot after fit of the exponential decay function.

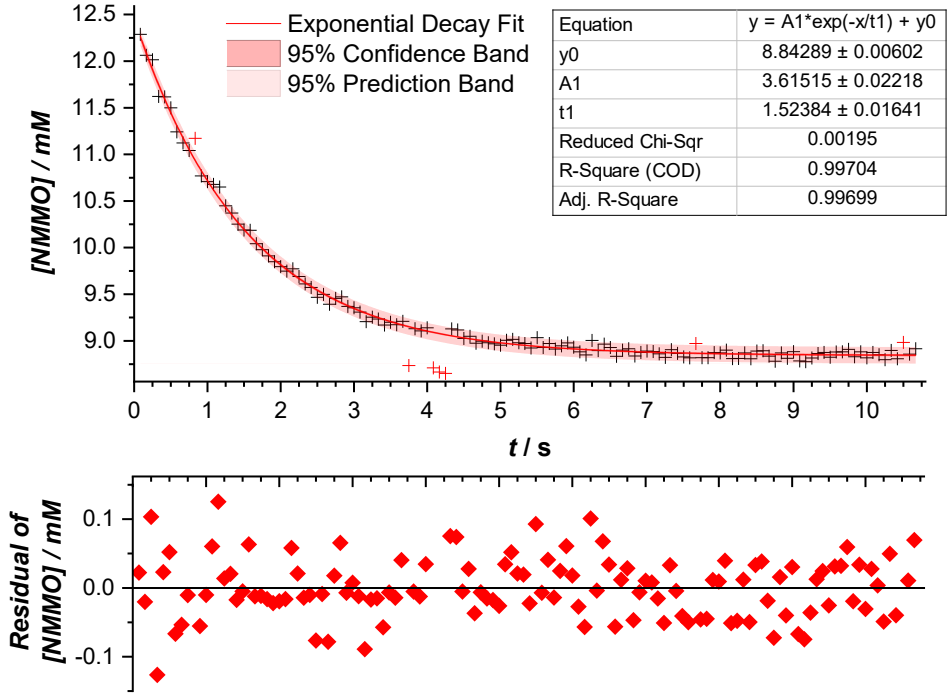

Figure B.9—Plot of the measured concentration of NMMO against reaction time in the O1+P system stacked with the regular residual plot after fit of the exponential decay function.

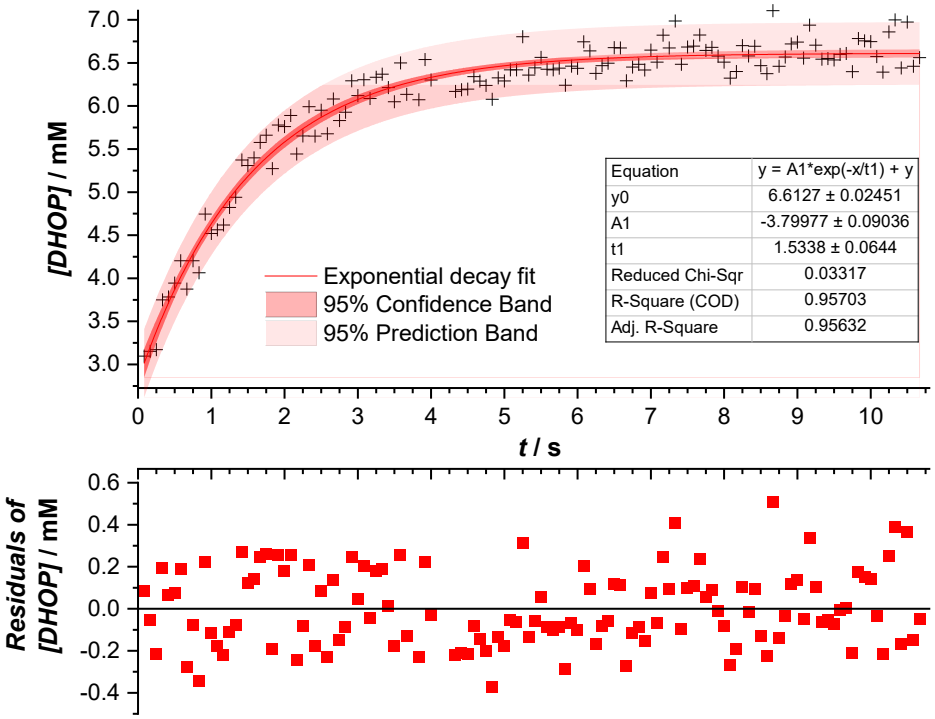

Figure B.10— Plot of the measured concentration of DHOP against reaction time in the O1+P system stacked with the regular residual plot after fit of the exponential decay function.

• The present Dissertation was presented to the Jury in
December 2018 by João Miguel Pimenta Pereira •
• The definitive version was delivered to the University of Aveiro in January 2019 •
• The body text was typed in Calluna and the headings and subtitles in Calluna Sans •